NASA Contractor Report 159029

NATURAL LAMINAR FLOW AIRFOIL ANALYSIS AND TRADE STUDIES

ENERGY EFFICIENT TRANSPORT PROGRAM

BOEING COMMERCIAL AIRPLANE COMPANY
P.O. BOX 3707, SEATTLE, WA 98124

CONTRACT NAS1-14742, TASKS 4.1.1 AND 4.1.2
MAY 1979

NASA
National Aeronautics and Space Administration
Langley Research Center
Hampton, Virginia 23665
AC 804 827-3966

FOREWORD

This document constitutes the final report for the 4.1.1 and 4.1.2 portions of Task 4.1, Natural Laminar Flow (NLF), one of five major tasks covered by the Statement of Work for Contract NASI-14742. The report covers work conducted from August 1977 through June 1978. The NASA Technical Monitor for all contract tasks was Mr. D. B. Middleton of the Energy Efficient Transport Project Office at Langley Research Center.

The investigations were conducted within the Preliminary Design Department of the Vice President—Engineering Organization of The Boeing Commercial Airplane Company. Contractor personnel who participated and their areas of contribution are:

G. W. Hanks	Program Manager
C. W. Clay	Task Manager—Airfoil and Trade Studies
G. R. Swinford	Configuration
T. C. Versteegh	Airfoil Design
R. L. Sullivan	Aero Performance
J. A. Paulson	Low-Speed Aerodynamics
R. N. Gornstein	High-Speed Aerodynamics
K. H. Hartz	Weights
M. D. Taylor	Stability and Control
V. D. Bess	Structures
A. C. Wery	Loads
C. R. Pratt-Barlow	Flutter

Principal measurements and calculations used during this study were in customary units.

CONTENTS

		Page
1.0	SUMMARY	1
2.0	INTRODUCTION	7
3.0	SYMBOLS AND ABBREVIATIONS	9
4.0	NLF AIRFOIL AND WING DESIGN	15
	4.1 Airfoil Design Sequence and Procedure	15
	4.2 Airfoil Design Evolution	19
	4.2.1 Starting Airfoil—Airfoil 1	19
	4.2.2 Design Modifications--Airfoils 2, 3, and 4	22
	4.2.3 Final Airfoil—Airfoil 5	26
	4.3 Airfoil 5 Boundary Layer Stability Analysis	29
	4.4 Wing Geometry Selection	30
5.0	AIRCRAFT DESIGN TRADE STUDY	35
	5.1 Trade Study Methods	35
	5.2 Trade Study Airplanes	35
	5.2.1 Turbulent Reference Airplane Configuration	35
	5.2.2 NLF Airplane Configurations	38
	5.2.3 NLF Wing Structure Design and Analysis	41
	5.3 Airplane Sizing and Performance	62
	5.3.1 Sizing and Performance	64
	5.3.2 Sensitivity Study	67
	5.3.3 Mission Analysis	69
	5.3.4 Turbulent Reference and NLF-AR10.24 Airplane Mission Analysis Comparison	70
	5.4 Economic Study	71
	5.5 Trade Study Results	71

Page

6.0 CONCLUSIONS AND RECOMMENDATIONS 73

6.1 NLF Airfoil and Wing Design 73

6.1.1 Conclusions 73

6.1.2 Recommendations 73

6.2 Aircraft Design Trade Study 74

6.2.1 Conclusions 74

6.2.2 Recommendations 74

7.0 REFERENCES 77

FIGURES

		Page
1	NLF Airfoil Design Criteria	16
2	Airfoil Design Sequence	17
3	Boundary Layer Stability Analysis Method	18
4	Airfoil 1 Pressure Distribution and Contour	19
5	Airfoil 1 Pressure Distributions, M = 0.76	20
6	Airfoil 1 Pressure Distributions, M = 0.78	20
7	Airfoil 1 Pressure Distributions, M = 0.80	21
8	Airfoil 1 Effect on Mach Number on Pressure Distribution	21
9	Airfoil 1 Application Boundaries	22
10	Pressure Distribution Comparison, Airfoils 1 and 2	22
11	Pressure Distribution Comparison, Airfoils 1 and 3	23
12	Lower Surface Pressure Distribution Comparison, Airfoils 3 and 4	23
13	Application Boundary Comparison, Airfoils 1 and 4	24
14	Airfoil 4 Pressure Distributions	25
15	Pressure Distribution Comparison, Airfoils 4 and 5	26
16	Airfoil 5 Lift Curve	27
17	Airfoil 5 Application Boundaries	27
18	Airfoil 5 Upper-Surface Boundary Layer Transition Prediction	29
19	Airfoil 5 Lower-Surface Boundary Layer Transition Prediction Disturbance	30
20	Effect of Pressure Distribution on Disturbance Amplification	31
21	Effect of Sweep on Transition Location	32
22	NLF Airplane Wing Spanwise t/c_{max} Distribution	33
23	Cruise Spanload Distribution	34
24	Design Development Method and Sequence	36
25	Reference Tubulent Airplane General Arrangement	37
26	Reference NLF-AR10.24 Airplane General Arrangement	38

		Page
27	Reference NLF-AR12 Airplane General Arrangement . . .	39
28	NLF Wing Structural Concept	42
29	NLF-AR10.24 Wing Aerodynamic Panels	43
30	NLF-AR12 Wing Aerodynamic Panels	43
31	Wing Stiffness Distribution, Aspect Ratio 10.24 . . .	44
32	Wing Stiffness Distribution, Aspect Ratio 12.0 . . .	44
33	Wing-Box Skin Panel	45
34	Tail-Off Lift Curve Slope Comparison	46
35	Structural Design Airspeed Comparison	46
36	Wing Lift Distribution Comparison in Terms of c_ℓ . .	47
37	Wing Lift Distribution Comparison in Terms of $c_\ell c$ . .	47
38	Wing Design Bending Moments at Elastic Axis Comparison .	48
39	Maneuver/Critical Positive Gust Bending Moment Comparison .	48
40	Wing Maximum Thickness Comparison	49
41	NLF-AR10.24 Airplane Gust Response at Maximum Zero Fuel Weight	50
42	NLF-AR12 Airplane Gust Response at Maximum Zero Fuel Weight	50
43	Airplane Gust Response Comparison	51
44	NLF Airplane Horizontal-Tail Sizing Selection . . .	55
45	NLF Airplane Flap System Geometry	56
46	Reference Airplane Low-Speed Characteristics . . .	57
47	NLF-AR10.24 Airplane Low-Speed Characteristics . . .	58
48	NLF-AR12 Airplane Low-Speed Characteristics . . .	59
49	NLF-AR10.24 Airplane Drag Characteristics Summary . .	60
50	NLF-AR10.24 Airplane Drag Polar	61
51	NLF-AR12 Airplane Drag Characteristics Summary . . .	61
52	NLF-AR12 Airplane Drag Polar	62
53	Reference Airplane Design Selection Chart	64
54	NLF-AR10.24 Airplane Design Selection Chart . . .	66
55	NLF-AR12 Airplane Design Selection Chart	66
56	Wing Loading Trade Study	67

Page

57 NLF-AR10.24 Airplane Sensitivity to Change in Selected Airplane Characteristics 68
58 NLF Final Airplane General Arrangement 69
59 NLF Final Airplane Mission Profile 70
60 Optimized Pressure Distribution Characteristics . . . 75

TABLES

		Page
1	Airfoil Evolution	19
2	Airfoil 5 Geometric Definition	28
3	Reference Airplane Principal Characteristics	37
4	Reference NLF-AR10.24 Airplane Principal Characteristics	39
5	Reference NLF-AR12 Airplane Principal Characteristics	40
6	NLF Wing Structure Material/Allowables	41
7	Airplane Characteristics/Gust Response Comparison	51
8	Cantilever Wing Uncoupled Modes	52
9	Wing Flutter Speed Ratios	52
10	Unsized Airplane Wing Weight Comparison; Constant Area 232.3 m^2	53
11	Sized Airplane Characteristics and Performance Requirements	63
12	Mission Analysis and Economic Data Comparison	65

1.0 SUMMARY

This study of natural laminar flow (NLF) is a segment of a program to investigate the application of new technologies to large transport aircraft with an objective of providing next-generation, energy-efficient civil transports. The NLF segment consists of two subtasks; airfoil and wing design analysis, and a preliminary evaluation of the efficiency and economics of an NLF airplane as compared to a conventional turbulent flow transport. The two subtasks were conducted concurrently.

Airfoil and Wing Design Analysis—The subtask objective was to establish, through application of the latest aerodynamic boundary layer analysis methods, the feasibility of developing an airfoil having a high degree of natural laminar flow.

A laminar flow airfoil, developed by Boeing prior to this contract, was selected as a base point for airfoil and wing design analysis. Effects of thickness ratio, off-design Mach number, and lift coefficient were evaluated, followed by airfoil modification to increase its thickness and to improve the extent of favorable pressure gradient, while minimizing wave drag. The final airfoil has a thickness of 10.1% chord, a design section lift coefficient of 0.5, and is intended to cruise at M = 0.78. The pressure distribution for those conditions is shown below.

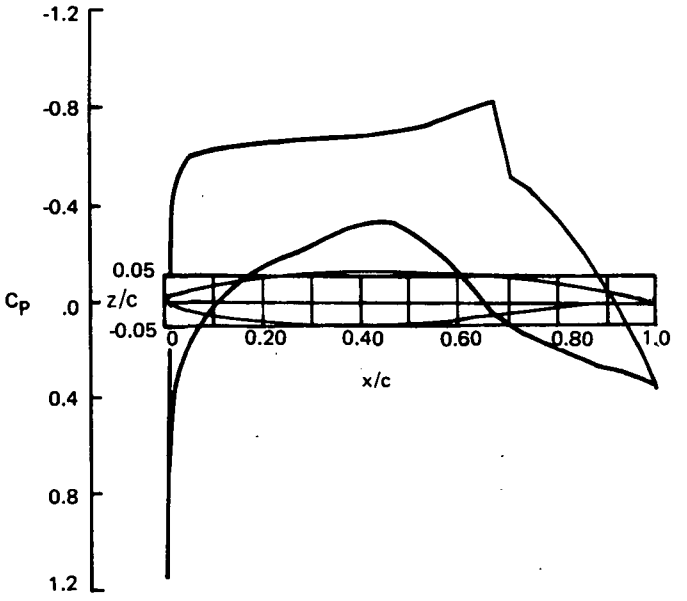

Final NLF Airfoil

Boundary layer stability was evaluated at the design section lift coefficient and Mach number, for a series of Reynolds numbers. It was assumed that transition would occur when the boundary layer disturbance amplitude ratio, e^n, had exceeded any of the several selected values. Numbers of amplification factors, n, have been established in the past, with results indicating maximum values ranging from 10 to 14. Upper surface transition location on the final NLF airfoil was quite sensitive to change in the selected values of n, while the lower surface transition location showed little variation. On the final developed airfoil, for n = 12, transition is calculated to occur at 35% chord on the upper surface despite a pressure gradient favorable to 60% chord, while the lower surface transition is delayed to 50% chord.

Although several iterations were required to evolve the airfoil shown, the results indicate that, through the use of advanced boundary layer flow analysis and stability calculations, an airfoil that should provide a high degree of natural laminar flow can be designed.

Laminar Flow Wing Design—Early transition can be caused not only by surface irregularities and adverse pressure gradient, but also by boundary-layer crossflow instability. A wing sweep and boundary-layer stability analysis, based upon a representative pressure distribution, revealed that crossflow instability could cause transition on natural laminar flow airfoils at very low sweep angles depending on airfoil pressure gradient. For the particular pressure distribution used in the present analysis, crossflow was found to cause transition for leading-edge sweep angles larger than 0.12 rad (7 deg), as shown below.

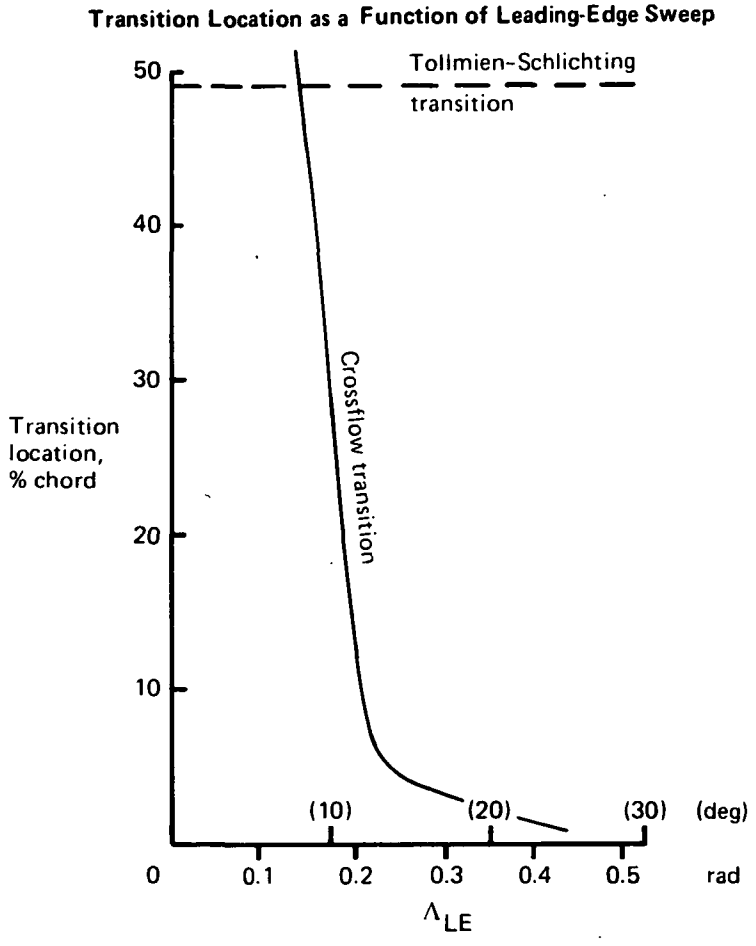

Effect of Sweep on Transition Location

However, a different airfoil pressure gradient could allow a higher leading-edge sweep but also adversely affect the Tollmien-Schlichting stability. The integration of a natural laminar flow airfoil into a three-dimensional swept wing is a very complex task requiring in-depth studies of optimum pressure distribution versus sweep angle, Reynolds number effects, and Mach number effects. Since such in-depth studies were beyond the scope of the present work, it was necessary to choose a leading-edge sweep angle that would provide some margin from crossflow instability, based upon the representative distribution developed for this study. Therefore, a leading-edge sweep angle of 0.09 rad (5 deg) was chosen for the present study.

Aircraft Trade Studies—The aircraft trade studies were conducted on the assumption that insect contamination of the wing leading edge was nonexistent; i.e., either the bug problem was greatly exaggerated or some system was installed on the airplane to prevent contamination.

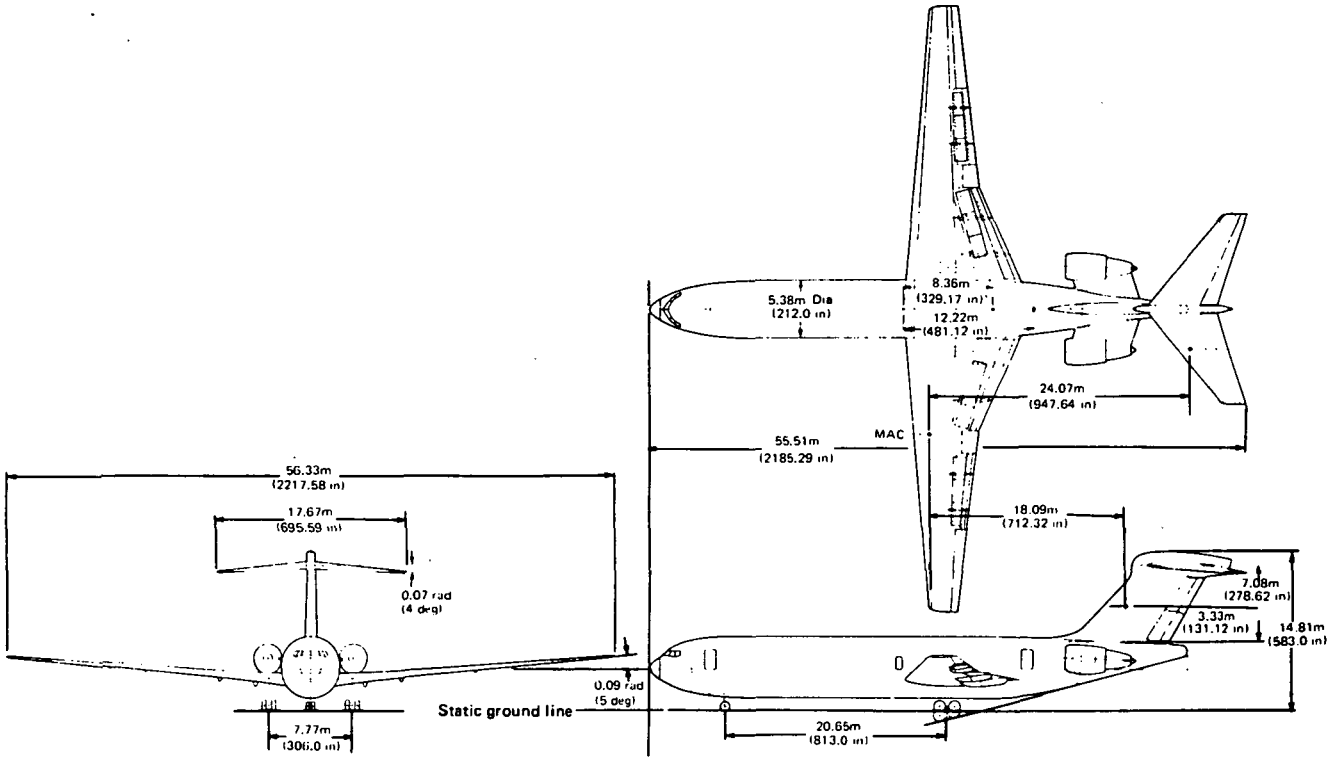

NLF Final Airplane General Arrangement

Using the results of the airfoil analysis (low sweep, low thickness ratio, etc.), a transport with an NLF wing was configured and compared with a conventional turbulent flow transport. Both airplanes were designed to perform the same mission; transport 196 passengers over a range of 3704km (2000 nmi). Fuel consumption and direct operating cost were compared, using a Boeing proprietary computer program. The computer program determines the airplane size, weight, thrust, and fuel required to satisfy the range requirement and other operational constraints, and computes the resultant direct operating cost.

Gust load conditions determined the structural strength of the unswept NLF wing and analysis showed it to be free from flutter. To provide a smooth aerodynamic surface, bonded aluminum-honeycomb construction was selected, even though it proved to be structurally less efficient than a conventional skin and stiffener wing in this application. To obtain laminar flow as far inboard as possible, the NLF wing thickness ratio at the side of the body was limited to 11% of gross chord as compared to 15% for the turbulent reference airplane. To eliminate wing pressure variations due to engines and struts, the engines were located on the aft body. When compared to the wing engine installation of the turbulent reference airplane, the NLF configuration showed a wing and aft body weight increase. The aeroelastic effects associated with unswept wings are found to increase wing-root bending moment over that of a rigid wing. For these reasons, the NLF wing was heavier, on a weight-per-unit area basis, than the swept wing of the turbulent reference aircraft.

To avoid gaps and discontinuities on the forward portion of the wing, the NLF airplane was configured without leading-edge devices, resulting in a maximum landing lift coefficient lower than that of the turbulent reference wing. When the 231.5 km/hr (125 kt) approach speed constraint was applied during the sizing program, the result was a substantial increase in the NLF wing area, causing a large weight increase. This negated the 20% improvement in lift-drag ratio attributable to NLF.

Results of the final mission analysis and economic study are listed below:

Mission Analysis and Economic Data Comparison

	Reference airplane	NLF final airplane
Payload, kg (lb)	18 225 (40 180)	18 225 (40 180)
Still air range, km (nmi)	3 704 (2 000)	3 704 (2 000)
M_{cruise}	0.80	0.78
Operating empty weight, kg (lb)	76 861 (169 450)	91 290 (201 260)
Manufacturer's empty weight, kg (lb)	71 690 (158 050)	86 119 (189 860)
Brake release gross weight, kg (lb)	121 985 (268 930)	137 490 (303 070)
Block fuel, kg (lb)	20 600 (45 415)	21 310 (46 980)
Block time, hr	4.769	4.885
Reserves (ATA domestic), kg (lb)	6 681 (14 730)	7 058 (15 560)
Relative direct operating cost	Base	*107.8% base

*Based upon 1967 ATA DOC equations adjusted to 1976 costs.

This study has demonstrated that the combination of boundary layer stability analysis techniques with standard airfoil design techniques can be used to satisfactorily define a two-dimensional airfoil having natural laminar flow over a major portion of a wing chord typical of a large contemporary civil transport. However, it has also demonstrated that the integration of such an airfoil into a three-dimensional swept wing is the most challenging problem to be solved before natural laminar flow can be successfully applied to a commercial airplane.

The basic problem involved in obtaining natural laminar flow on a swept wing, as opposed to unswept wing, is that the two basic types of laminar boundary layer instabilities which occur on a swept wing, crossflow instability and Tollmien-Schlichting instability, are affected oppositely by pressure gradient. Crossflow is caused by the combination of sweep and pressure gradient. As a result, a large extent of favorable pressure gradient on a swept wing will result in the development of large crossflow velocities in the boundary layer and large crossflow disturbance amplification rates. On the other hand, a large extent of favorable pressure gradient is required for the stabilization of Tollmien-Schlichting disturbances. As shown below, the typical optimum pressure distribution for crossflow stability has very large initial pressure gradients (where the boundary layer is thinner and more stable than further back). It then rapidly flattens out,

resulting in the decay of crossflow disturbances. The typical optimum pressure distribution for Tollmien-Schlichting stability has large favorable pressure gradients occuring over a large percentage of the chord. The integration, in an optimum manner, of a two-dimensional natural laminar flow airfoil (which has been optimized for Tollmien-Schlichting stability) into a three-dimensional swept wing would require that the airfoil be modified to have acceptable crossflow stability characteristics at the desired sweep angle, while not allowing the resulting degradation of Tollmien-Schlichting stability to become too severe. The resulting pressure distribution would be a compromise between that which is optimum for Tollmien-Schlichting stability and that which is optimum for crossflow stability. There will be some upper bound on the sweep angle beyond which it will not be possible to stabilize both types of disturbances without making other changes to the wing, such as reducing the chord Reynolds number. The aircraft trade study identified several areas where further iterations of the NLF airplane might have improved the design, such as thicker wing section at side-of-body; however, the biggest benefit would result from increasing wing sweep as high as possible. The airfoil-wing integration problem and the resulting determination of a realistic upper bound in the allowable sweep angle is one of the most fruitful areas for additional natural laminar flow studies.

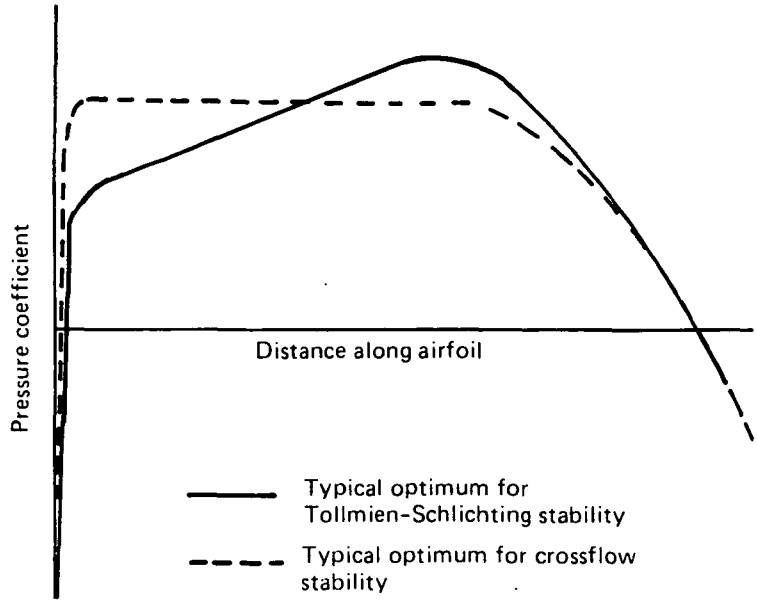

Optimized Pressure Distribution Characteristics

2.0 INTRODUCTION

The theoretical possibility of achieving laminar airflow over airplane wings and realizing the performance benefits of the resultant drag reduction has been recognized for many years. At first, the incentive for investigation in this field was the need for a more efficient airplane permitting longer ranges or higher payload. Today's escalating fuel prices have increased the necessity for research in this fuel-saving technology.

Laminar flow control, the maintenance of laminar flow by controlled suction through an airplane's skin, offers the largest gain in aircraft performance and reduced fuel consumption of any of the currently envisioned technology advances. However, design of a smooth, efficient wing structure through which controlled suction can be applied has presented formidable challenges.

Natural laminar flow may be achieved by a wing having a smooth airfoil with a contour producing favorable pressure gradients over a large portion of its upper and lower surfaces. If such an airfoil also provides a weak shock wave at high subsonic Mach numbers and maintains attached flow in the aft pressure-rise region, the resultant drag reduction benefits will approach those of laminar flow control, with little of its complexity.

Recent development of advanced computer techniques for boundary layer analyses and airfoil design, and advances in manufacturing methods for low-cost, smooth-surfaced bonded structure have combined to provide new interest in natural laminar flow technology. As a result of these advances, The Boeing Company funded research of natural laminar flow airfoils prior to this contract.

Data from Boeing's research was used as a starting point in the performance of Task 4.1, Natural Laminar Flow, one of five major tasks in the Contractor's Energy Efficient Transport program being conducted for NASA.

This document constitutes the final report of two of the Task 4.1 subtasks, of Contract NASI-14742. The first subtask was to define an airfoil for a large commercial transport cruising at Mach 0.8. The second subtask was to incorporate the airfoil into a natural laminar flow transport configuration and compare its fuel requirements and operating costs to those of an equivalent turbulent flow transport.

A third subtask was pursued as a separate study and is reported in NASA Final Report CR-158954, "Aircraft Surface Coatings Study" (ref 1).

Section 4.0 of this document pertains to the first subtask, NLF Airfoil and Wing Design Analysis. Subtask 2, Aircraft Design Trade Studies, is discussed in Section 5.0. The conclusions and recommendations resulting from completion of the study comprise Section 6.0.

3.0 SYMBOLS AND ABBREVIATIONS

A	amplitude
A_0	amplitude at neutral stability point
AR	aspect ratio
ATA	Air Transport Association
BLKF	block fuel
c	chord
$\bar{c}$	mean chord length
c_ℓ	section lift coefficient
C_c	compressibility correction
C_D	drag coefficient
C_{D_L}	induced drag coefficient
C_{D_M}	Mach drag coefficient
C_{D_P}	profile drag coefficient
CG	center of gravity
C_L	lift coefficient
C_{L_α}	lift curve slope, $dC_L/d\alpha$
C_p	pressure coefficient
C_{n_ℓ}	derivative of yawing moment with slideslip
DMF	dynamic magnification factor
DOC	direct operating cost
e	natural base of logarithms
E	Young's modulus

FAR	Federal Air Regulation
g	acceleration of gravity
G	torsional modulus
I	moment of inertia
ICAC	initial cruise altitude capability
J	polar moment of inertia
kPa	kilopascal
kt	knot
KEAS	knots, equivalent air speed
L/D	lift-drag ratio
LE	leading edge
LRA	load reference axis
M_∞	freestream Mach number
MAC	mean aerodynamic chord
M_C	cruise Mach number
M_D	dive limit Mach number
M_ℓ	local Mach number
M_{EA}	moment at elastic axis
MEW	manufacturer's empty weight
MTOW	maximum takeoff weight
MZFW	maximum zero fuel weight
n_ℓ	transition criterion, load factor—as defined in text
nmi	nautical mile
NLF	natural laminar flow
N-m	newton-meter

OEW	operating empty weight
R	momentum thickness x velocity ÷ kinematic viscosity
RN	Reynolds number
s	distance along surface
strw	streamwise
S	area
SFC	specific fuel consumption
SL	sea level
SLST	sea level static thrust
SOB	side-of-body
STA	station
S_W	wing area
t	thickness
T	thrust
TOFL	takeoff field length
TOGW	takeoff gross weight
U	velocity
U_{de}	derived gust velocity
V	airspeed
V_{app}	approach speed
V_B	gust penetration speed
V_C	cruise speed
V_D	limit dive speed

V_e	eqivalent airspeed
V_R	takeoff rotation speed
V_S	stalling speed
V_2	speed at start of second-segment climb
W	weight
x	distance, horizontal or along reference plane
X_0	amplitude at neutral stability point of laminar boundary layer
z	distance, vertical or normal to reference plane
ZFW	zero fuel weight
α	angle of attack
δ	angular deflection
δ^*	boundary layer displacement thickness
δ_F	flap deflection
Δ	increment
η	semispan fraction
θ	momentum thickness
Λ	sweep angle
ν	kinematic viscosity
ω	frequency
ω^*	disturbance frequency
ψ	disturbance propagation direction relative to local velocity at edge of boundary layer

Subscript

C	chordwise
c/4	quarter chord
des	design
e	equivalent
EA	elastic axis
f	flap
F	flutter
H	horizontal
max	maximum
MU	minimum unstick
o	initial condition
ref	reference
s	stall
V	vertical
∞	freestream condition

4.0 NLF AIRFOIL AND WING DESIGN

The objectives of this portion of the advanced technology NLF Study were:

- Design an airfoil section having, at typical flight conditions for large transport aircraft, the potential to produce laminar flow over 55 to 60% chord on the upper surface and 35 to 40% chord on the lower surface.
- Predict airfoil pressure distributions for a range of Mach numbers, lift coefficients, and Reynolds numbers (RNs).
- Determine the NLF operating regime by establishing the range of section lift coefficients and Mach numbers for which continuous, favorable pressure gradients exist.
- Predict boundary layer transition locations on the final airfoil, using specified boundary layer stability criteria. (The transition point, or location, is defined as that point at which the boundary layer has reached a fully developed turbulent flow character.)
- Define a three dimensional wing incorporating the final airfoil and having planform, twist, and thickness characteristics suitable for attainment of natural laminar flow.

4.1 AIRFOIL DESIGN SEQUENCE AND PROCEDURE

The starting airfoil (Airfoil 1) for this study was defined during previous Boeing-funded research. In the airfoil design process, it was assumed that extended regions of favorable pressure gradient would correspond to extended regions of laminar flow. Therefore, it was required that the pressure gradients be favorable as far aft as the design transition points. To limit wave drag, the local Mach number was to be limited to a value less than Mach = 1.2. To ensure attached flow, the maximum slope of the aft pressure gradient, $dC_p/d(x/c)_{max}$, was to be less than 3.0. These design criteria are summarized in Figure 1.

The development of the starting airfoil is summarized in the design sequence chart (fig. 2) under the section entitled "Boeing-funded research".

At the start of this study, an evaluation was conducted to determine the effects of off-design operating conditions upon the starting airfoil pressure distribution. Because the off-design pressure distributions were found to be unsuitable for attainment of extensive laminar flow, a revised target pressure distribution was defined.

An airfoil design procedure consisting of the following 10 steps was used for the refining cycle (fig. 2), as well as for the Boeing-funded research.

1. Computation of velocity distribution associated with starting pressure distribution and meeting NLF pressure gradient and peak local Mach criteria. This is the target velocity distribution.
2. Calculation of starting airfoil velocity distributions, using Korn-Garabedian transonic analysis (ref 2) for selected Mach and c_ℓ.
3. Calculation of the velocity-increment difference between the airfoil and target velocity distributions.

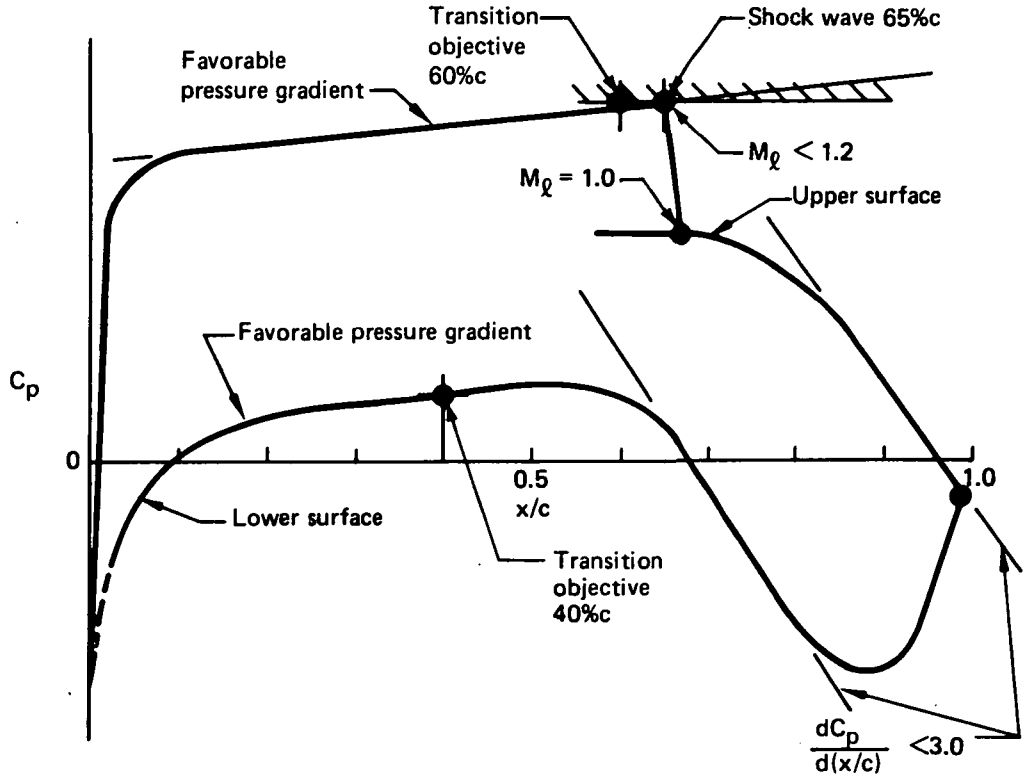

Figure 1. NLF Airfoil Design Criteria

4. Recontouring of the starting airfoil, using the streamline curvature approximation defined in Reference 3:

$$\left(\frac{d^2z}{dx^2}\right)_{new} = \left[1 + 10(1 - M^2)\left(\frac{\Delta U}{U}\right)\frac{d^2z}{dx^2}\right]_{initial}$$

$\Delta U/U$ is the ratio of velocity increment to local velocity. The new contour is obtained by integrating $(d^2z/dx^2)_{new}$, using initial boundary conditions z/c and dz/dx at the point where the velocity starts to deviate from the target velocity distribution.

5. Calculation of velocity distribution and the associated pressure distribution for the recontoured airfoil.

6. Repetition of Steps 2 through 5 until target pressure distribution is achieved.

7. Calculation of the boundary layer for a given RN on the resultant airfoil and addition of displacement thickness to the contour, using boundary layer calculations based upon the Nash-McDonald turbulent viscous flow method (ref 4), aft of the assumed transition location; the laminar region ahead of this location is assumed to have zero displacement thickness.

8. Calculation of airfoil contour pressure distribution with superimposed displacement thickness, using Korn-Garabedian equations.

9. Repetition of the boundary layer calculations (Steps 7 and 8) until the resultant pressure distributions converge.

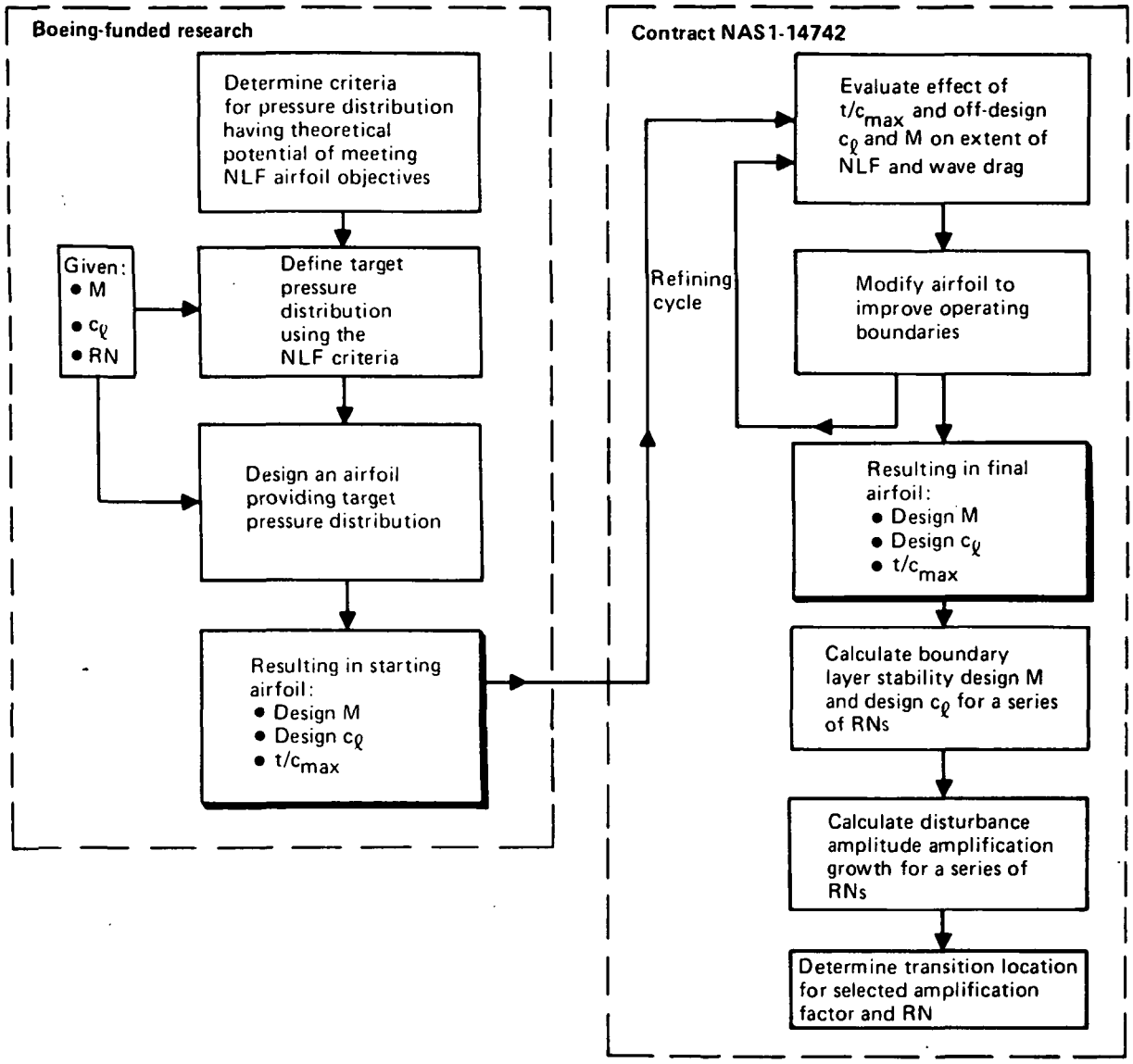

Figure 2. Airfoil Design Sequence

10. Iteration of final pressure distribution, including viscosity effects, until the target pressure distribution is achieved.

The product of these 10 steps was the final airfoil (Airfoil 5), which possessed an operating regime and a pressure distribution meeting the NLF criteria of Figure 1.

The calculation method used to determine the boundary layer stability characteristics of the two dimensional airfoil at a given Mach number and lift coefficient (fig. 3) consists of two major parts:

- Boeing boundary layer calculation code TEM 139 (ref 5 and 6)
- Revised boundary layer stability code developed by Mack (ref 7)

A separate computer program (ref 8) served as an interface between the TEM 139 boundary layer code and Mack's boundary layer stability code.

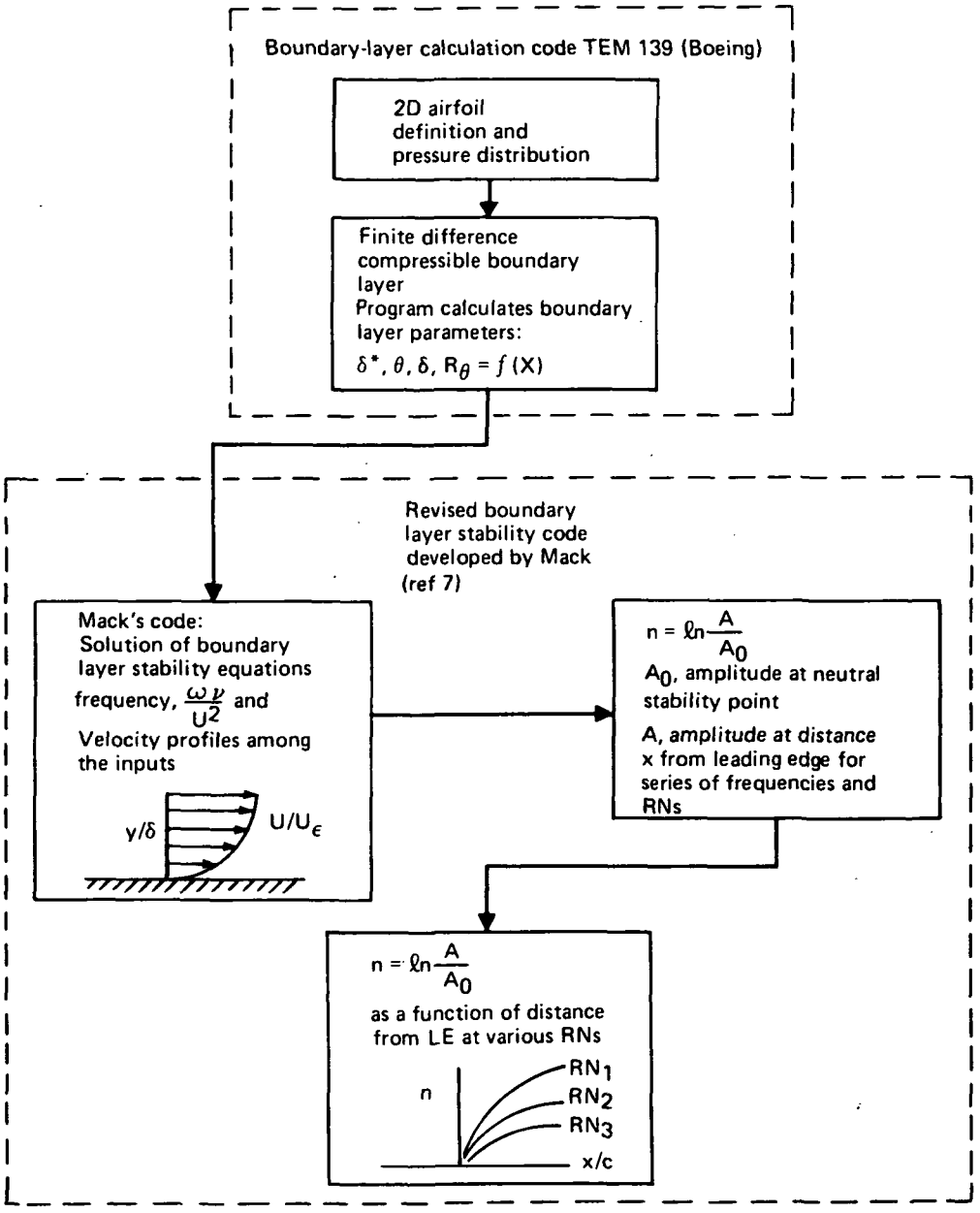

Figure 3. Boundry Layer Stability Analysis Method

TEM 139 calculates both the laminar and turbulent segments of the boundary layer, as well as details of the boundary layer flow, velocity profiles, temperature, total pressure, displacement thickness, momentum thickness, shape factor, and momentum Reynolds number.

Mack's boundary layer stability calculation is based upon a linear stability theory that postulates transition originating from a very small initial wave-type disturbance, amplitude A_O, inside the boundary layer. This disturbance is amplified as it sweeps downstream until it reaches a large enough amplitude, A, to cause a finite distortion in the mean velocity profiles, which leads to eventual transition. Transition is assumed to occur when the wave-type disturbance imposed upon the flow is amplified to a critical value of $\ell n = A/A_O$.

4.2 AIRFOIL DESIGN EVOLUTION

A series of five airfoils was designed, following the sequence outlined in Paragraph 4.1. Table 1 lists these airfoils in the order of their development and their distinguishing differences are noted. Each airfoil is discussed in the following text.

Table 1. Airfoil Evolution

Airfoil	t/c_{max}	Modification
1 (starting)	0.087	———
2	0.087	Recontoured lower surface in leading-edge area
3	0.101	Thickened by increasing lower surface ordinates
4	0.101	Smoothed lower surface
5 (final)	0.101	Recontoured upper surface

4.2.1 Starting Airfoil - Airfoil 1

The selected starting airfoil (Airfoil 1) was designed during a Boeing-funded study, using methods described in Paragraph 4.1. Figure 4 shows the contour of Airfoil 1 and the pressure distribution for 0.78M, $0.50c_{\ell}$, and 20 x 10^6 RN. Target pressure distribution (also shown on the figure) is close to that of Airfoil 1.

Analysis of pressure distributions at a given lift coefficient for various Mach numbers and at a given Mach number for various lift coefficients was made to determine their effect upon the extent of laminar flow and upon the local Mach number at the shockwave.

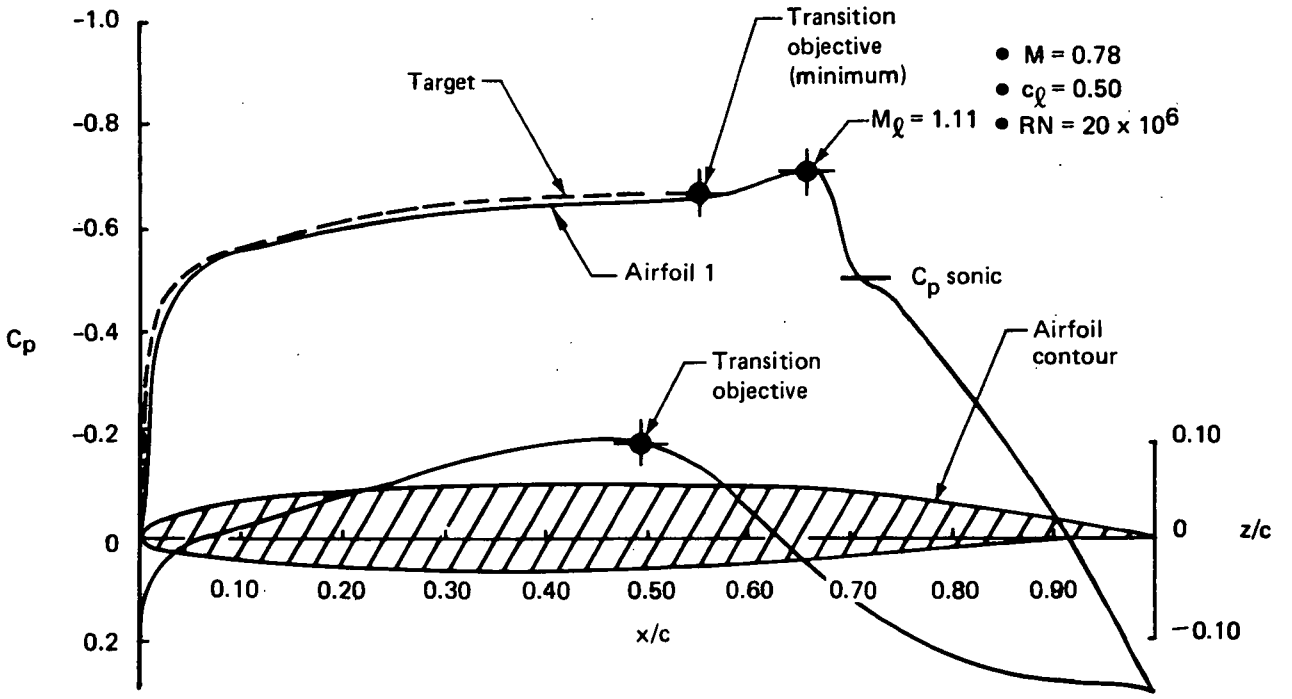

Figure 4. Airfoil 1 Pressure Distribution and Contour

Figures 5, 6, and 7 (0.76, 0.78, and 0.80M respectively) show Airfoil 1 pressure distributions for various c values. Each figure shows a region of adverse pressure gradient contained within the pressure variations existing on the forward lower surface for c_ℓ values of 0.50 and below. These adverse pressure gradients were expected to cause occurrence of transition substantially ahead of the 0.40 x/c lower-surface design objective.

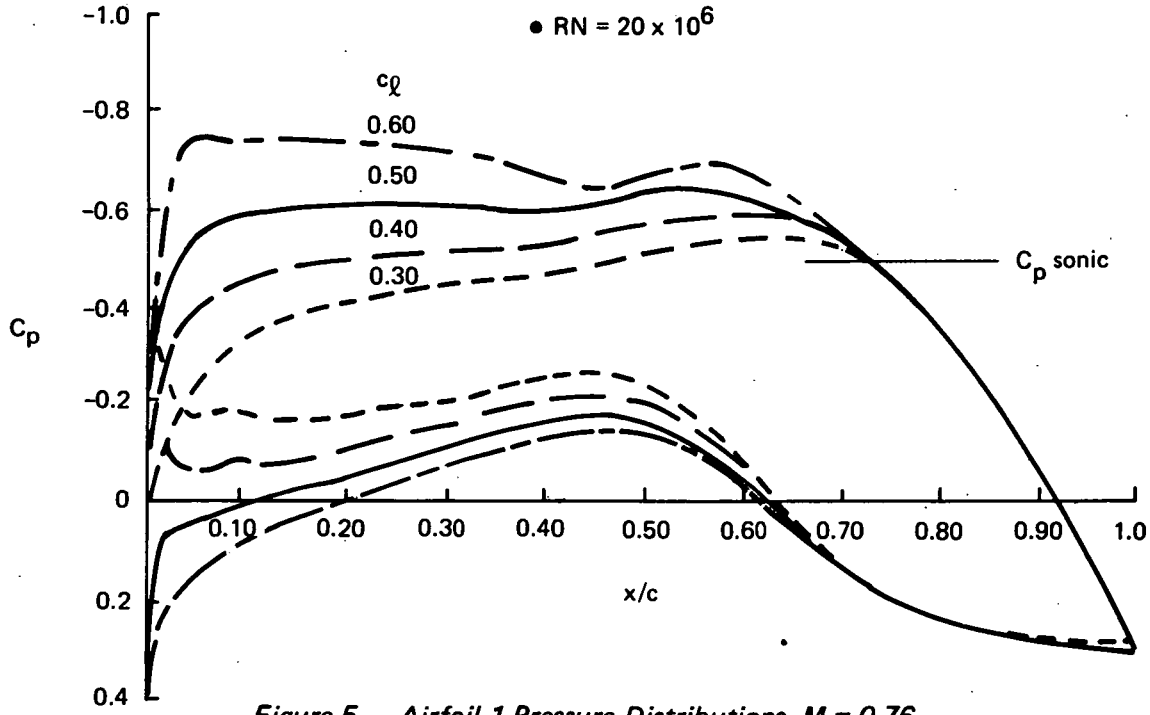

Figure 5. Airfoil 1 Pressure Distributions, M = 0.76

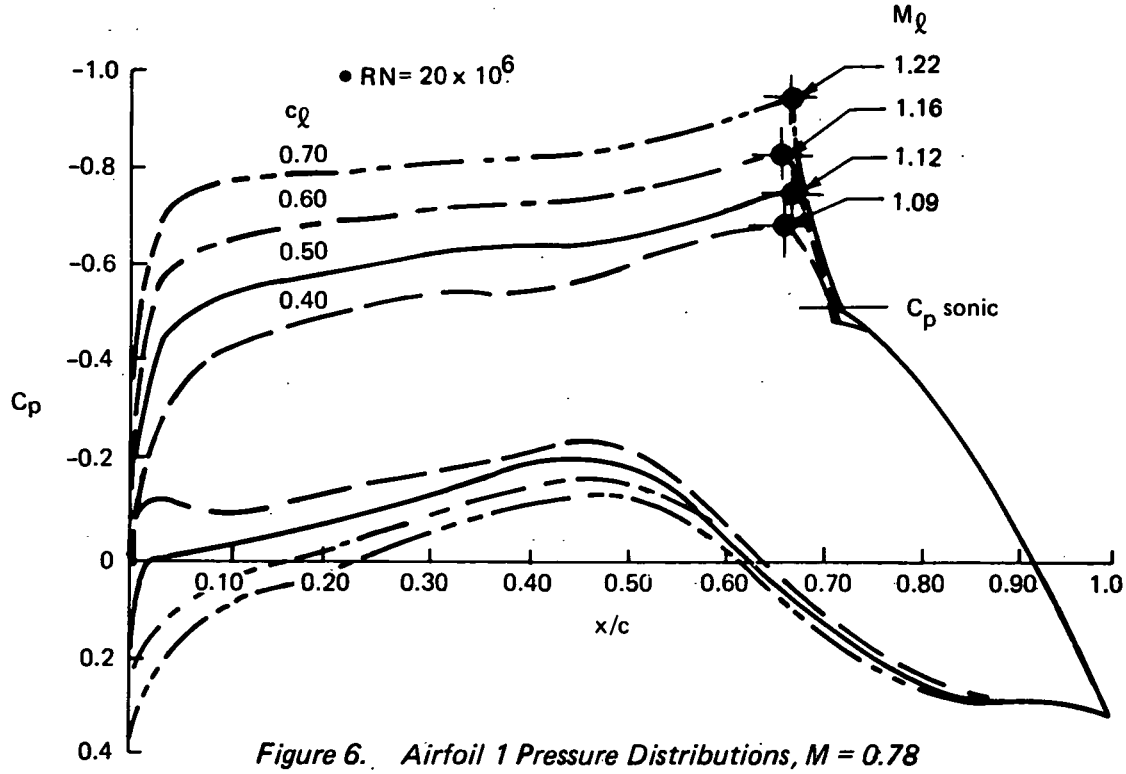

Figure 6. Airfoil 1 Pressure Distributions, M = 0.78

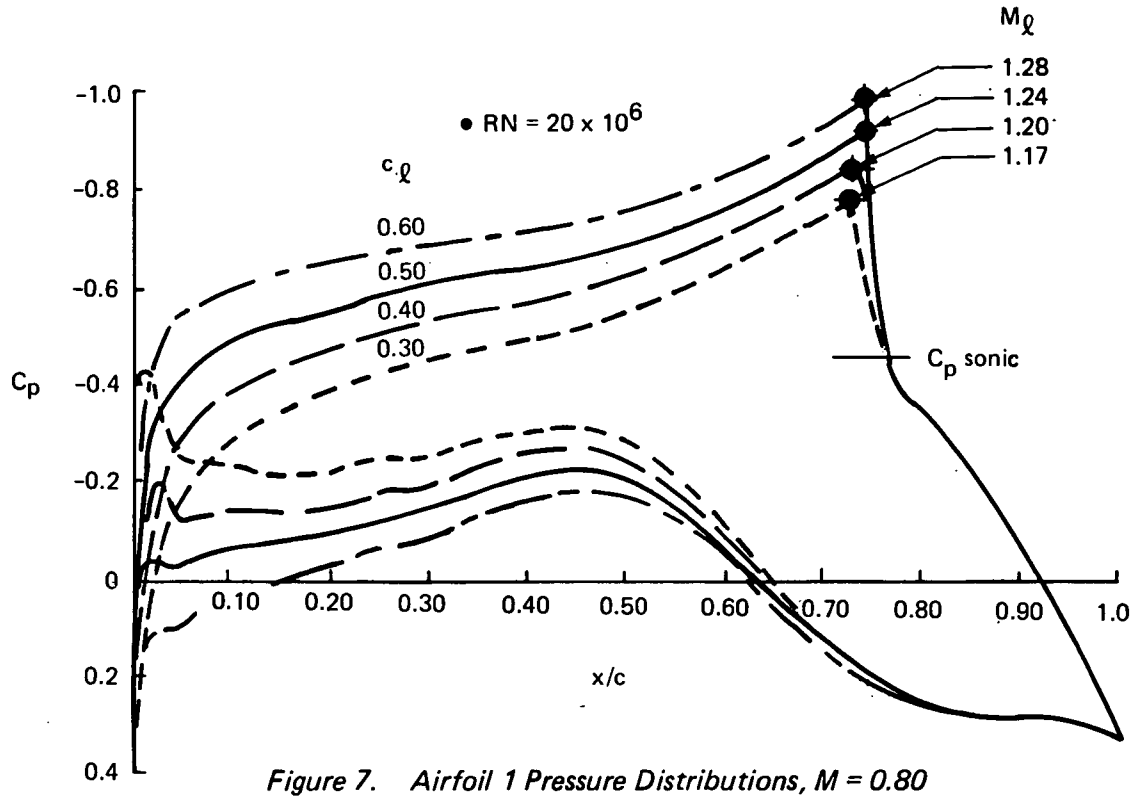

Figure 7. Airfoil 1 Pressure Distributions, M = 0.80

The pressure distributions for Mach numbers 0.74, 0.76, 0.78, and 0.80 at c_ℓ = 0.50 are shown in Figure 8. The Airfoil application boundaries (fig. 9) show a very limited M, c_ℓ region, which required modification of the airfoil, especially on the lower surface.

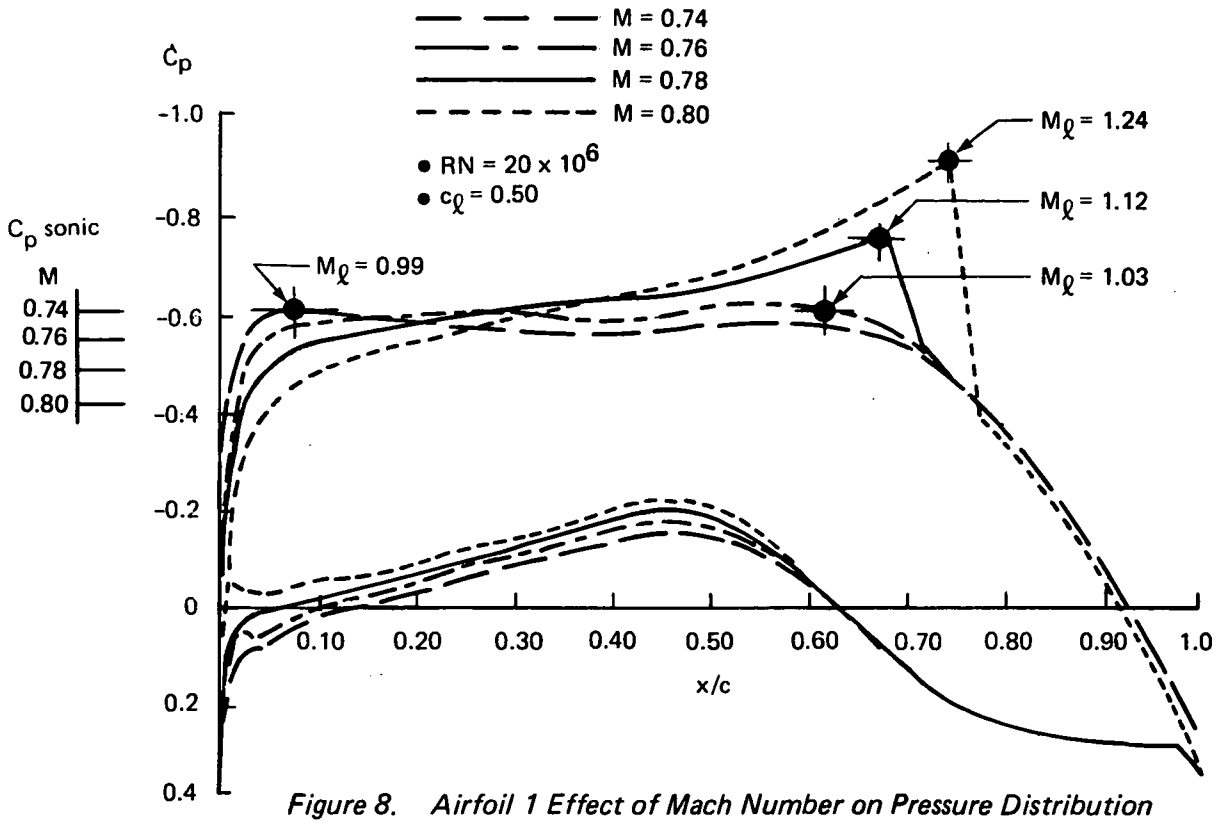

Figure 8. Airfoil 1 Effect of Mach Number on Pressure Distribution

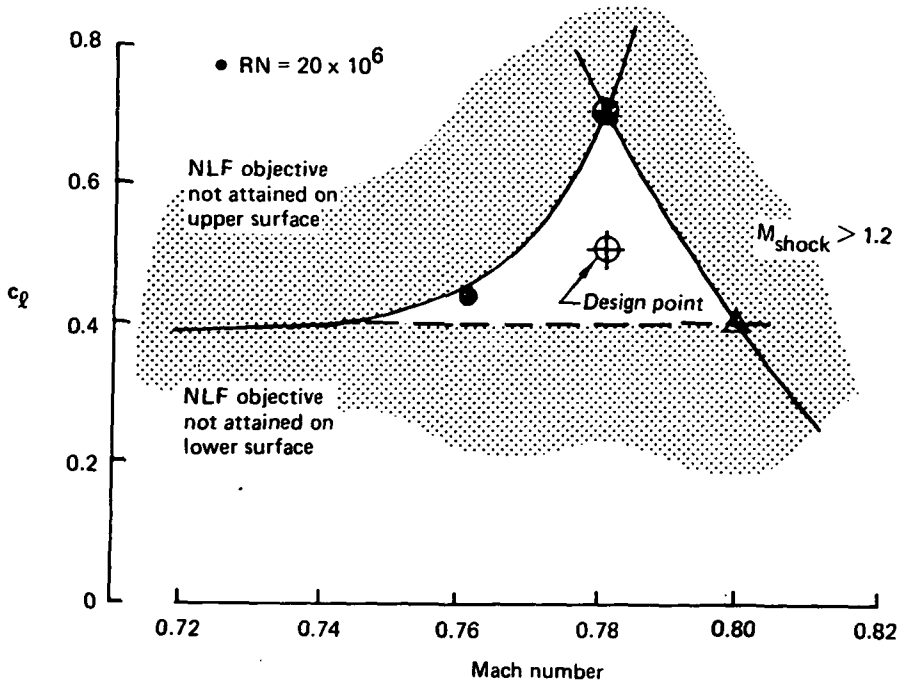

Figure 9. Airfoil 1 Application Boundaries

4.2.2 Design Modifications - Airfoils 2, 3, and 4

Recontouring of the lower surface near the leading edge was the initial design modification. It was in this region that a pressure "bump" occurred on Airfoil 1 for off-design conditions. An initial attempt, Airfoil 2, failed. Figure 10 shows evidence of this failure in that the lower-surface pressure distribution exhibits serious waviness.

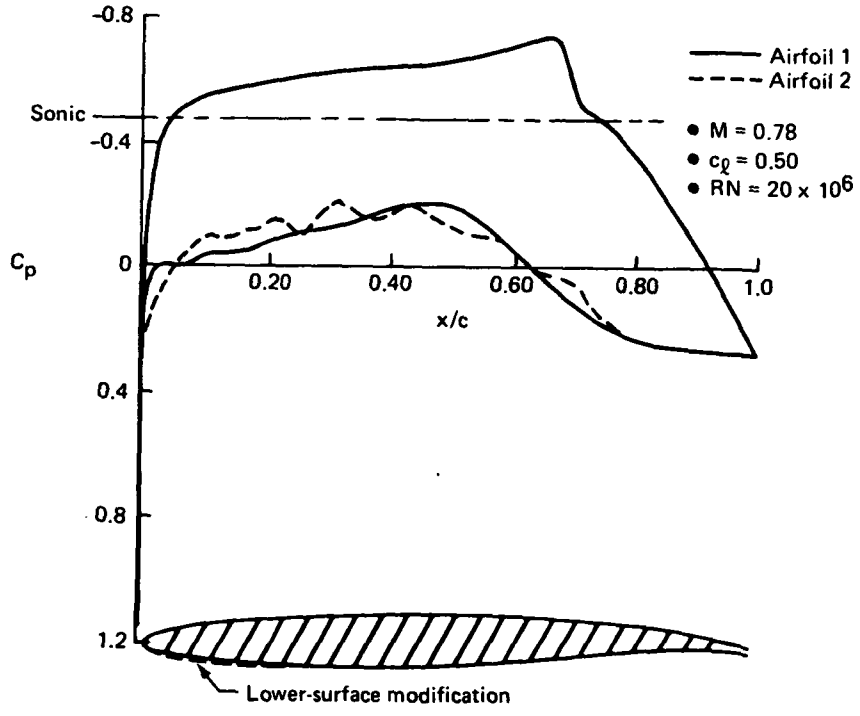

Figure 10. Pressure Distribution Comparison, Airfoils 1 and 2

As waviness of the lower-surface pressure distribution was addressed, the effect of airfoil thickness also was examined. The maximum thickness was increased from 8.7% chord to 10.1% chord to allow lighter, more practical wing construction. This increase was obtained by increasing the lower surface ordinates. Figure 11 (Airfoil 3) shows the effect of thickening the airfoil and, most significantly, the negligible change in shockwave strength.

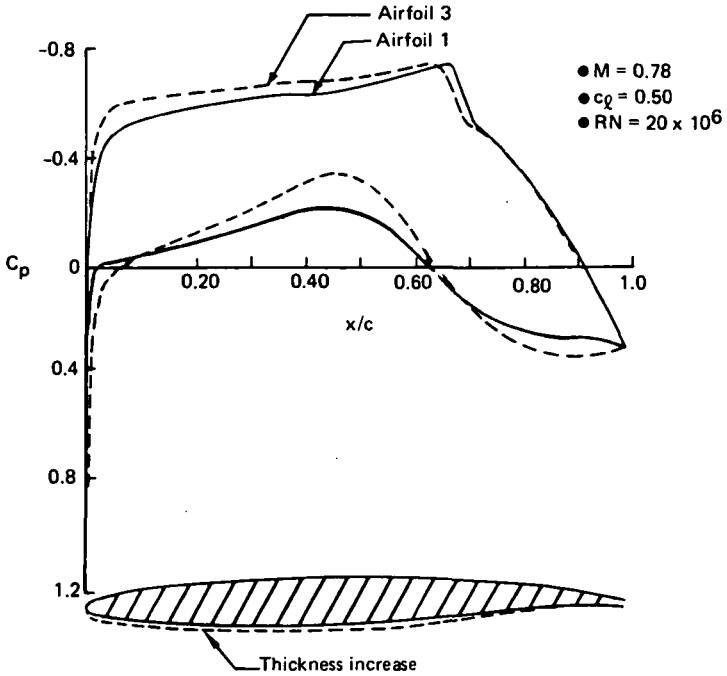

Figure 11. Pressure Distribution Comparison, Airfoils 1 and 3

Smoothing of the lower surface pressure distribution still was required and this process resulted in another 10.1% chord airfoil (Airfoil 4), shown in Figure 12. After smoothing, a favorable pressure gradient was obtained on the lower surface for all positive lift coefficients and Mach numbers of interest.

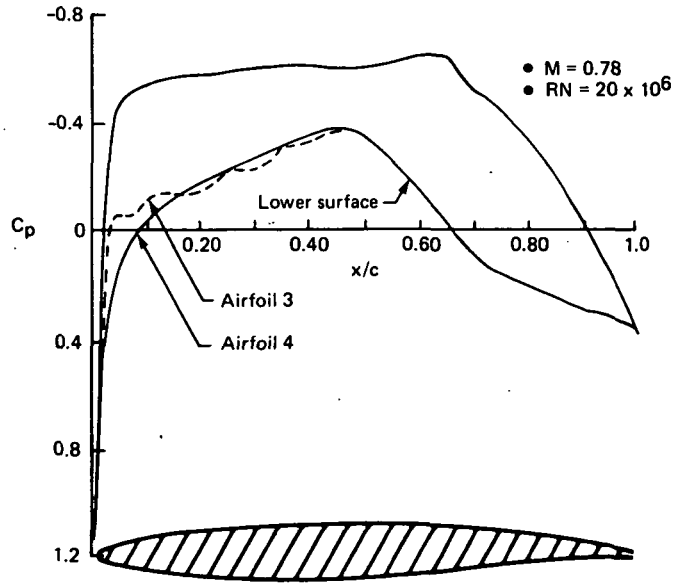

Figure 12. Lower Surface Pressure Distribution Comparison, Airfoils 3 and 4, c_ℓ = 0.40

The change in the lower-surface pressure distribution is reflected in the application boundaries (fig. 13) for the 8.7% t/c_{max} starting airfoil (Airfoil 1) and for the 10.1% t/c_{max} Airfoil 4. Figure 14 shows Airfoil 4 pressure distributions for the following conditions:

c_ℓ = 0.50, Mach number = 0.78 (target)
c_ℓ = 0.40, Mach number = 0.74, 0.76, and 0.78
c_ℓ = 0.20, Mach number = 0.70 and 0.76

Views A, C, and D of this figure show a sonic line, within which the local Mach number exceeds 1.0.

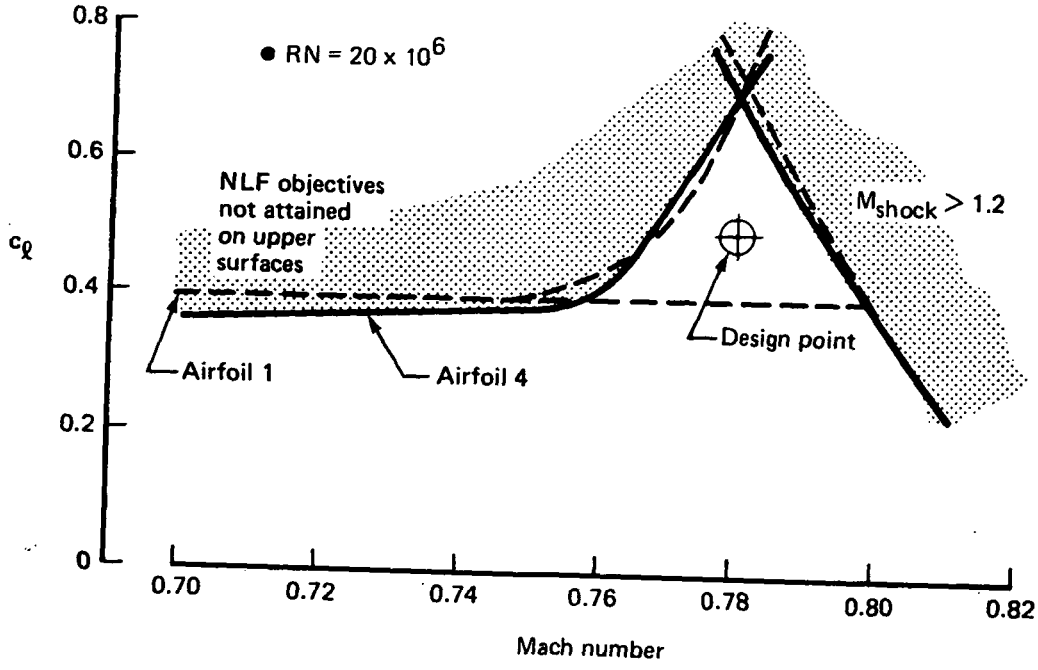

Figure 13. Application Boundaries Comparison, Airfoils 1 and 4

Under the transition assumptions of Paragraph 4.1, the strong, favorable lower-surface pressure gradients shown indicate that the lower surface boundary layer will likely meet the design objectives at any positive lift coefficient for any cruise Mach numbers considered. The application boundary is determined only by the upper-surface contour (fig. 13). Therefore, attempts were made to improve the upper surface, producing more favorable pressure gradients capable of delaying transition.

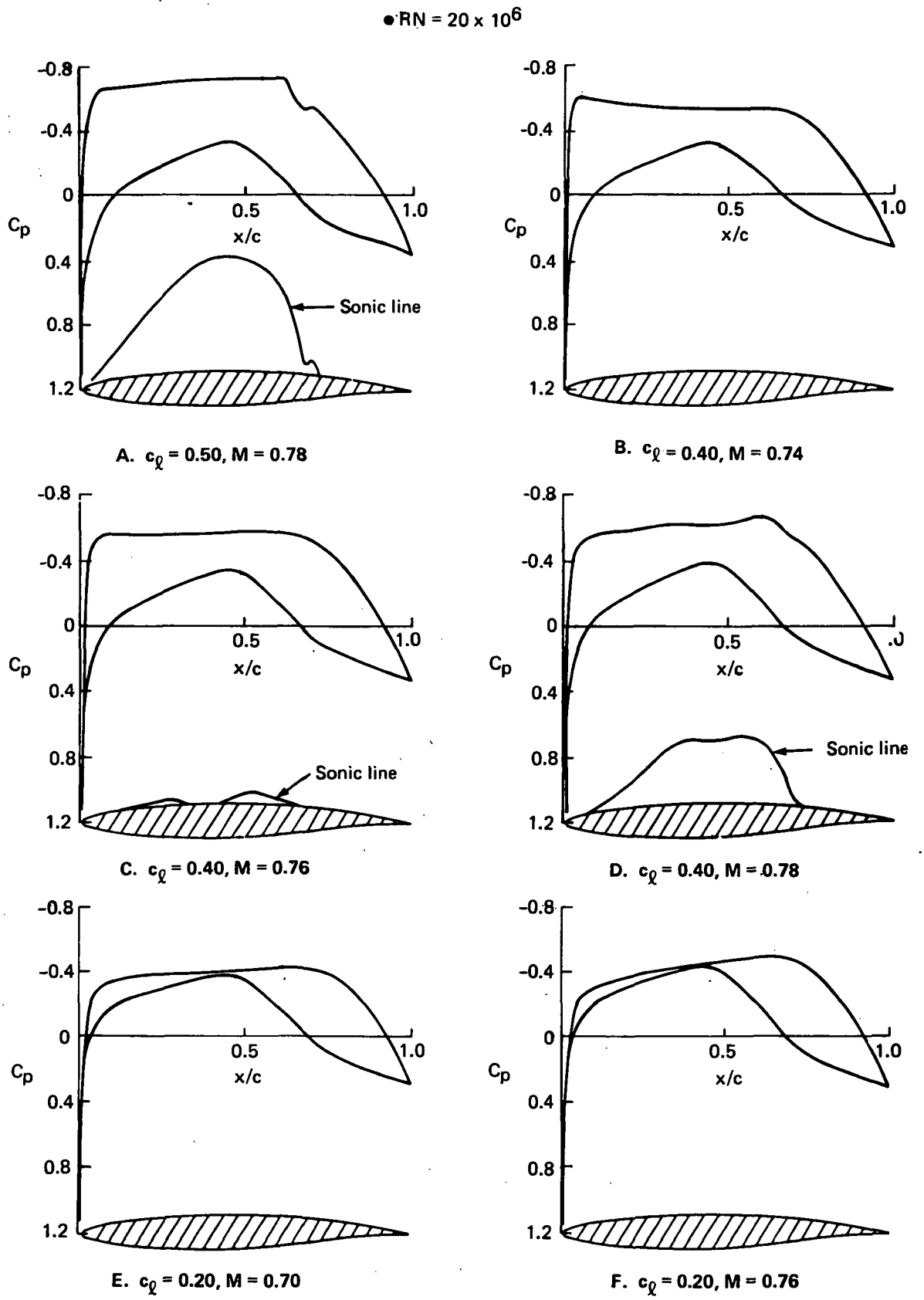

Figure 14. Airfoil 4 Pressure Distributions

4.2.3 Final Airfoil - Airfoil 5

The upper surface of Airfoil 4 was recontoured, resulting in Airfoil 5. The results of this process are shown in Figure 15. Airfoil 5 achieved a slightly more favorable pressure gradient than did Airfoil 4, with a slightly stronger shockwave. The maximum local Mach number for this airfoil was still less than the 1.20 initial criterion, so Airfoil 5 was selected as the final airfoil upon the basis of the more favorable pressure gradient.

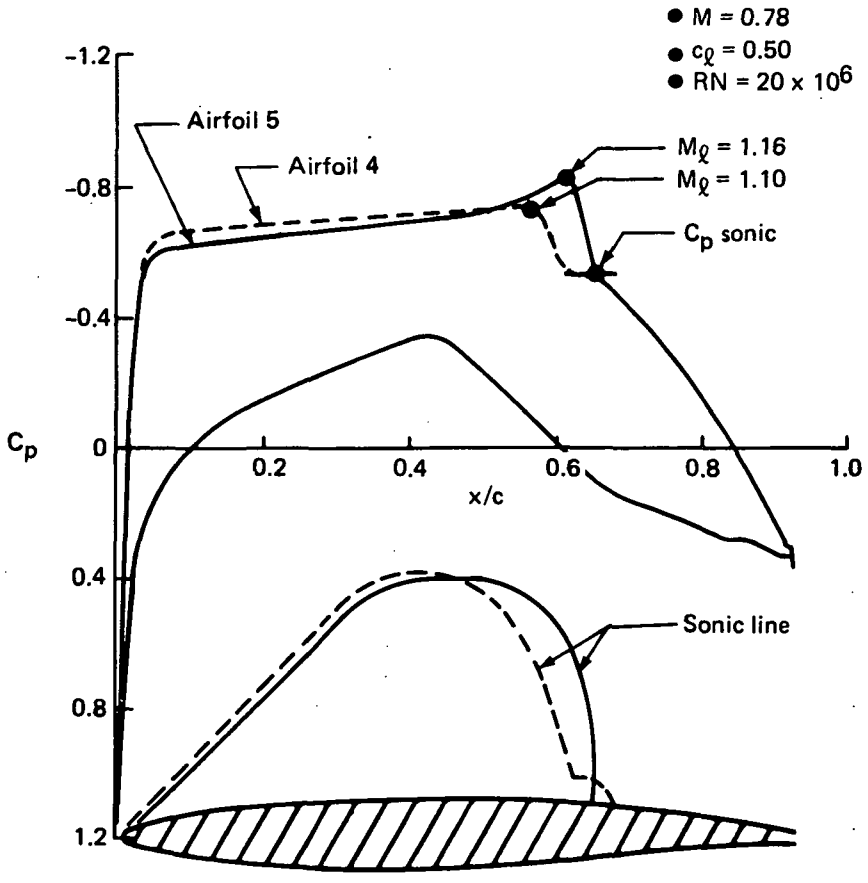

Figure 15. Pressure Distribution Comparison, Airfoils 4 and 5

The Airfoil 5 lift curve at 0.78M is shown in Figure 16. The application boundaries for Airfoil 5, Figure 17, are nearly the same as those for Airfoil 4, Figure 13, except that the shock strength criterion boundary (M shock<1.2) is encountered at slightly lower Mach numbers for Airfoil 5.

Geometric definition of Airfoil 5 is contained in Table 2.

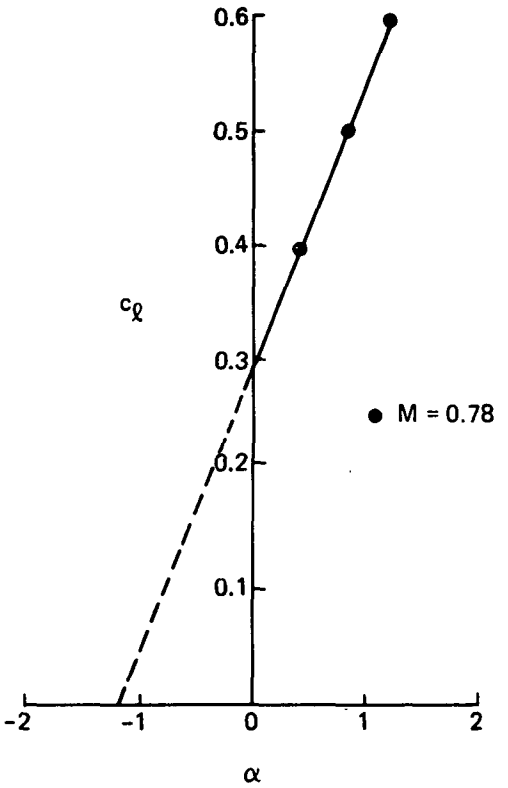

Figure 16. Airfoil 5 Lift Curve

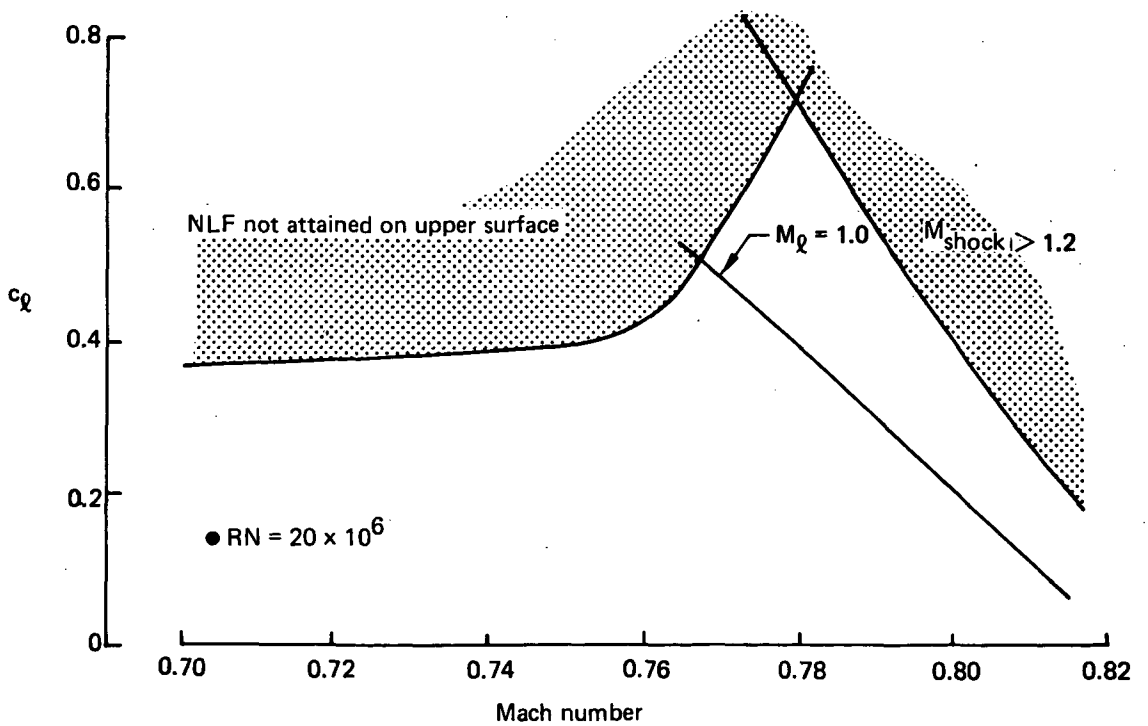

Figure 17. Airfoil 5 Application Boundaries

Table 2. Airfoil 5 Geometric Definition

Upper Surface

x/c	z/c	x/c	z/c	x/c	z/c
0.00010	0.002410	0.17121	0.041920	0.53886	0.056126
0.00080	0.004443	0.18584	0.043259	0.55738	0.055904
0.00231	0.006498	0.20091	0.044560	0.57576	0.055582
0.00441	0.008545	0.21642	0.045793	0.59393	0.055128
0.00719	0.010574	0.23232	0.046977	0.61202	0.054540
0.01067	0.012576	0.24861	0.048082	0.64761	0.052992
0.01485	0.014570	0.26524	0.049138	0.66516	0.052008
0.01973	0.016517	0.28221	0.050106	0.68256	0.050905
0.02531	0.018446	0.29948	0.051014	0.71681	0.048343
0.03159	0.020357	0.31703	0.051843	0.73351	0.046902
0.03855	0.022241	0.33483	0.052604	0.75006	0.045324
0.04619	0.024076	0.35286	0.053295	0.78208	0.041873
0.05450	0.025885	0.37109	0.053917	0.81261	0.038063
0.06347	0.027655	0.38948	0.054469	0.82725	0.036060
0.07309	0.029407	0.40801	0.054962	0.85522	0.031935
0.08334	0.031122	0.42664	0.055376	0.88141	0.027725
0.09419	0.032789	0.44533	0.055709	0.90556	0.023557
0.10565	0.034428	0.46406	0.055971	0.92746	0.019582
0.11767	0.036018	0.48280	0.056141	0.95562	0.014212
0.13027	0.037561	0.50153	0.056228	0.97094	0.011200
0.14340	0.039056	0.52023	0.056222	1.00000	0.005400
0.15706	0.040512				

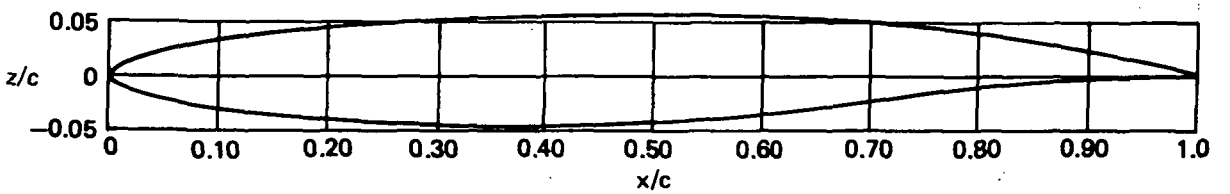

Lower Surface

x/c	z/c	x/c	z/c	x/c	z/c
0.00000	0.000000	0.10000	−0.028781	0.70000	−0.022603
0.00120	−0.003418	0.12000	−0.031347	0.74000	−0.017930
0.00200	−0.004381	0.14000	−0.033615	0.77000	−0.014833
0.00300	−0.005334	0.16000	−0.035637	0.80000	−0.011738
0.00500	−0.006725	0.19000	−0.038272	0.83000	−0.009066
0.00800	−0.008333	0.22000	−0.040503	0.85000	−0.007252
0.01200	−0.010079	0.26000	−0.042926	0.87000	−0.005726
0.01800	−0.012250	0.30000	−0.044762	0.89000	−0.004199
0.02400	−0.014133	0.35000	−0.046207	0.91000	−0.003054
0.03200	−0.016336	0.40000	−0.046621	0.93000	−0.002099
0.04000	−0.018294	0.45000	−0.045813	0.95000	−0.001241
0.05000	−0.020467	0.50000	−0.043518	0.97000	−0.000668
0.06000	−0.022422	0.55000	−0.039757	0.98000	−0.000477
0.07000	−0.024208	0.60000	−0.034778	0.99000	−0.000382
0.08000	−0.025846	0.65000	−0.028855	1.00000	−0.000382

4.3 AIRFOIL 5 BOUNDARY LAYER STABILITY ANALYSIS

The stability of the final airfoil boundary layer was analyzed by the method outlined in Paragraph 4.1, for the design conditions M = 0.78, c_ℓ = 0.50.

Boundary layer transition locations, thus determined, were found to be sensitive to changes of the selected value of amplification factor n and of RN. Some experimental determinations of the value of n have yielded results ranging from n = 10 (ref 9) to n = 14 (ref 10).

In this study, values of n = 12, 14, and 16 were considered. Figure 18 shows upper-surface transition locations. The curves represent the envelopes of a series of disturbance frequencies, as shown for RN = 30 x 10^6. The predicted transition location is quite sensitive to the value of n. As an example, for the case of RN = 20 x 10^6: if n = 12, transition is predicted at about x/c = 0.35. If n = 14, transition will occur between x/c = 0.50 and x/c = 0.60, while a value of n = 16 would presumably allow laminar flow back to x/c = 0.60, where transition would occur due to pressure gradient changes.

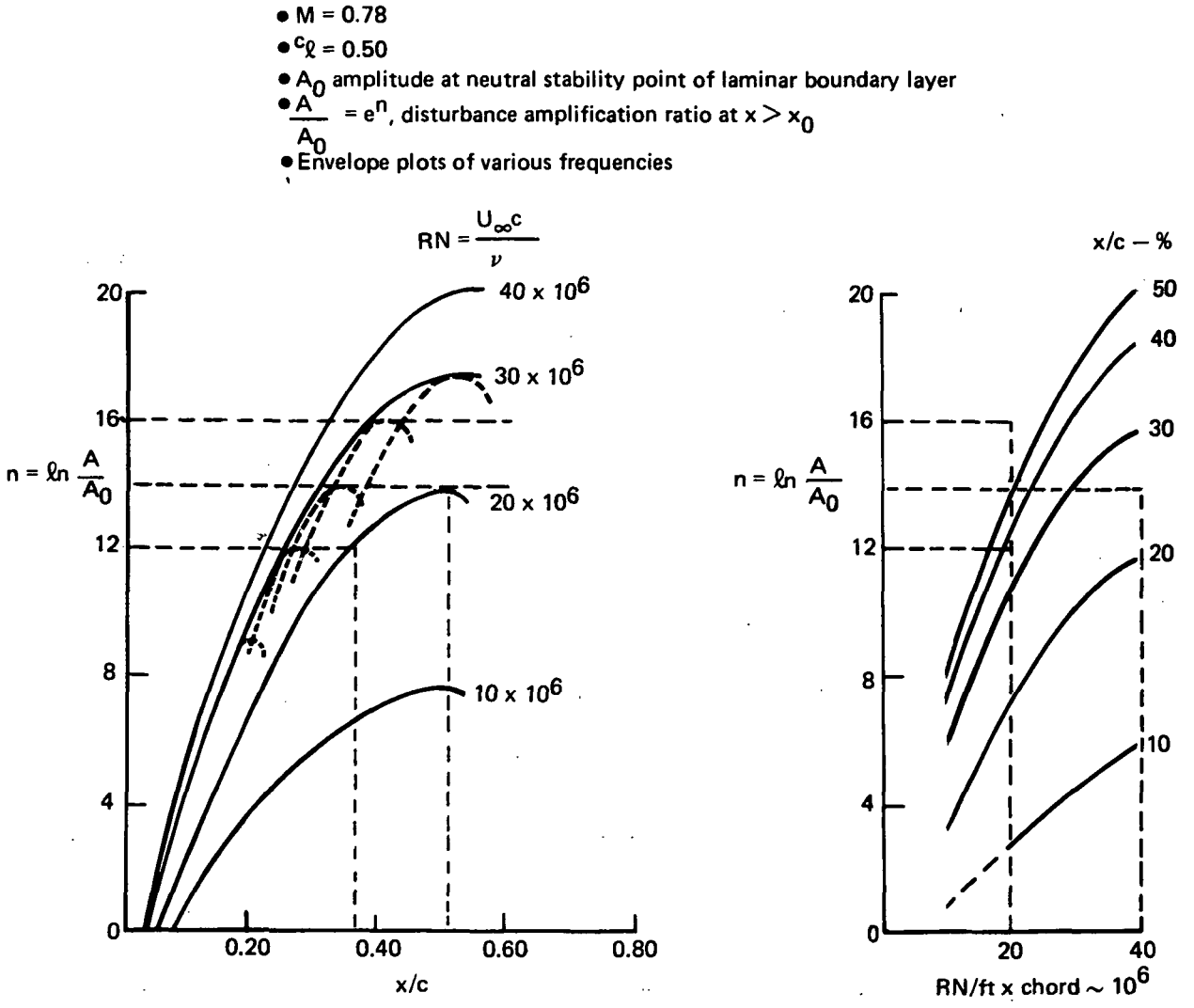

Figure 18. Airfoil 5 Upper Surface Boundary Layer Transition Prediction

The predicted upper-surface transition location also is quite sensitive to change in RN. For n = 14, changing the value of RN from 20 x 10^6 to 40 x 10^6 causes the predicted transition location to move forward from x/c = 0.50 to x/c = 0.32.

Lower-surface transition location is quite insensitive to variation in n, as shown in Figure 19. For n = 12, transition is predicted at x/c = 0.53.

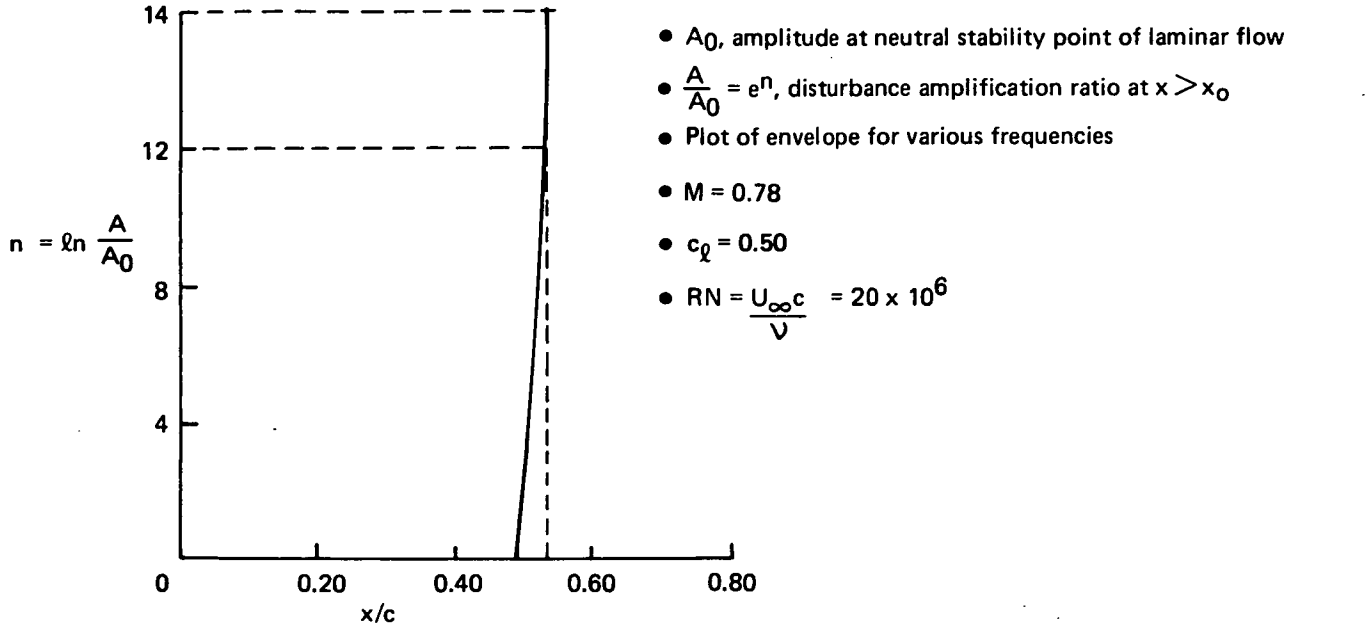

Figure 19. Airfoil 5 Lower Surface Boundary Layer Transition Prediction Disturbance

4.4 WING GEOMETRY SELECTION

When airfoil sections with pressure distributions characteristic of extensive natural laminar flow are used on a swept wing, significant spanwise pressure gradients occur and boundary layer crossflow develops. Crossflow velocity, that component of velocity within the boundary layer which is normal to the local velocity at the edge of the boundary layer, tends to increase as wing sweep increases. Boundary layer crossflow results in the development of crossflow vortices that, when amplified, cause transition. Therefore, wing sweep for an NLF airplane must be less than that for which crossflow vortices will cause transition.

Two pressure distributions are shown in Figure 20A. Type 1 has a large initial favorable pressure gradient but flattens out rapidly and has zero pressure gradient from about 5 to 60% chord. On a swept wing, this type of pressure distribution reduces the amplification of boundary layer crossflow vortices. However, the zero pressure gradient aft of 5% chord can permit rapid amplification (at representative flight Reynolds numbers) of Tollmien-Schlichting waves so that transition could occur well forward on the airfoil. The Type 2 pressure distribution represents an airfoil type that tends to damp amplification of the Tollmien-Schlichting waves. However, applied to a swept wing, it would result in extensive regions over which spanwise pressure gradient would occur, thus allowing continued amplification boundary layer crossflow vortices.

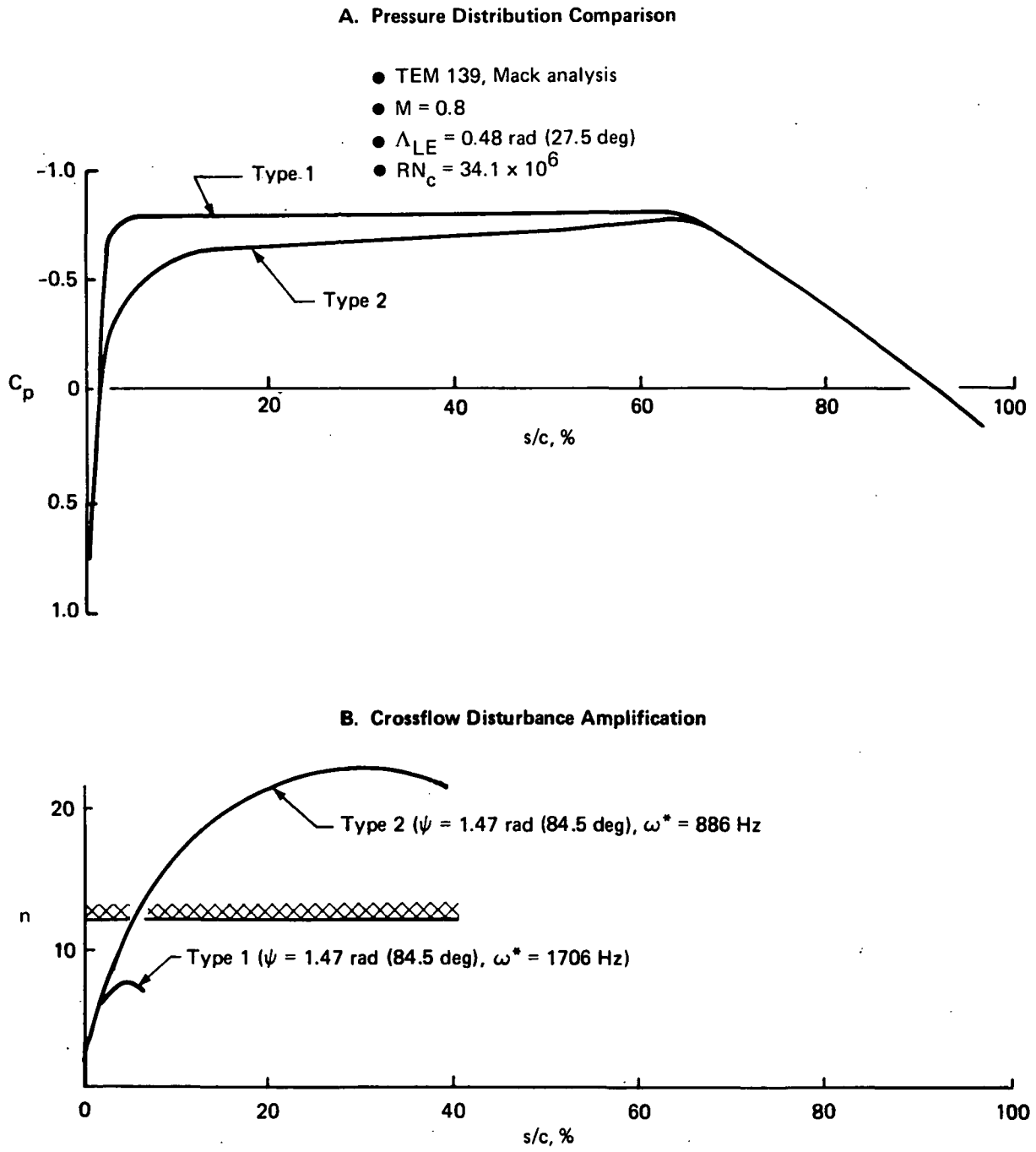

Figure 20. Effect of Pressure Distribution on Disturbance Amplification

Figure 20B shows the amplification of the most critical crossflow disturbance for each type, applied to a 0.48 rad (27.5 deg) sweptback wing, as computed by the MACK code (ref 7). For type 1, the maximum value of n is 7.5. Assuming transition to occur when n = 12, transition due to crossflow will not occur for this case. For type 2, the maximum value of n is 22, and transition occurs at about 5% chord. These results indicate that for airfoils with extensive regions of favorable pressure gradient, necessary for extensive natural laminar flow on an unswept wing, large sweep angles are unacceptable.

To determine the allowable sweep for an NLF airplane, the analysis and results of a sweep analysis performed as part of the Contractor's aerodynamic research program also were reviewed. Figure 21 presents the applicable results from this analysis and review. The pressure distribution (fig. 21A) is typical of those for NLF lower surfaces, the rear pressure rise starting at about 50% chord. Because the pressure gradient characteristic of either surface of an NLF airfoil, conclusions of the sweep analysis were assumed to apply for both upper and lower.

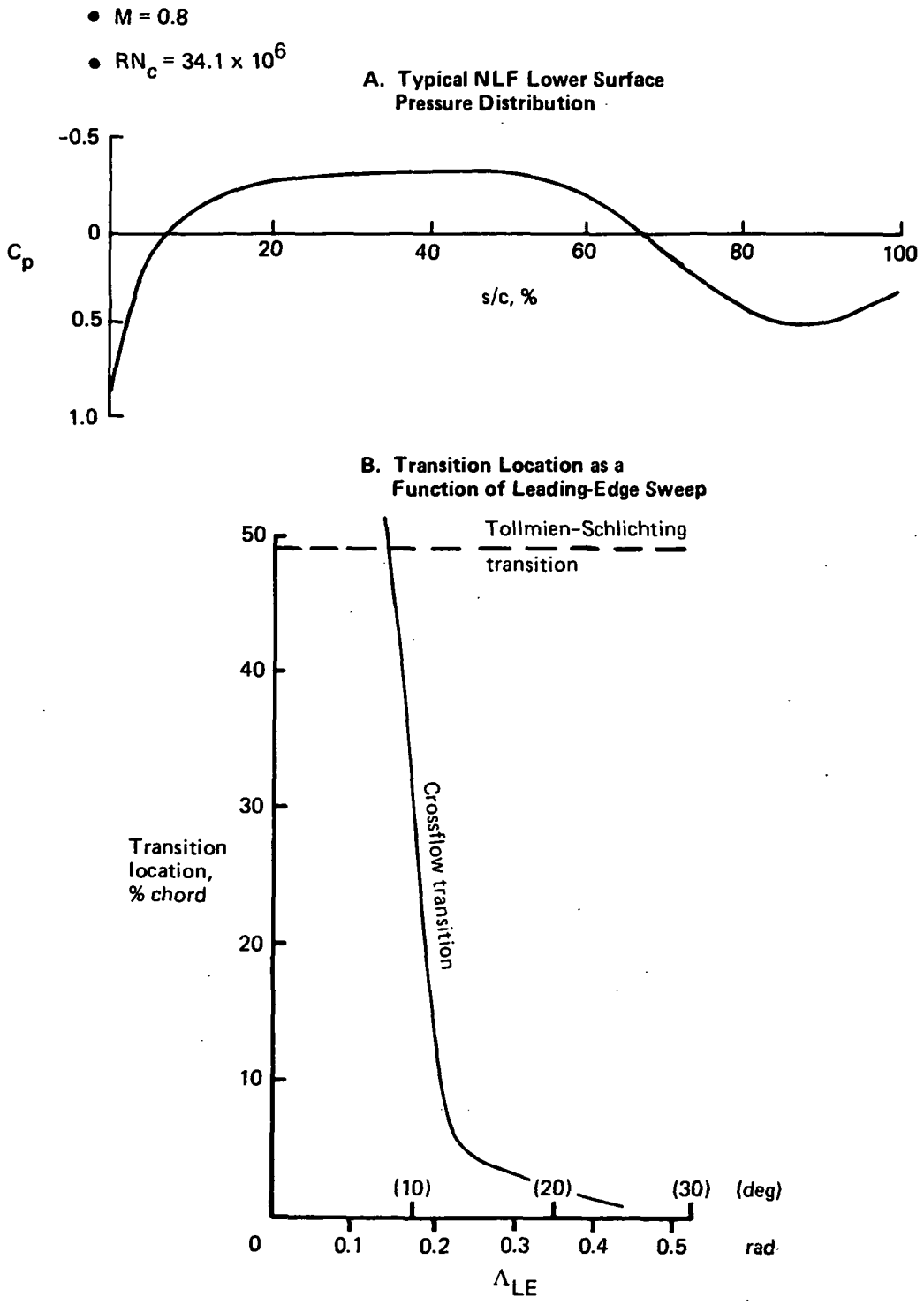

Figure 21. Effect of Sweep on Transition Location

Figure 21B shows transition location as a function of leading-edge sweep. The solid line shows transition due to crossflow disturbances, and the dashed line shows transition due to Tollmien-Schlichting disturbances. For sweep angles less than 0.122 rad (7 deg), transition occurs at about 49% chord and is of the Tollmien-Schlichting type. For sweep angles larger than 0.122 rad (7 deg), crossflow disturbances determine the transition location. At a sweep angle of 0.262 rad (15 deg) transition occurs at about 4% chord, and it moves forward at higher sweep angles. With an allowance for a small amount of slideslip during cruise, it was concluded that use of a leading-edge sweep angle no greater than 0.087 rad (5 deg) would result in a wing free from transition due to crossflow.

The results shown in Figure 21B were obtained using the same pressure distribution normal to the wing leading edge at all sweep angles for a constant freestream Mach number and Reynolds number. This assumes that the airfoil shape is different at each sweep angle. However, the optimum pressure distribution (i.e., the one resulting in the greatest extent of laminar flow) will vary with the sweep angle as the relative importance of Tollmien-Schlichting and crossflow disturbance changes. It is likely, therefore, that the indicated limitation on sweep could be improved if a different, more optimum, airfoil that attenuates the crossflow effect while maintaining a favorable pressure gradient were used for each sweep angle. It also should be recognized that Reynolds number has a very powerful effect on the crossflow-induced transition. Lower Reynolds numbers would delay to higher values the sweep angle at which crossflow disturbances cause transition.

Maximum thickness distribution versus span is illustrated in Figure 22. The wing thickness at the side-of-body is 11% chord, decreasing to 10.1% at 40% semispan and maintained at 10.1% to the wing tip. Normalized cruise spanload distribution is shown in Figure 23.

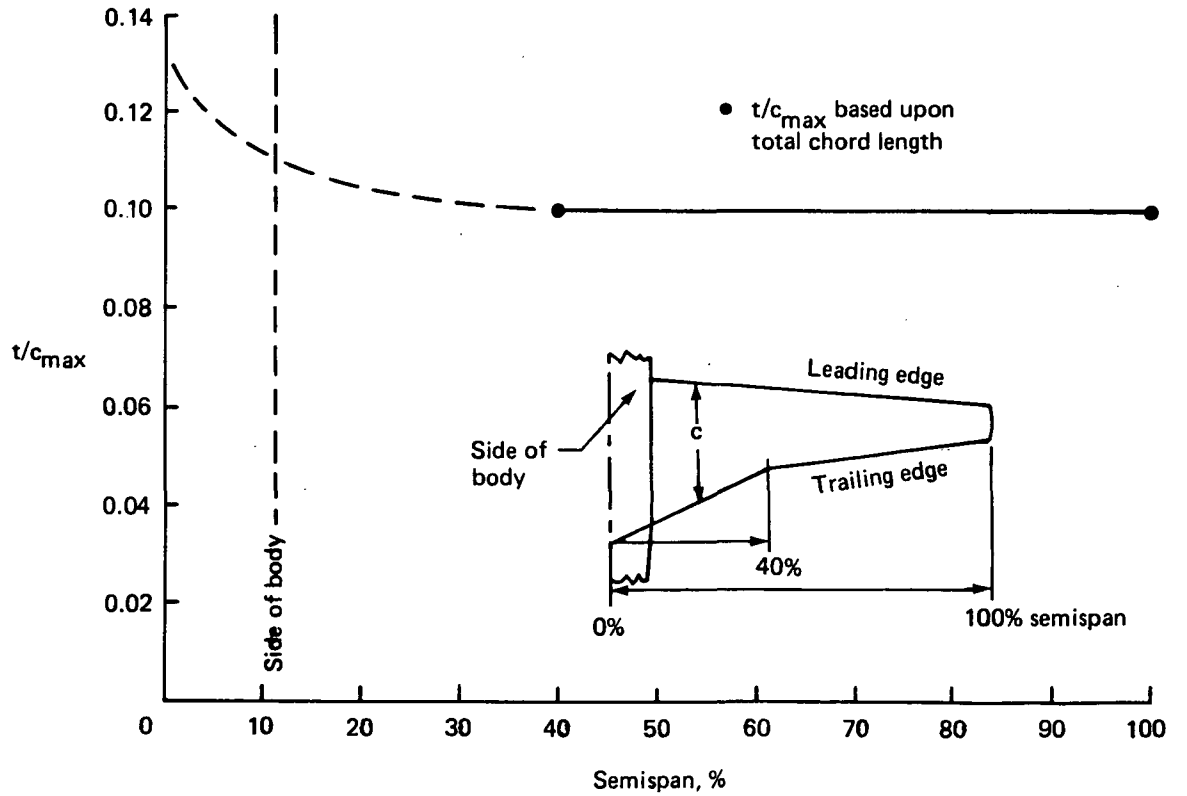

Figure 22. NLF Airplane Wing Spanwise t/c_{max} Distribution

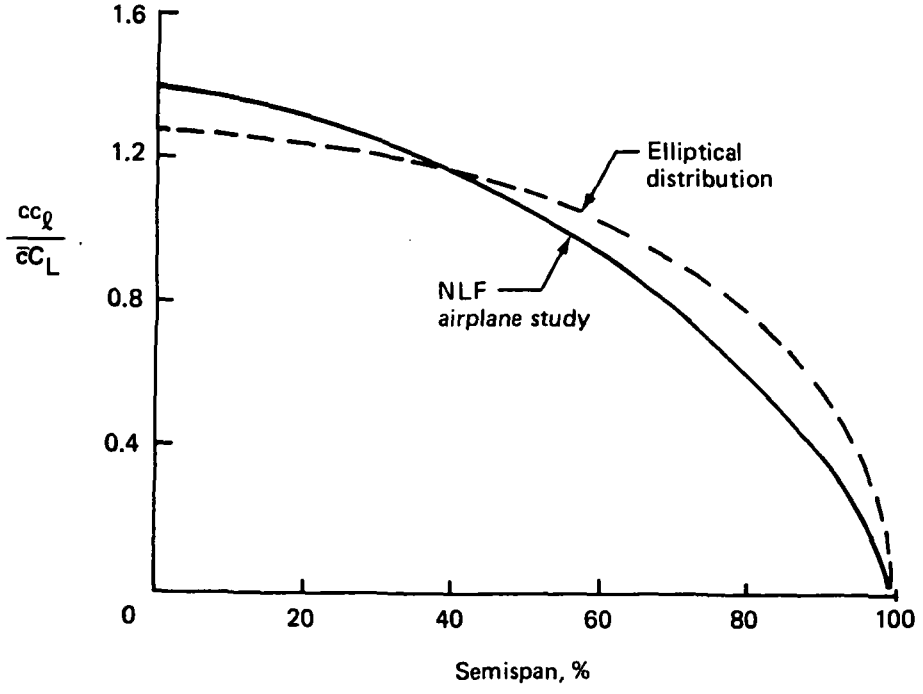

Figure 23. Cruise Spanload Distribution

5.0 AIRCRAFT DESIGN TRADE STUDY

Trade studies were conducted to determine if the NLF airfoil and wing selected during the design and analyses task would yield fuel savings and performance and economic benefits sufficient to warrant further development for large subsonic transport application.

5.1 TRADE STUDY METHODS

To assess the benefits of natural laminar flow, NLF airplanes were developed and their performance compared to that of a turbulent reference airplane. The trade study method and sequence is shown in Figure 24.

The configuration characteristics for the items listed in Step 1 (fig. 24) were selected from results of previous related research. A detailed configuration drawing of the initial turbulent reference airplane was developed from sketches; studies of weight and balance, stability and control, and aerodynamics; and layout drawings.

The THUMBPRINT parametric performance analysis program (Steps 2 and 3) computes the gross weight, block fuel, wing and tail areas, and thrust required to perform the design mission. A mission-sized airplane is selected in Step 4 and, when compared to study objectives, is accepted or the process is reiterated.

5.2 TRADE STUDY AIRPLANES

5.2.1 Turbulent Reference Airplane Configuration

A turbulent reference airplane was selected as the basis of comparison for the NLF airplane configuration studies. It is a wide-bodied, twin-engine airplane designed to carry 196 passengers in seven-abreast seating over a still air range of 3704 km (2000 nmi). The general arrangement of the reference airplane is shown in Figure 25 and its principal characteristics are listed in Table 3.

The airplane study process to compare turbulent and NLF designs involved comparison of initial designs that were similar except for those characteristics impacted by turbulent or NLF requirements. This approach is discussed in Paragraphs 5.2.1, 5.2.2, and 5.2.3 where basic internal design features and trapezoidal wing area were held constant. Paragraph 5.3 continues with the scaling process to mission-sized airplanes.

A 5.38-m (212-in) fuselage diameter was selected, permitting double aisle economy and six-abreast first class seating. An arrangement of first class seats at 0.97-m (38-in) pitch and economy seats at 0.86-m (34-in) pitch, assuming a 15%/85% mix, permits the 35.66-m (1404-in) cabin length to accommodate 196 passengers. A total of 17 LD3 containers can be carried in the lower lobe. The wing has an aspect ratio of 10.24 and is swept 0.52 rad (30 deg). It incorporates a Boeing-developed transonic airfoil section and tapers in thickness ratio from 0.15 (gross chord) at side-of-body to 0.103 at the tip. The dihedral angle is 0.13 rad (7.5 deg). Variable-camber, Krueger leading-edge flaps and double-slotted Fowler-type trailing-edge flaps are incorporated.

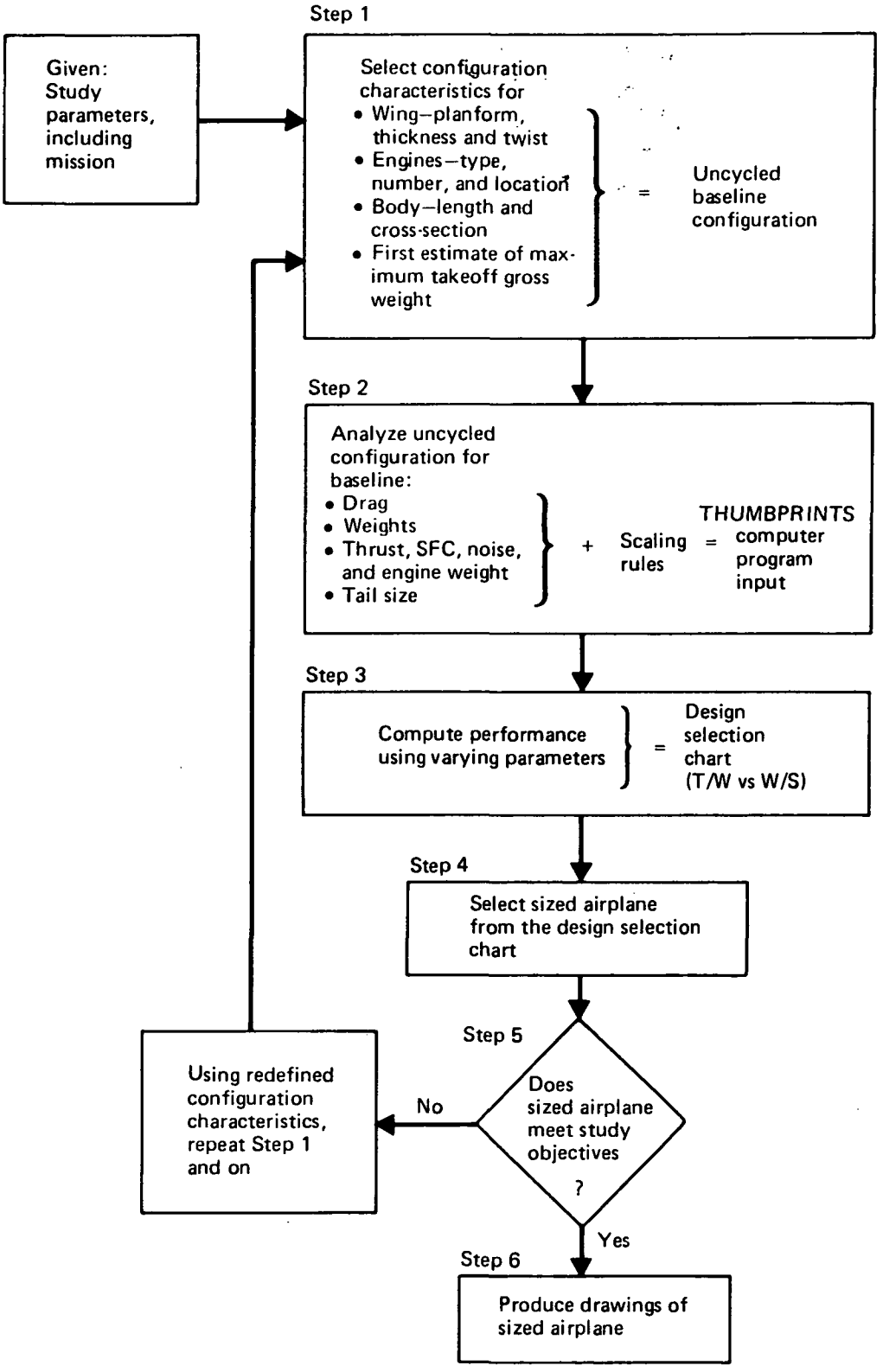

Figure 24. Design Development Method and Sequence

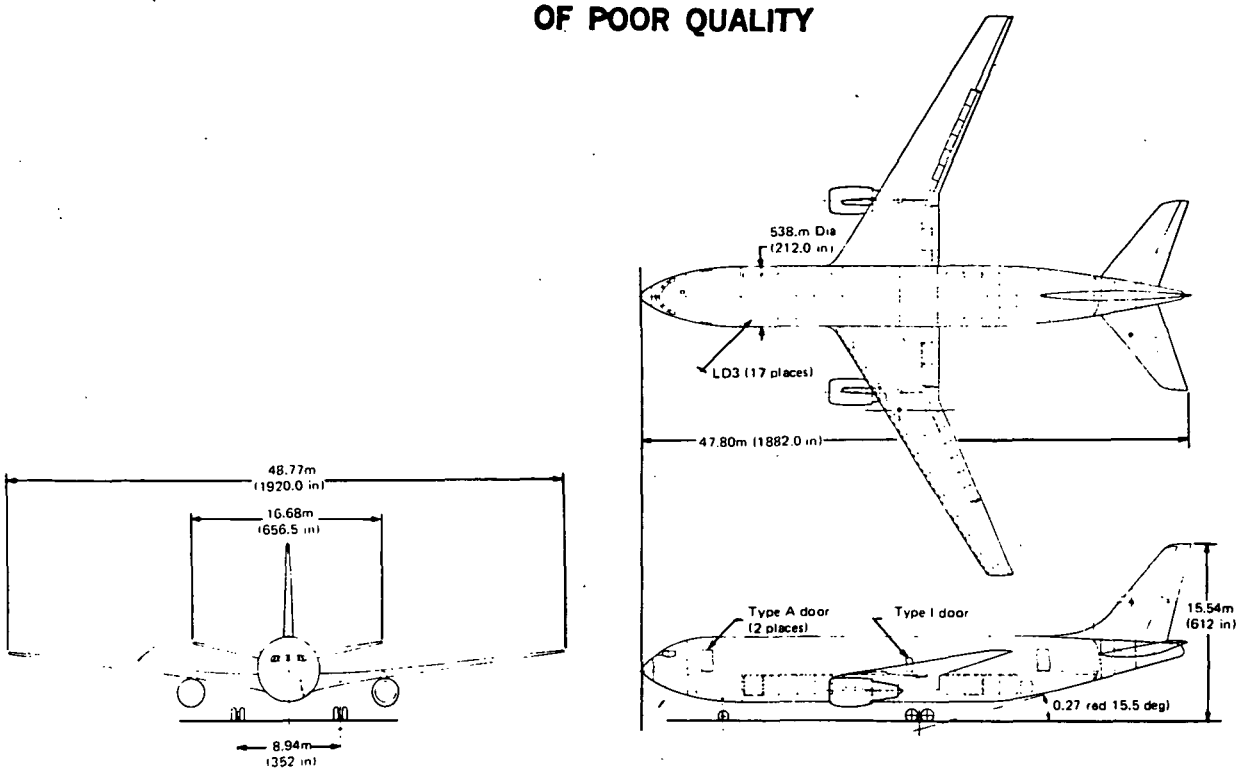

Figure 25. Reference Turbulent Airplane General Arrangement

Table 3. Reference Airplane Principal Characteristics

Surface	Wing	Horizontal tail	Vertical tail
Area, m^2 (ft^2)	232.26 (2500.0)	69.49 (748.00)	41.25 (444.00)
Aspect ratio	10.24	4.0	1.8
Taper ratio	0.3158	0.35	0.30
Sweep—c/4, rad (deg)	0.52 (30.0)	0.61 (35.00)	0.61 (35.00)
Dihedral, rad (deg)	0.13 (7.5)	0.12 (7.00)	–
t/c (root/tip), % gross chord	15/10.3	11/19	11.5/8.5
MAC, m (in)	5.19 (204.4)	4.49 (176.81)	5.25 (206.68)
Span, m (in)	48.77 (1920.0)	16.68 (656.50)	8.62 (339.24)
Tail arm, m (in)	–	20.29 (799.00)	20.32 (800.00)
Tail volume coefficient	–	1.171	0.074
Body			
Length, m (in)	47.55 (1872)		
Diameter, m (in)	5.38 (212)		
Power plants			
Number	2		
SLST, kN (lb)	169.03 (38 000)		
Landing gear			
Nose—number, tire size	(2) 37 x 14		
Main—number, tire size	(8) 49 x 19		

Note: Planform characteristics refer to basic trapezoidal shape.

The all-flying horizontal tail with segmented geared elevators is conventionally mounted on the aft fuselage. It is swept 0.61 rad (35 deg), has a dihedral angle of 0.12 rad (7 deg), and tapers in thickness ratio from 0.11 to the root to 0.09 to the tip.

The vertical tail has an aspect ratio of 1.8 and is swept 0.61 rad (35 deg). It incorporates a double-hinged rudder and tapers in thickness ratio from 11.5% at the root to 8.5% at the tip. It incorporates a double-hinged rudder and tapers in thickness ratio from 11.5% at the root to 8.5% at the tip.

The power plants are two scaled CF6-50C turbofans mounted on underwing struts located at approximately 35% semispan. The main landing gear consists of a pair of conventionally arranged four-wheeled trucks located at 57.9% MAC.

5.2.2 NLF Airplane Configurations

NLF airplane configurations were derived from the turbulent reference configuration by introducing those changes necessary to make extensive laminar flow possible. The principal changes were unsweeping the wing and relocating the engines to the aft fuselage. Engine relocation required reconfiguring the horizontal and vertical tail.

General arrangements of the two reference NLF airplanes define in this study, models NLF-AR10.24 and NLF-AR12, are shown in FIgure 26 and 27. Their principal characteristics are listed in Tables 4 and 5. These models share a common fuselage configuration. The cockpit and cabin are identical to the turbulent reference airplane. The aft fuselage was lengthened and refaired to accommodate the aft engine installation and a larger vertical fin of lower aspect ratio.

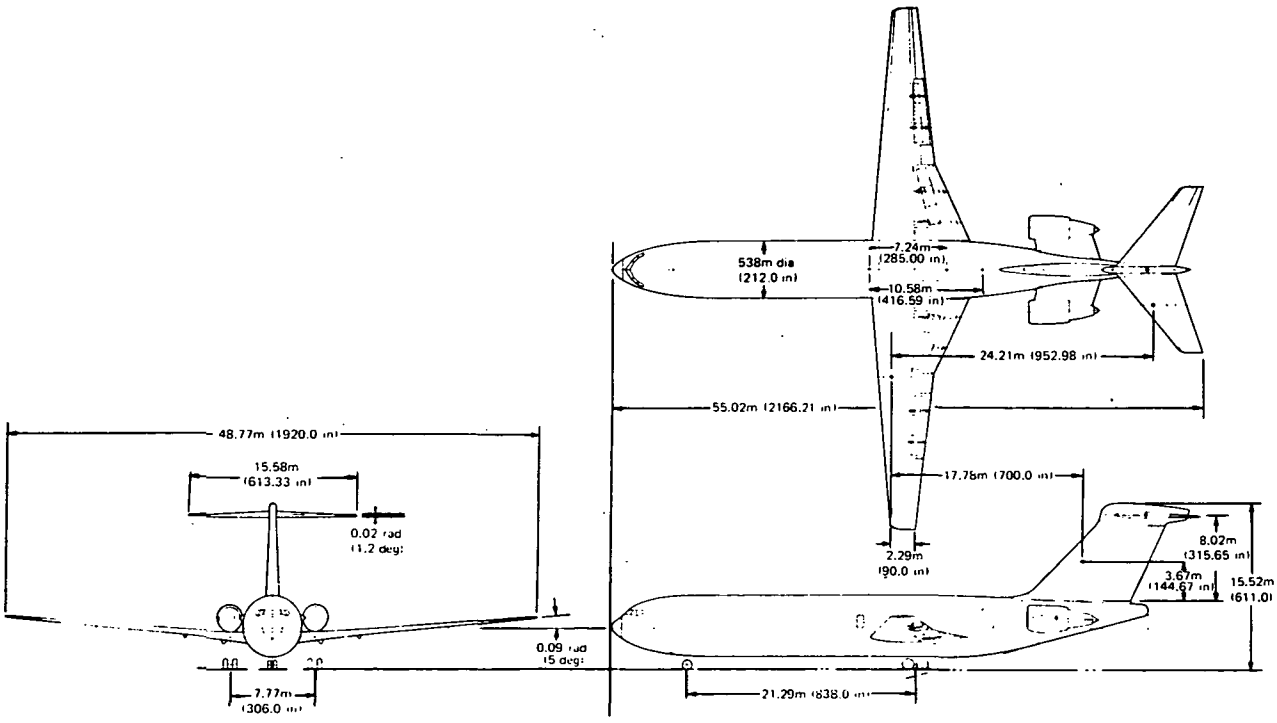

Figure 26. Reference NLF-AR10.24 Airplane General Arrangement

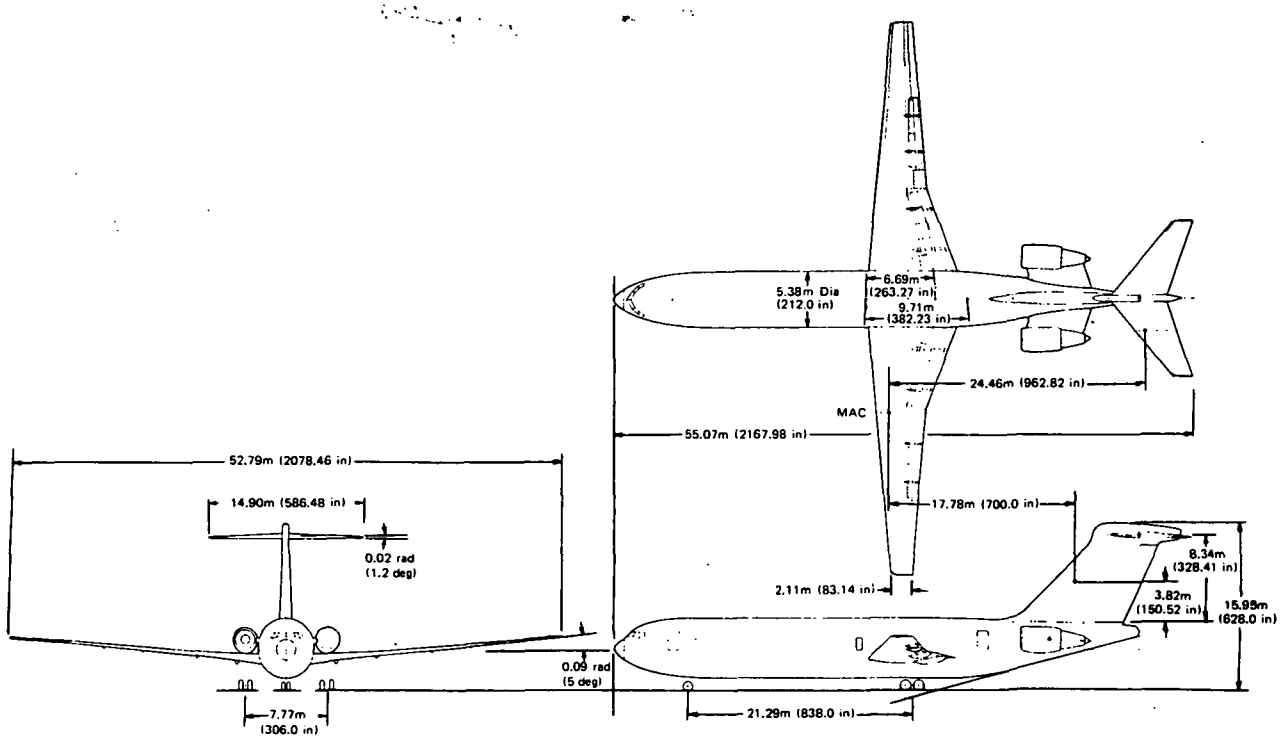

Figure 27. Reference NLF-AR12 Airplane General Arrangement

Table 4. Reference NLF-AR10.24 Airplane Principal Characteristics

Surface	Wing	Horizontal tail	Vertical tail
Area, m^2 (ft^2)	232.26 (2500.000)	60.670 (653.09)	64.28 (691.89)
Aspect ratio	10.24	4.0	1.0
Taper ratio	0.3158	0.35	0.6
Sweep—c/4, rad (deg)	0.037 (2.102)	0.610 (35.00)	0.70 (40.00)
Dihedral, rad (deg)	0.087 (5.000)	-0.020 (-1.20)	–
t/c (root/tip), % gross chord	11/10	11/19	12
MAC, m (in)	5.19 (204.400)	4.200 (165.18)	8.18 (322.22)
Span, m (in)	48.77 (1920.000)	15.580 (613.33)	8.67 (341.32)
Tail arm, m (in)	–	24.210 (952.98)	17.78 (700.00)
Tail volume coefficient	–	1.218	0.1009
Body			
Length, m (in)	50.01 (1969)		
Diameter, m (in)	5.38 (212)		
Power plants			
Number	2		
SLST, kN (lb)	169.03 (38 000)		
Landing gear			
Nose—number, tire size	(2) 38 x 11		
Main—number, tire size	(8) 44 x 16		

Note: Planform characteristics refer to basic trapezoidal shape.

Table 5. Reference NLF-AR12 Airplane Principal Characteristics

Surface	Wing	Horizontal tail	Vertical tail
Area, m^2 (ft^2)	232.26 (2500.0)	55.48 (597.15)	69.58 (748.99)
Aspect ratio	12.0	4.0	1.0
Taper ratio	0.3158	0.35	0.6
Sweep—c/4, rad (deg)	0.04 (2.53)	0.61 (35)	0.70 (40)
Dihedral, rad (deg)	0.087 (5)	-0.02 (-1.2)	–
t/c (root/tip), % gross chord	11/10	11/9	12
MAC, m (in)	4.80 (188.82)	4.01 (157.95)	8.52 (335.26)
Span, m (in)	52.79 (2078.46)	14.90 (586.48)	8.34 (328.41)
Tail arm, m (in)	–	24.46 (962.82)	17.78 (700.0)
Tail volume coefficient	–	1.218	0.1009
Body			
Length, m (in)	50.01 (1969)		
Diameter, m (in)	5.38 (212)		
Power plants			
Number	2		
SLST, kN (lb)	169.03 (38 000)		
Landing gear			
Nose—number, tire size	(2) 38 x 11		
Main—number, tire size	(8) 44 x 16		

Note: Planform characteristics refer to basic trapezoidal shape

Initially, the wing area of the two NLF airplanes was maintained at 232.3 m^2 (2500 ft^2) to match the turbulent reference airplane. Model NLF-AR10.24 has the same aspect ratio as the reference airplane, while model NLF-AR12 has an aspect ratio of 12.0. To make extensive natural laminar flow possible, the leading-edge sweep must be limited to a small angle. A 0.087 rad (5 deg) leading-edge sweep was chosen for both models. To obtain the desired extent of laminar flow at the design conditions (M = 0.78, C_L=0.5), it was necessary to limit wing thickness ratios to 10.1% chord. Inboard of $\eta = 0.4$, the wing was increased in thickness ratio to 11% at side-of-body (fig. 22). To increase the structural depth at the side of body, the wing trailing edge was extended inboard of $\eta = 0.4$. The inboard lift distribution was tailored to decrease life coefficient in this region, permitting laminar flow to exist over a significant percent of chord. At the side-of-body, the wing thickness is 15% of the basic trapezoidal chord. The assumed cruise span load distribution is shown in the same figure.

High-lift devices consist of large chord, double-slotted, trailing-edge flaps. Leading-edge devices are not fitted because they disrupt the smooth surface required for natural laminar flow. Conventional low- and high-speed ailerons and flight ground spoilers are included.

The horizontal tail is an all-flying surface with geared elevators, located at the top of the vertical fin. Because this surface is affected by the noise field of the engines, it was assumed to have turbulent flow. It retains the planform features of the reference airplane tail, including the 0.61-rad (35-deg) sweep angle. The tail also retains the turbulent airplane's thickness distribution.

The vertical fin is substantially larger in area than that of the turbulent reference airplane, its aspect ratio is reduced and taper ratio increased to provide for adequate mounting of the horizontal tail. It has a constant 0.12 thickness ratio. As on the turbulent reference airplane, the rudder is double-hinged.

The power plants are two scaled CF6-50C engines supported on struts from the aft fuselage.

5.2.3 NLF Wing Structure Design and Analysis

The turbulent reference airplane was assumed to have a wing of conventional construction, with structural characteristics typical of modern wings of similar sweep. Because the turbulent reference airplane was defined for performance comparison purposes, its structural definition and analysis was not considered necessary for this study. The model NLF-AR10.24 and NLF-AR12 wings were compared, instead, to a current production airplane, the Boeing 727.

The structural arrangement of the NLF wing is shown in Figure 28. Bonded aluminum-honeycomb wing box construction was selected for its excellent smoothness and fidelity to contour. Minimum spar web thickness is 1.60 mm (0.063 in). Allowable stresses for the NLF wing are listed in Table 6. These allowable stresses are based upon current 2024 and 7075 alloy allowables, adjusted to account for future material improvement and for fatigue effects not otherwise included in the wing analysis program.

Wing and fuel spanwise deadweight distribution and wing aerodynamic coefficients were calculated and lift curve slopes were corrected for speeds greater than the critical Mach number. Aerodynamic panels analyzed are shown in Figures 29 and 30 with resultant wing stiffness shown in Figures 31 and 32.

Table 6. NLF Wing Structure Material/Allowables

	Allowable stress	
	kPa	(lb/in^2)
Spar shear	233 044	(33 800)
Upper surface tension	434 372	(63 000)
Lower surface tension	365 424	(53 000)
Upper surface shear	232 355	(33 700)
Lower surface shear	196 502	(28 500)
Upper surface compression	434 372	(63 000)
Lower surface compression	253 729	(36 800)
	Gage	
	mm	(in)
Minimum skin gage	2.03	(0.080)
Minimum spar gage	1.60	(0.063)

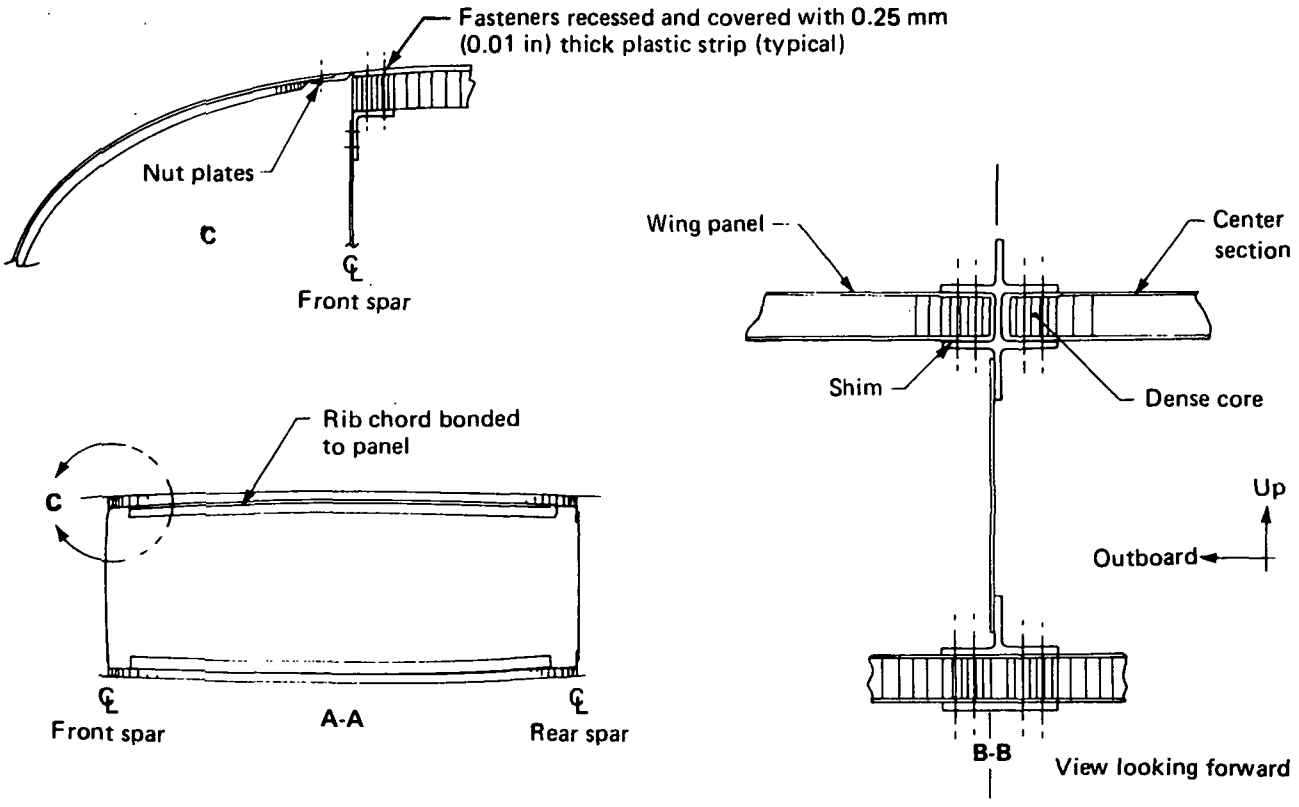

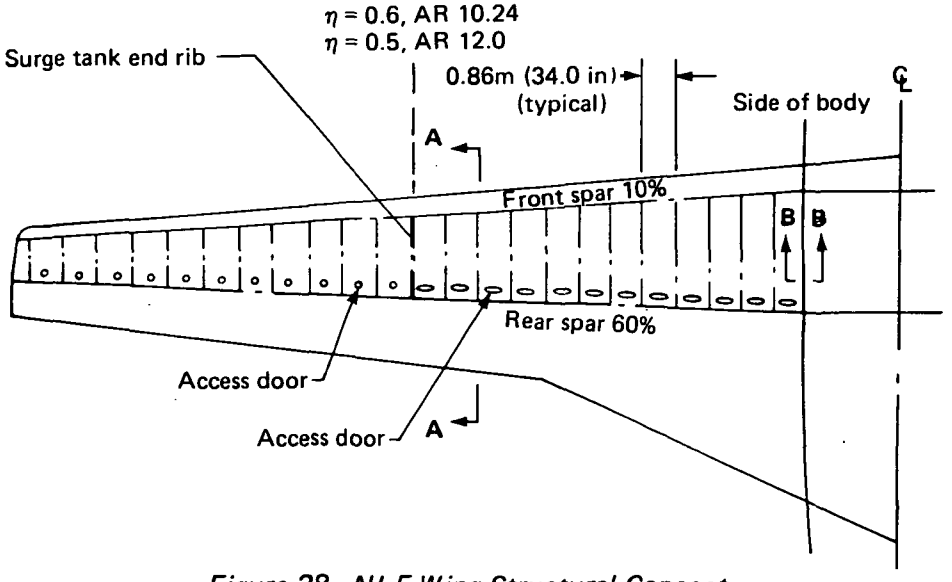

Figure 28. NLF Wing Structural Concept

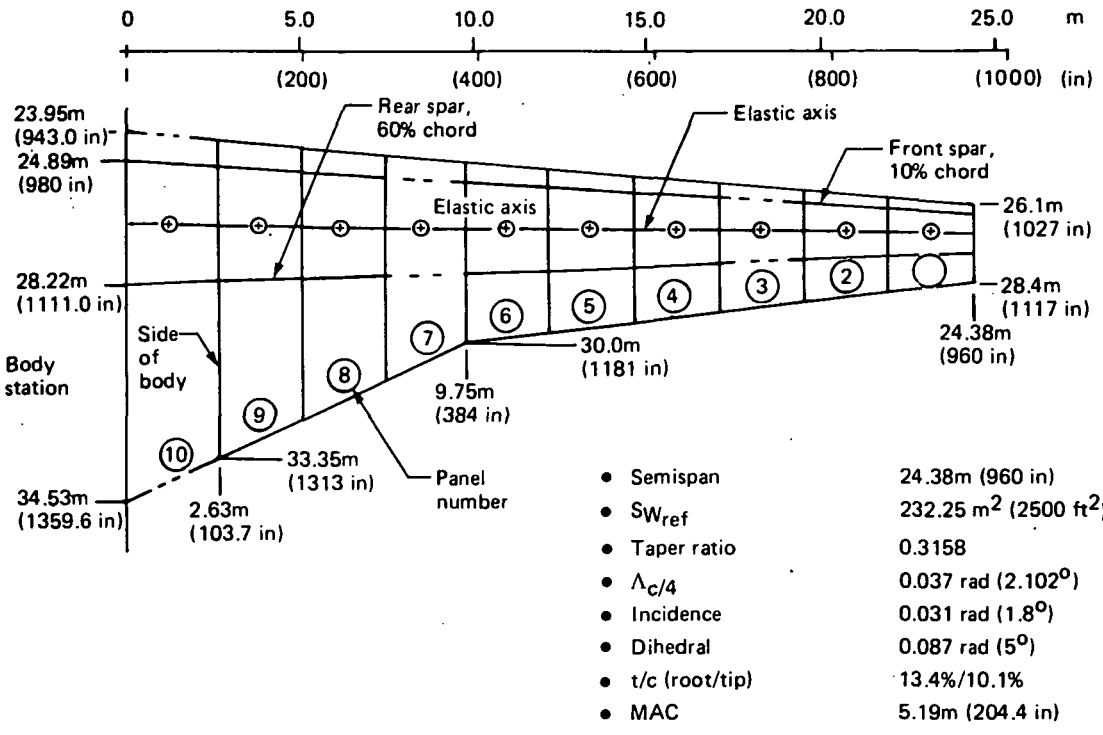

Figure 29. NLF-AR10.24 Wing Aerodynamic Panels

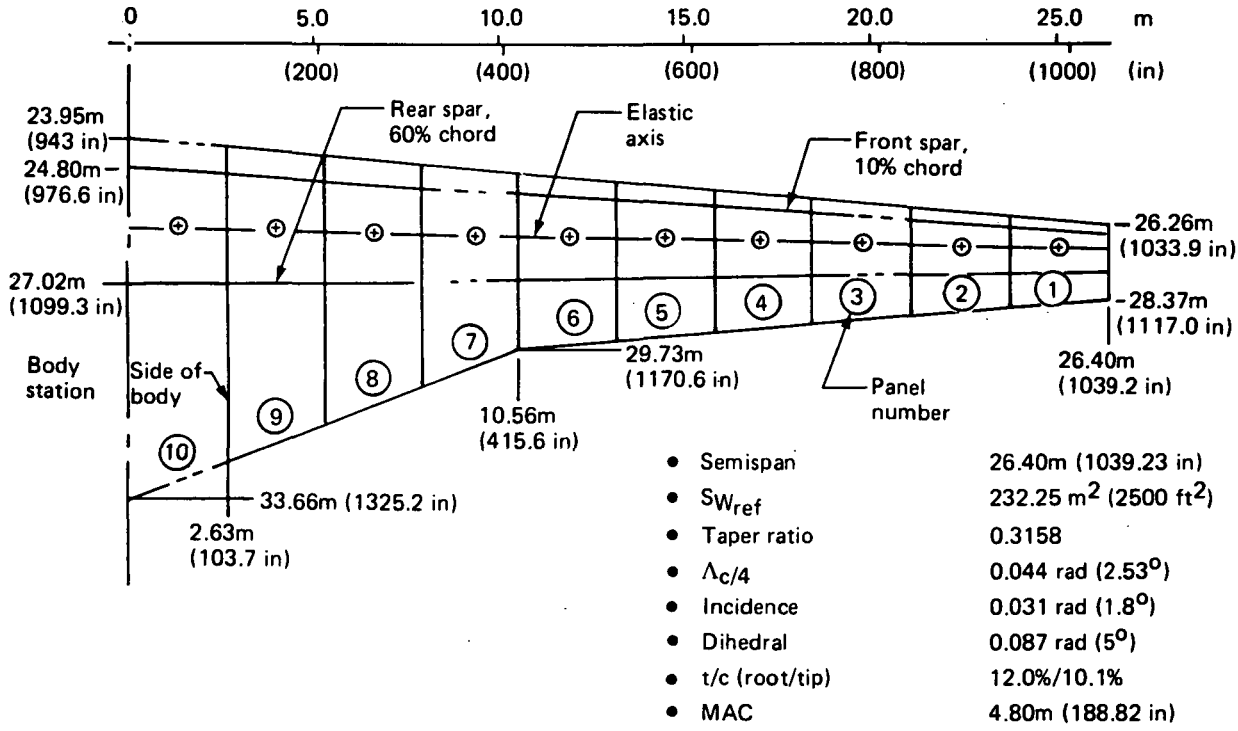

Figure 30. NLF-AR12 Wing Aerodynamic Panels

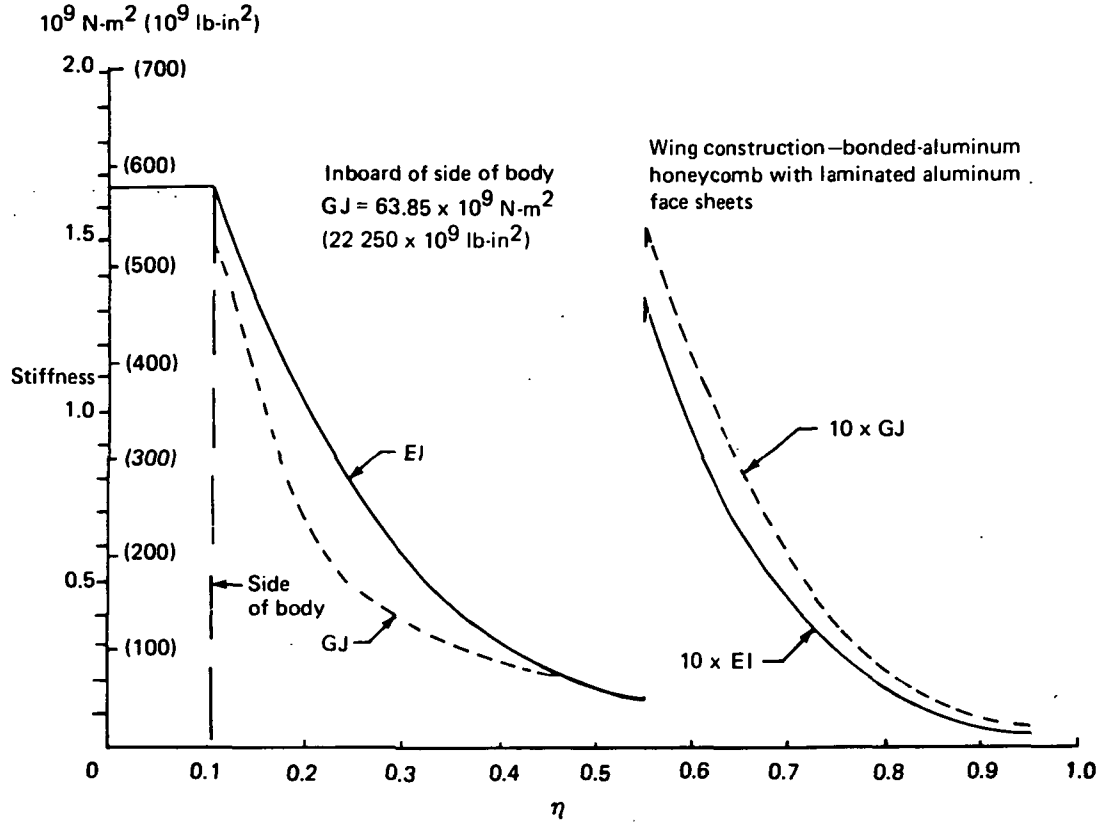

Figure 31. Wing Stiffness Distribution, Aspect Ratio 10.24

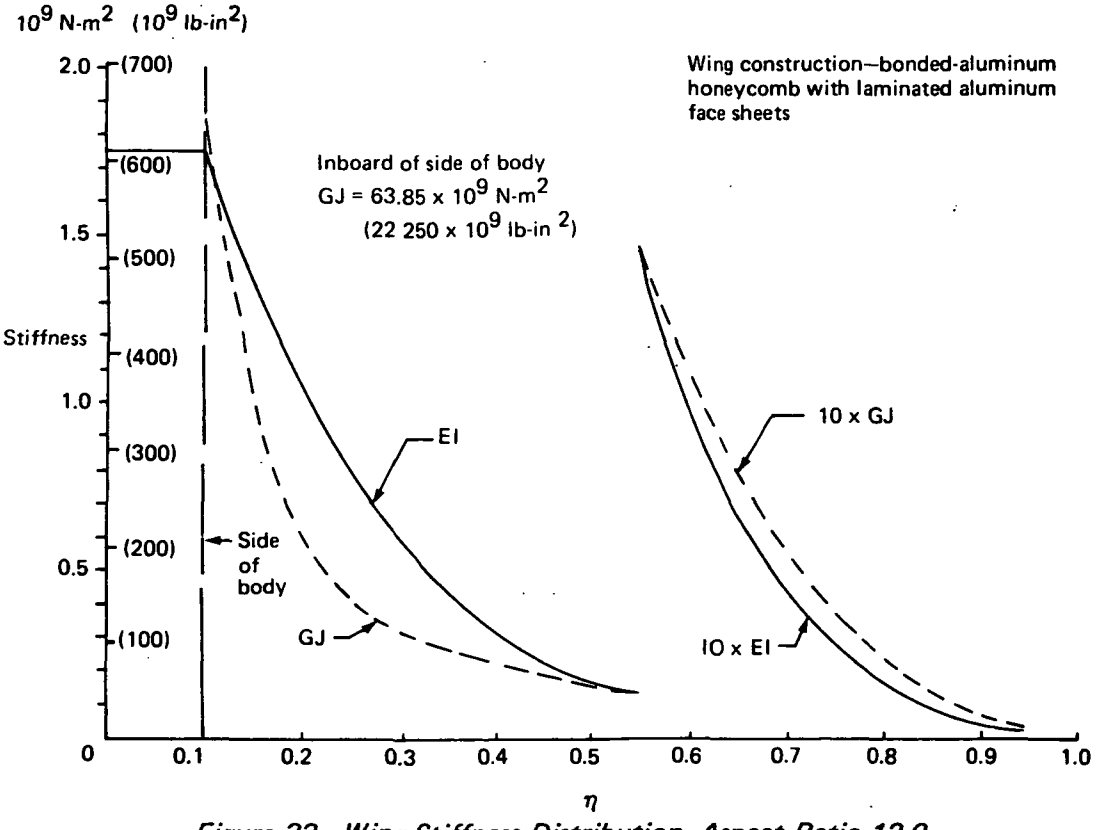

Figure 32. Wing Stiffness Distribution, Aspect Ratio 12.0

The NLF wing upper and lower surfaces consist of honeycomb sandwich construction. The inner and outer skins of each sandwich are the same thickness. Each skin consists of two, three, or four laminae, depending on location as illustrated by Figure 33. The thickness of each laminae varies as a function of load, but has a minimum thickness of 0.51 mm (0.02 in).

Figure 34 displays tail-off lift curve slopes, showing the effects of aspect ratio, sweep, and wing flexibility. The higher aspect ratios of the NLF wings produce steeper lift curve slopes throughout the Mach number range, which tends to make such wings more gust-critical. Wing twist due to wing bending increases the lift curve slope of the unswept NLF wings, while decreasing that slope for the 0.56-rad (32-deg) swept 727 wing.

The negligible sweep of the NLF wings implies a critical Mach number lower than that of the 727. Figure 35 provides a comparison of structural design airspeeds.

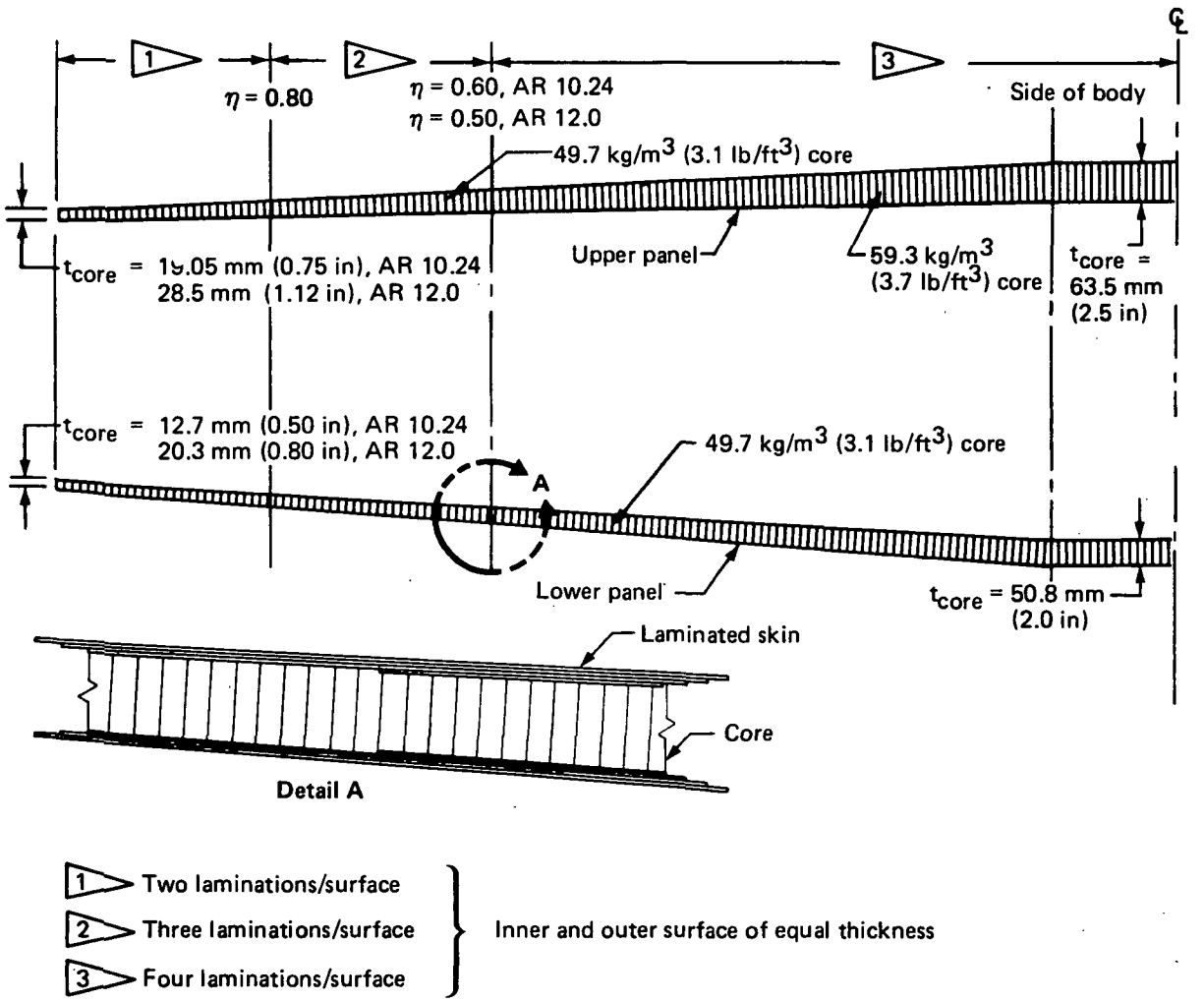

Figure 33. Wing-Box Skin Panel

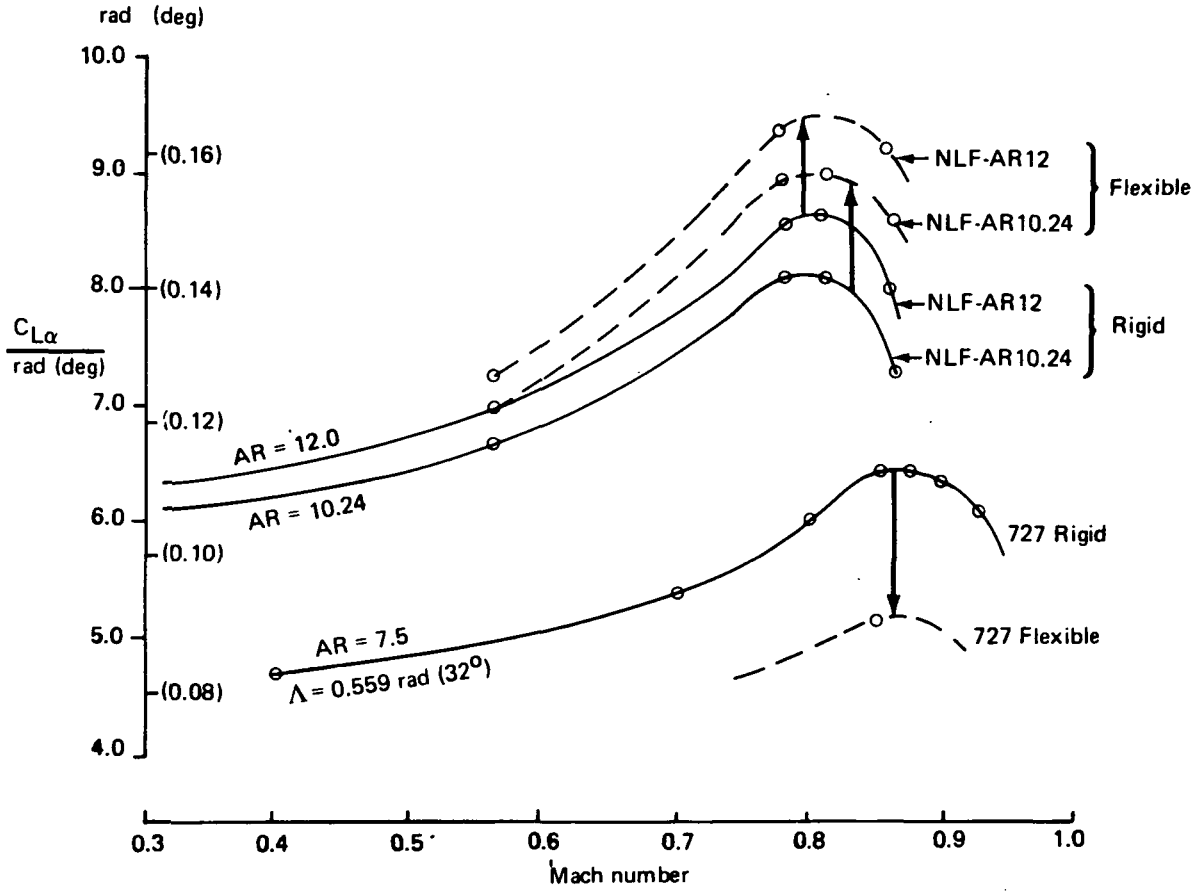

Figure 34. Tail-Off Lift Curve Slope Comparison

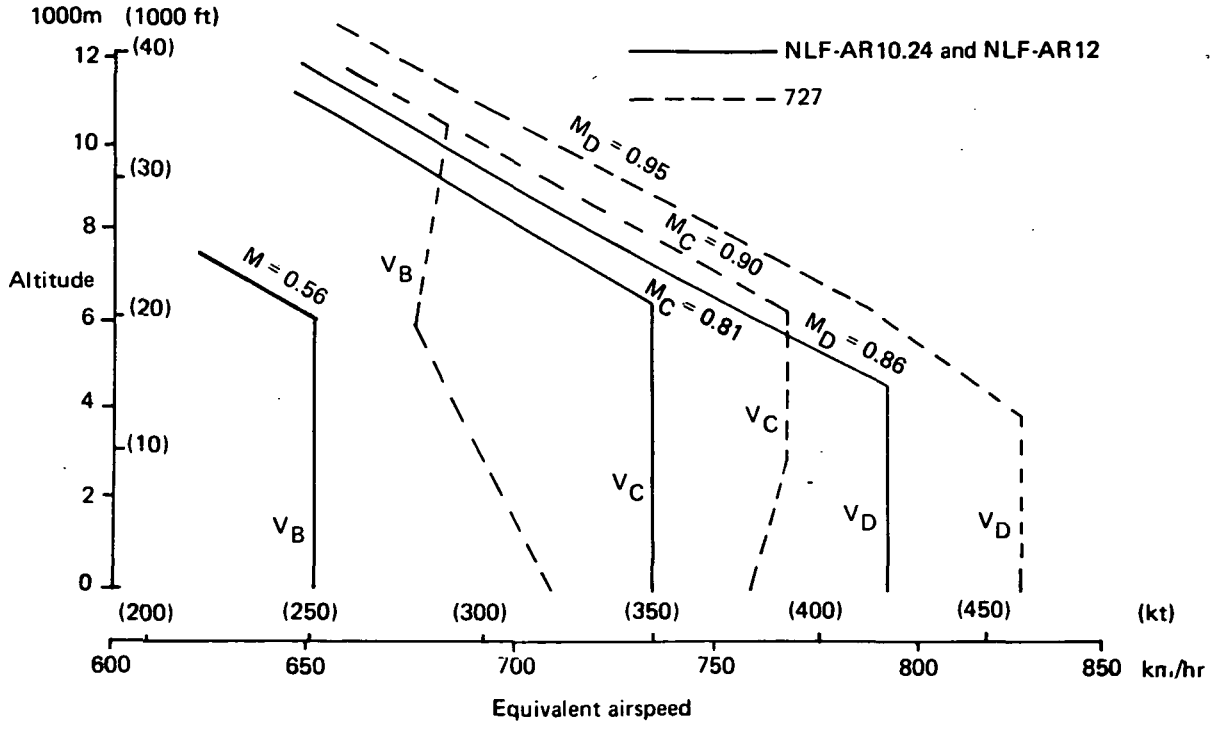

Figure 35. Structural Design Airspeed Comparison

One effect of flexure on unswept wings, a tendency to "wash-in" the wing tips, causes the center of pressure to move outboard. Figures 36 and 37 show this effect on spanwise distribution of nondimensional lift coefficient. The result of this tendency is illustrated in Figure 38, a comparison of wing design bending moments. Figure 39 shows the relative criticality of maneuver versus gust. Maneuver loads for models NLF-AR10.24 and NLF-AR12 are 68% and 63%, respectively, of design gust load at the wing root.

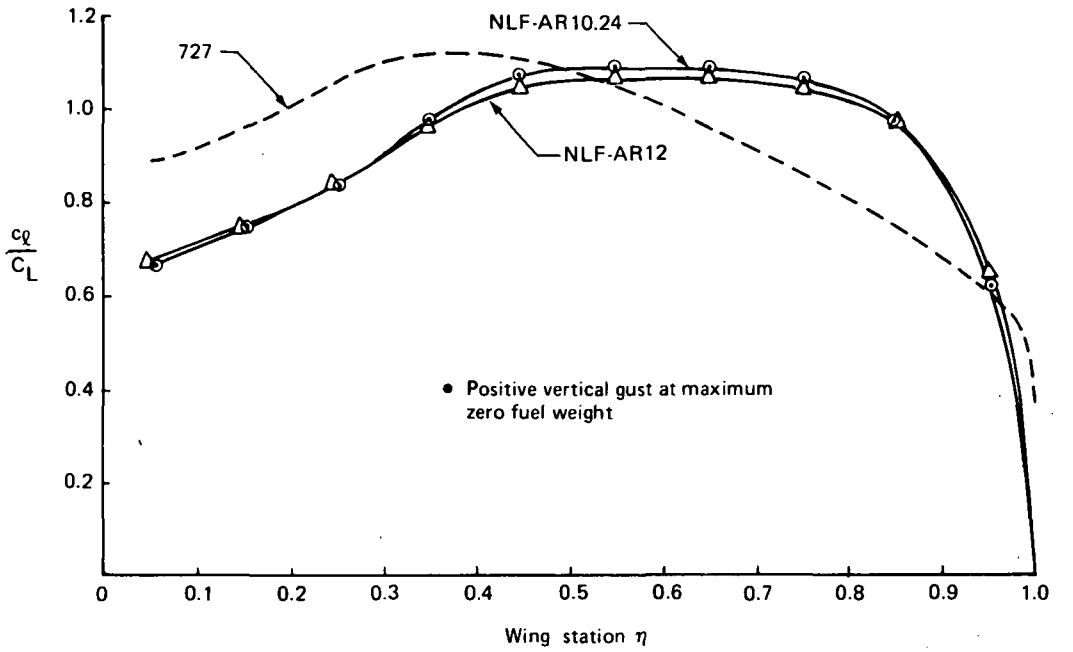

Figure 36. Wing Lift Distribution Comparison in Terms of c_ℓ

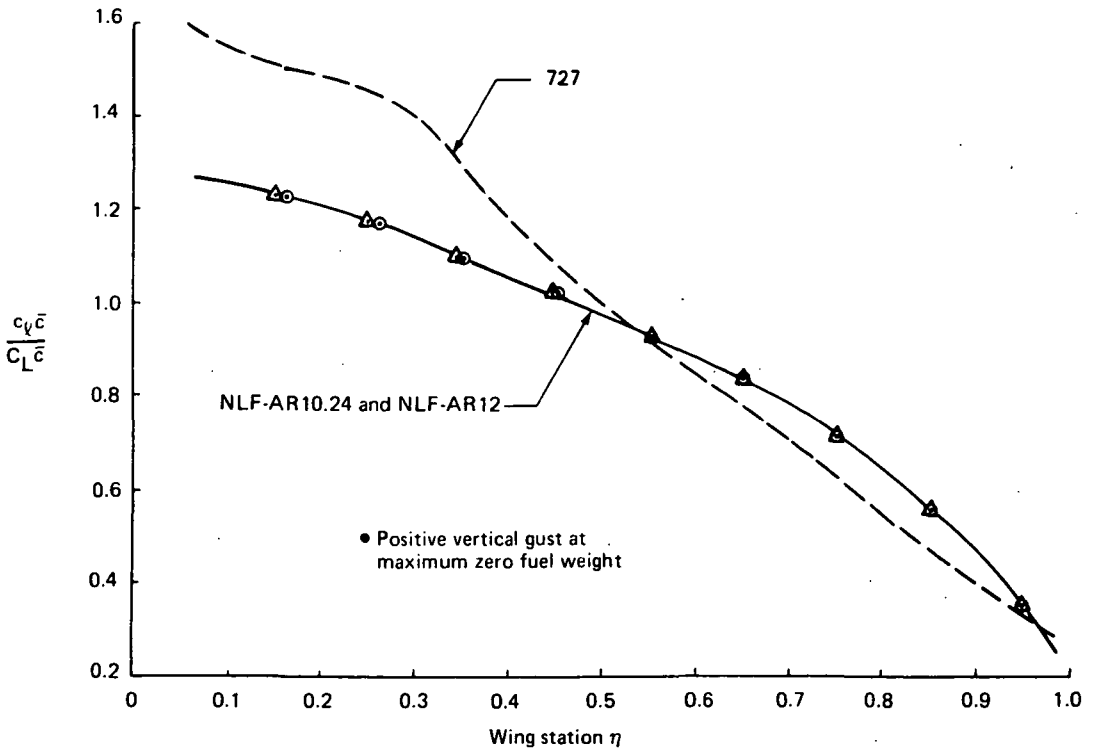

Figure 37. Wing Lift Distribution Comparison in Terms of $c_\ell c$

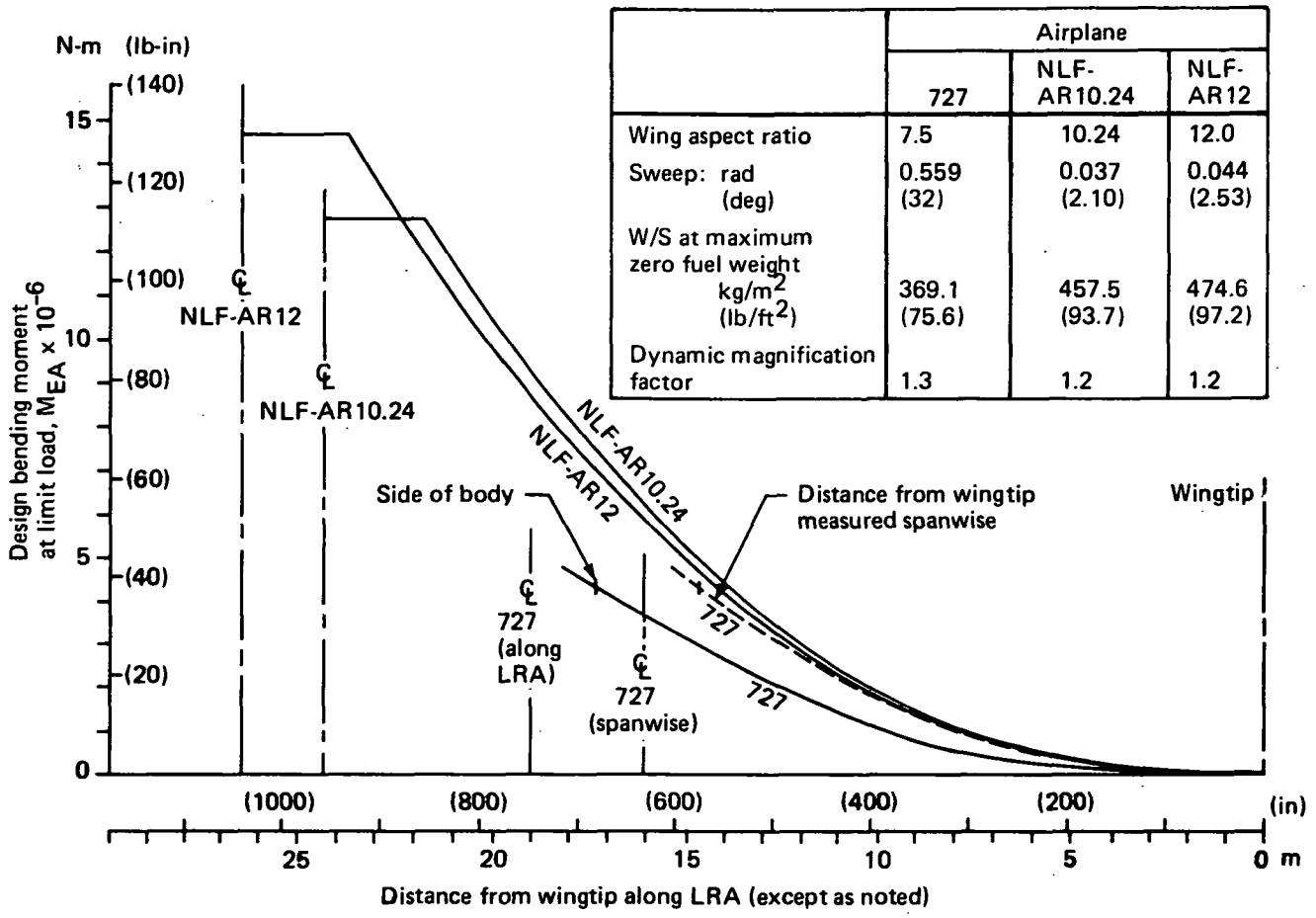

	Airplane		
	727	NLF-AR10.24	NLF-AR12
Wing aspect ratio	7.5	10.24	12.0
Sweep: rad (deg)	0.559 (32)	0.037 (2.10)	0.044 (2.53)
W/S at maximum zero fuel weight kg/m^2 (lb/ft^2)	369.1 (75.6)	457.5 (93.7)	474.6 (97.2)
Dynamic magnification factor	1.3	1.2	1.2

Figure 38. Wing Design Bending Moment at Elastic Axis Comparison

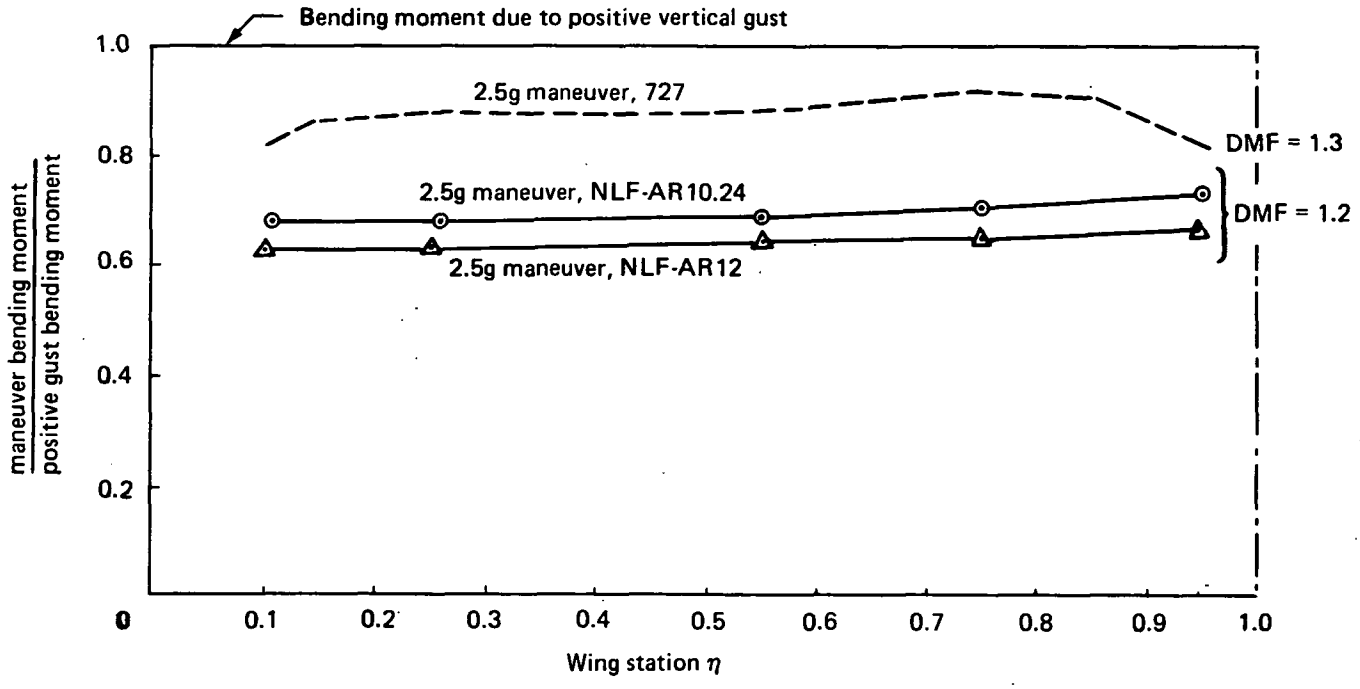

Figure 39. Maneuver/Critical Positive Gust Bending Moment Comparison

In Figure 40, relative wing thickness distributions are shown to be similar. This similarity implies that weight difference of the NLF wings is more dependent on the relative distributions of the loads than on thickness distribution.

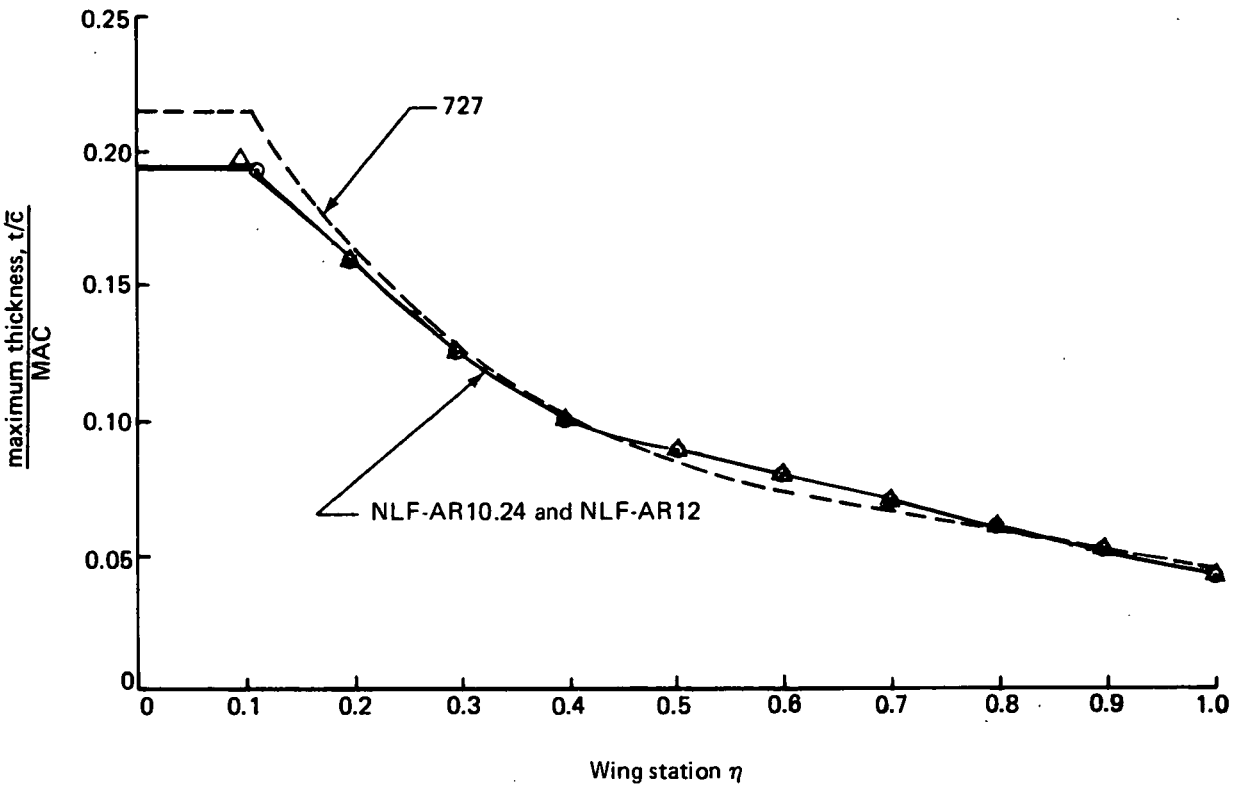

Figure 40. Wing Maximum Thickness Comparison

Airplane gust sensitivity is expressed as the ratio of incremental gust load factor to derived gust velocity ($\Delta n/U_{de}$), where n represents the load factor as calculated by the formula of FAR25.341C. Figures 41 and 42 show gust sensitivity values of the two unsized NLF airplanes for various points on the altitude/airspeed envelope, at the weight (MZFW) for greatest gust sensitivity. Figure 43 is a gust-response comparison of the two NLF airplanes and a number of current production airplanes, at typical flying weights. Decreasing values of $\Delta n/U_e$ correspond to decreasing gust sensitivity and improved ride quality. The comparison indicates that the NLF ride quality will be inferior to that of current airplane equipment. Table 7 lists the airplane charcteristics relevant to the comparison of Figure 43.

A flutter analysis of unsized model NLF-AR10.24 and NLF-AR12 wings was conducted to determine whether additional wing box material would be required. The analysis considered the free airplane with a single flexible wing beam tied to a rigid body and empennage. Wing paneling and mass and stiffness distributions were the same as those used in the static aeroelastic and strength design analysis.

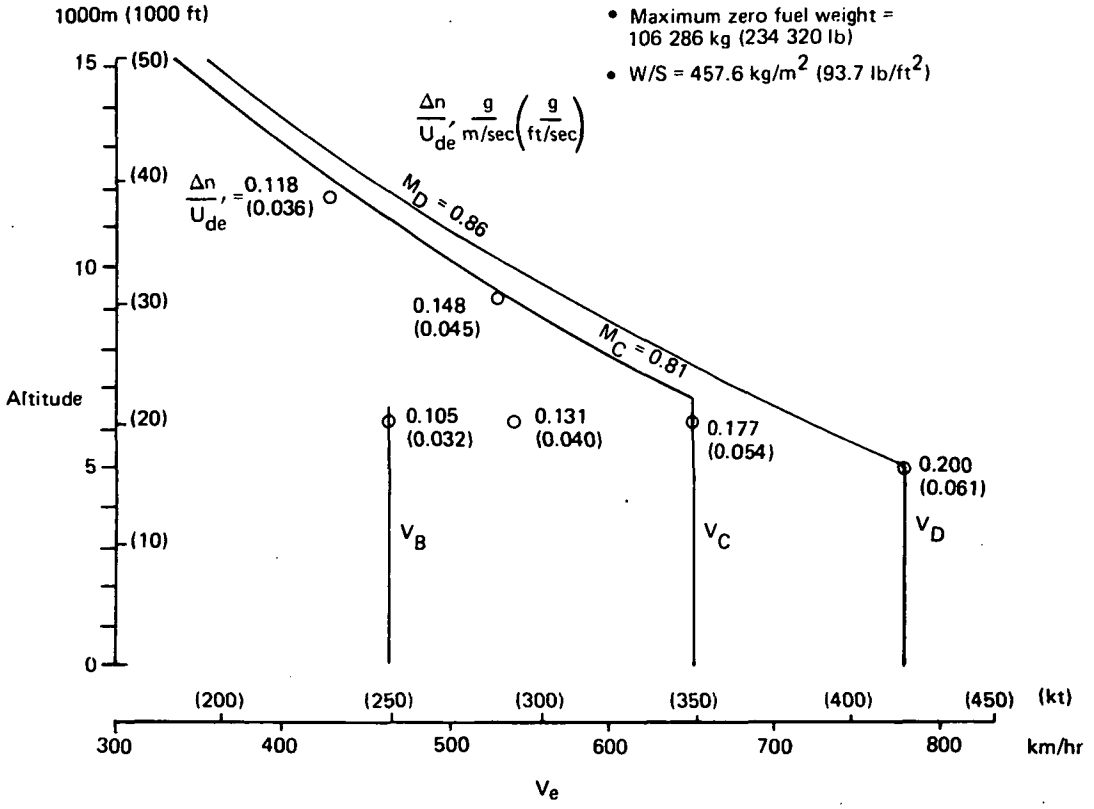

Figure 41. NLF-AR10.24 Airplane Gust Response at Maximum Zero Fuel Weight

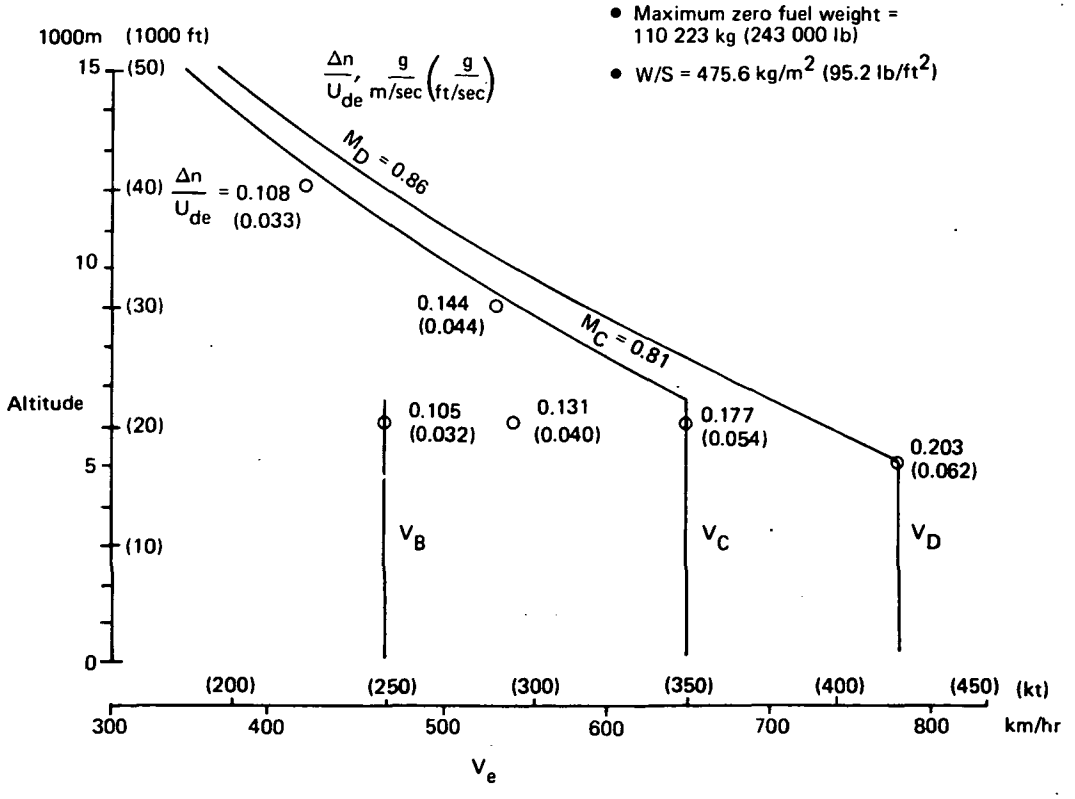

Figure 42. NLF-AR12 Airplane Gust Response at Maximum Zero Fuel Weight

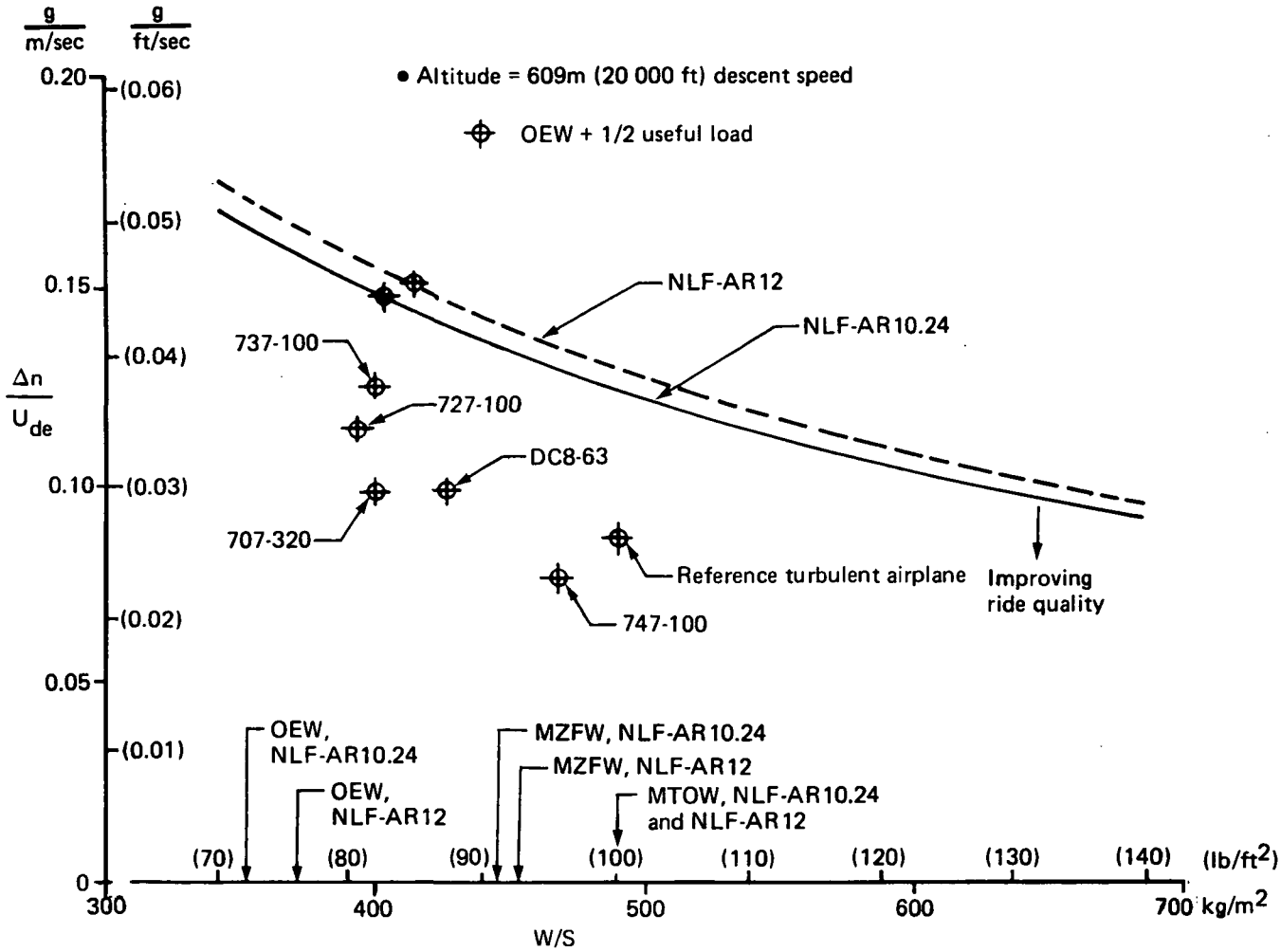

Figure 43. Airplane Gust Response Comparison

Table 7. Airplane Characteristics/Gust Response Comparison

Airplane	Aspect ratio	Wing area		Sweep—c/4		Equivalent airspeed	
		m^2	(ft^2)	rad	(deg)	km/hr	(kt)
Unsized reference	10.24	232.26	(2500)	0.524	(30.0)	557.45	(301)
NLF-AR10.24	10.24	232.26	(2500)	0.037	(2.1)	540.78	(292)
NLF-AR12	12.0	232.26	(2500)	0.044	(2.5)	540.78	(292)
747-100	6.96	510.97	(5500)	0.654	(37.5)	592.64	(320)
737-100	8.83	91.04	(980)	0.436	(25.0)	629.68	(340)
727-100	7.20	144.93	(1560)	0.559	(32.0)	629.68	(340)
707-320	7.06	279.73	(3011)	0.611	(35.0)	592.64	(320)
DC8-63	7.20	271.93	(2927)	0.524	(30.0)	592.64	(320)

Table 8 lists the cantilevered wing uncoupled bending- and torsion-mode frequencies calculated using a Boeing vibration analysis program. These modes, together with the relevant symmetric or antisymmetric rigid airplane freedoms, comprised the flutter analysis degrees of freedom. Panel lift slope and aerodynamic center data were used with static induction between the panels to obtain finite-span, incompressible unsteady air forces. Classical V-g flutter solutions were obtained for sea level air density with zero input structural damping. Calculated flutter speeds were then corrected for compressibility by multiplying the inverse square root of the wing lift slope ratio for M = 0.78 and a low Mach number. Altitude variations for the calculated sea level flutter speeds were assumed to occur at constant equivalent airspeed in applying the compressibility correction for the wing critical Mach number. The resulting flutter speed ratios are listed in Table 9.

Table 8. Cantilever Wing Uncoupled Modes

Uncoupled-mode description	Frequency (Hz)			
	NLF strength design			
	NLF-AR10.24		NLF-AR12	
	Tanks empty	Tanks full	Tanks empty	Tanks full
Bending–				
1st	1.75	1.55	1.48	1.42
2nd	5.00	3.92	4.22	3.56
3rd	10.27	8.25	8.60	7.28
4th	17.75	13.78	14.77	12.52
5th	27.35	21.73	22.57	18.91
Torsion–				
1st	11.01	9.93	10.16	9.57
2nd	18.74	17.40	17.66	16.60
3rd	26.12	23.70	24.51	23.15

Table 9. Wing Flutter Speed Ratios

Flutter type	Weight condition	Flutter speed ratio and frequency $V_F/1.2\ V_D$ (Hz)	
		NLF strength design	
		NLF-AR10.24	NLF-AR12
Symmetric	Tanks empty	1.312 (6.2)	1.218 (6.0)
	Tanks full	1.254 (6.5)	1.177 (6.1)
Antisymmetric	Tanks empty	1.246 (5.8)	1.169 (5.2)
	Tanks full	1.295 (4.9)	1.185 (4.9)

- Flutter analysis with rigid fuselage shows no sensitivity to payload condition
- Compressibility corrections applied to calculated flutter speeds are 0.826 for NLF-AR10.24 and 0.818 for NLF-AR12
- V_D = 777.8 km/hr (420 KEAS)
  $1.2\ V_D$ = 933.4 km/hr (504 KEAS)

The flutter analysis shows that flutter speeds exceed the 1.2 V_D requirement by 25% for the strength designed NLF-AR10.24 wing, and by 17% for the strength designed NLF-AR12 wing. The antisymmetric wing tanks empty condition is critical in both cases. Results were found to be insensitive to payload condition. In light of these results, no flutter weight penalty was included in the weight evaluation.

Weights—Weight analyses of all wings were conducted using a multistation beam-analysis computer program to determine the load-sensitive wing-box weight. Statistical-parametric techniques were used to estimate wing nonoptimum and secondary structure weight. Empennage, landing gear, and engine strut weights also were estimated by statistical-parametric methods. The body weight effects on the NLF designs of the aft-mounted engines were similarly determined. Nacelle, propulsion system, fixed equipment and standard and operational equipment weights are similar to those of the turbulent reference airplane. Table 10 shows the results of a wing weight study comparing the elements of wing weight at constant wing area for a turbulent wing and the two NLF wings.

Table 10. Unsized Airplane Wing Weight Comparison; Constant Area, 232.3 m^2 (2500 ft^2)

Item	Reference	NLF			
	AR = 10.24	NLF-AR 10.24		NLF-AR12	
	Weight/airplane, kg (lb)	Weight/airplane, kg (lb)	% change	Weight/airplane, kg (lb)	% change
Bending material	8777.0 (19 350)	12 637.1 (27 860)	+44.0	17 295.5 (38 130)	97.1
Shear material	562.5 (1240)	526.2 (1160)	- 6.5	562.5 (1240)	0.0
Ribs [1]	2426.7 (5350)	2154.6 (4750)	-11.2	2222.6 (4900)	-8.4
Secondary structure	3669.6 (8090)	3828.3 (8440)	+4.3	3991.6 (8800)	+8.8
Miscellaneous	412.8 (910)	362.9 (800)	-12.1	358.3 (790)	-13.2
Total wing	15 848.5 (34 940)	19 509.0 (43 010)	+23.1	24 430.5 (53 860)	+54.1
	kg/m^2 (lb/ft^2)	kg/m^2 (lb/ft^2)	% change	kg/m^2 (lb/ft^2)	% change
Total unit weight [2]	68.26 (13.98)	83.98 (17.20)	+23.1	105.17 (21.54)	+54.1
Total unit weight [3]	63.52 (13.01)	78.02 (15.98)	+22.8	97.75 (20.02)	+53.9

[1] Includes basic ribs, spanwise beams and side of body ribs
[2] Based on trapezoidal area
[3] Based on trapezoidal area plus additional exposed area

Increased wing weight was the major contributor to the increased operating empty weight of the NLF airplanes. The NLF-AR-10.24 wing would be 23% heavier than the turbulent reference wing at the same area. The weight of wing-bending material would be increased by 44%.

Some of the factors contributing to the increased weight of the NLF wings are:

- Reduction in the thickness ratio from 15% to 11% at the side-of-body to maintain inboard upper-surface laminar flow
- A 17% increase in gust load factor, due principally to a reduction in wing sweep
- A 10% greater bending moment at the side-of-body for the critical zero fuel weight condition, due to the increase in operating empty weight, loss of deadweight relief when engines were removed from the wing and to an outbord movement of the center of pressure due to reduction in wing sweep
- An 8% increase in bending material weight attributed to the use of bonded-aluminum-honeycomb wing skins in an application where such construction is less efficient structurally than skin and stringer construction

Increasing the NLF wing aspect ratio from 10.24 (model NLF-AR10.24) to 12.0 (model NLF-AR12) results in a 25% increase in wing weight. This is due to a 37% increase in the weight of wing bending material, resulting from the following factors:

- An 8% increase in structural span
- A 15% increase in bending moment at the side-of-body due to an outbord movement of the center of pressure, greater structural span, and the increase in airplane weight at the critical design condition
- A 7% decrease in actual wing-box depth at the side-of-body, which occurs when the wing chord is reduced while maintaining a constant thickness ratio
- A slight increase in the gust load factor resulting from the increase in aspect ratio

Propulsion—Powerplant performance data was generated by a CF6-50C specification deck, which includes Boeing installation losses. A 1.17 kg/sec (2.58 lb/sec) air-conditioning bleed schedule was applied. An additional 0.20% of fan duct airflow was included to simulate a 3.18 kg/sec (7 lb/sec) precooler bleed with 90% fan gross thrust recovery and a 0.23 kg/sec (0.5 lb/sec) bleed for foward core compartment ventilation.

Inlet recovery, nozzle C_Vs and fan duct pressure loss are Boeing estimates for an acoustically treated podded engine. Nozzle C_Ds are supplied by the CF6-50C computer deck. An applied 100.71 kW (135 hp) extraction is included as an installation loss throughout the flight envelope.

Stability and Control—The horizontal and vertical tails for the NLF airplanes were sized in accordance with current technology. With the center of gravity at the aft limit, the airplanes must have a 6% static margin for the approach condition. Cruise static margin requirement is 3% and dive static margin requirement is 0.0%. The NLF airplanes, like the turbulent reference airplane, have flying horizontal tails with geared elevators, and incorporate double-hinged rudders.

The NLF tail sizing chart is shown in Figure 44. The static neutral point on the NLF airplanes is further forward than that of the turbulent reference airplane, due to the destabilizing increase in forebody length, and to increase in lift curve slope and $C_{L_{elastic}}/C_{L_{rigid}}$ ratio associated with unswept NLF wings.

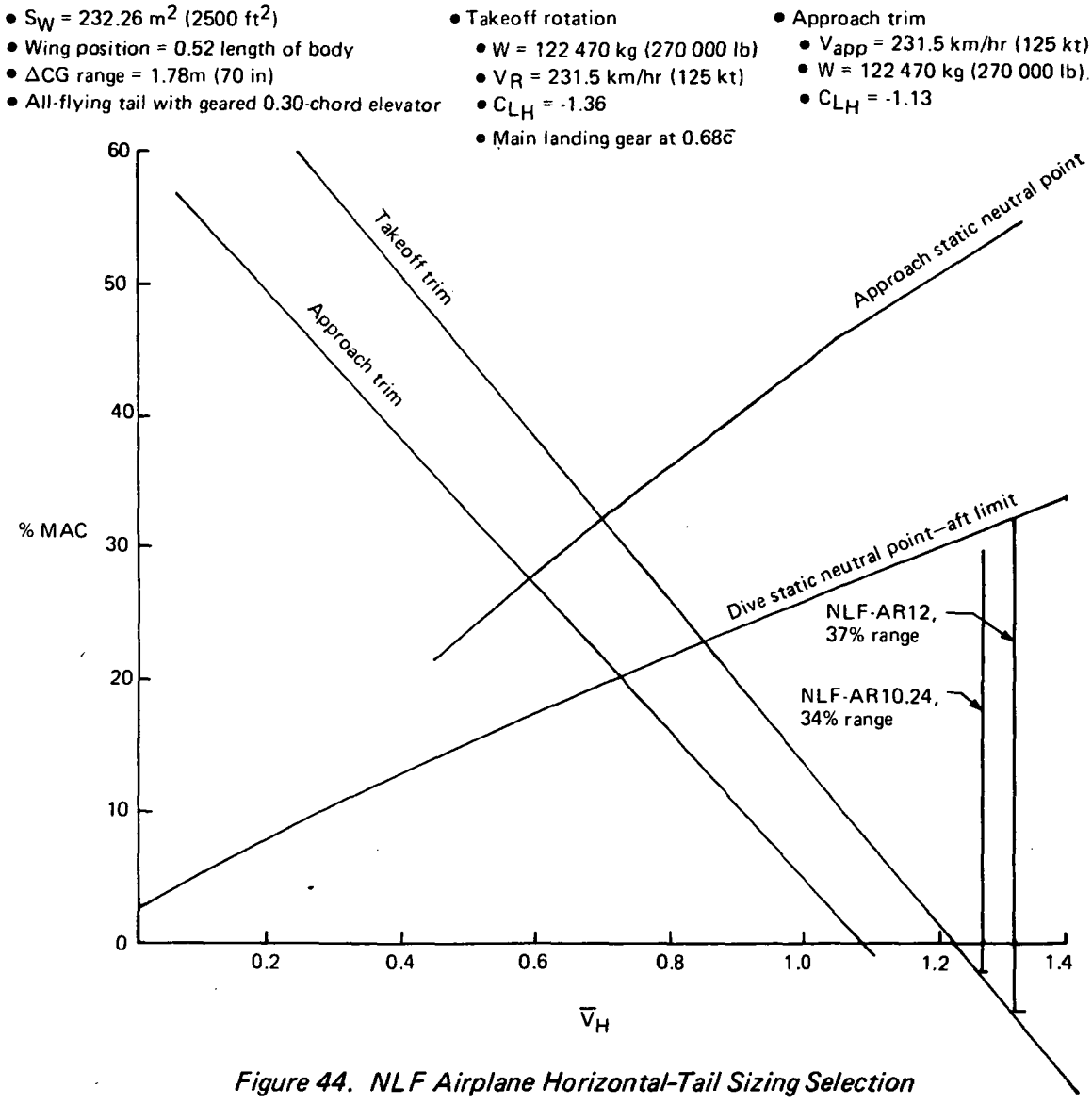

Figure 44. NLF Airplane Horizontal-Tail Sizing Selection

It was necessary to increase the loading (CG) range from the reference airplane's 1.60m (63 in) to 1.78m (70 in). The main landing gear position is 10% MAC further aft on the NLF airplanes, mainly due to the reduction in sweep. Each of these factors contributes to the NLF airplanes' requirement for a larger V_H, which results in a larger horizontal tail. The model NLF-AR12 has a loading range larger in percent MAC than the model NLF-AR10.24, requiring an additional increase in horizontal-tail size.

Low-Speed Aerodynamics—The low-speed aerodynamic characteristics for takeoff and landing performance estimation were defined for the flap geometry shown in Figure 45. The trailing-edge flap chord is 31% of the basic wing chord. Maximum flap extension angles are shown in the figure.

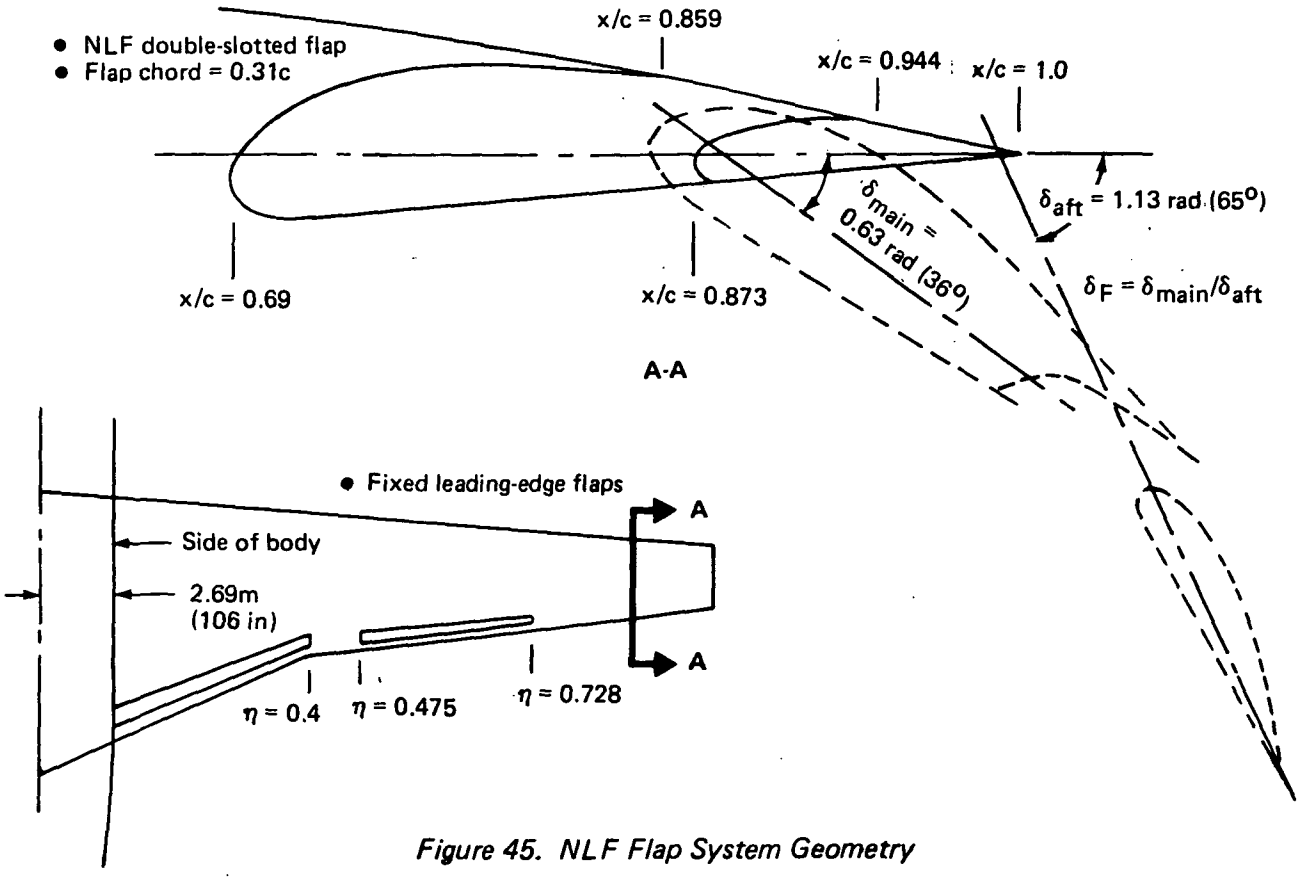

Figure 45. NLF Flap System Geometry

Figure 46 shows the low-speed characteristics of the unsized turbulent reference airplane. Figures 47 and 48 represent the low-speed characteristics of the unsized NLF-AR10.24 and NLF-AR12 airplanes. The gear-down $1.3V_S$ line represents the landing approach condition. Due to the absence of leading-edge devices, the NLF airplanes have a lower approach lift coefficient for a given flap setting. A lower approach lift coefficient will require a higher approach speed; or if, as in this study, a minimum approach speed is specified, a larger wing will be required. At maximum flap extension, the airplane will assume a nose-down attitude, which may lead to an undesirable nose-wheel-first touchdown.

The gear-up $1.2\ V_S$ ($= V_2$) line represents conditions at the start of the second-segment climb. For a given flap setting the NLF airplanes have lower lift coefficient under these conditions and, therefore, require higher V_2 speeds. For a specified field length, higher speeds require larger engines.

High-Speed Aerodynamics—The high-speed drag build-up based upon wind tunnel test data for a configuration similar to the turbulent reference airplane. The minimum profile drag coefficient of each component, except the wing, was corrected for the change from model to full-scale conditions. The wing profile drag (as a function of C_L) then was corrected using a Boeing derived analysis method. Profile drag factors were obtained from two dimensional airfoil data and simple sweep theory. Body and nacelle drags were obtained by standard Boeing drag prediction methods. Nacelle interference drag was derived from experimental data.

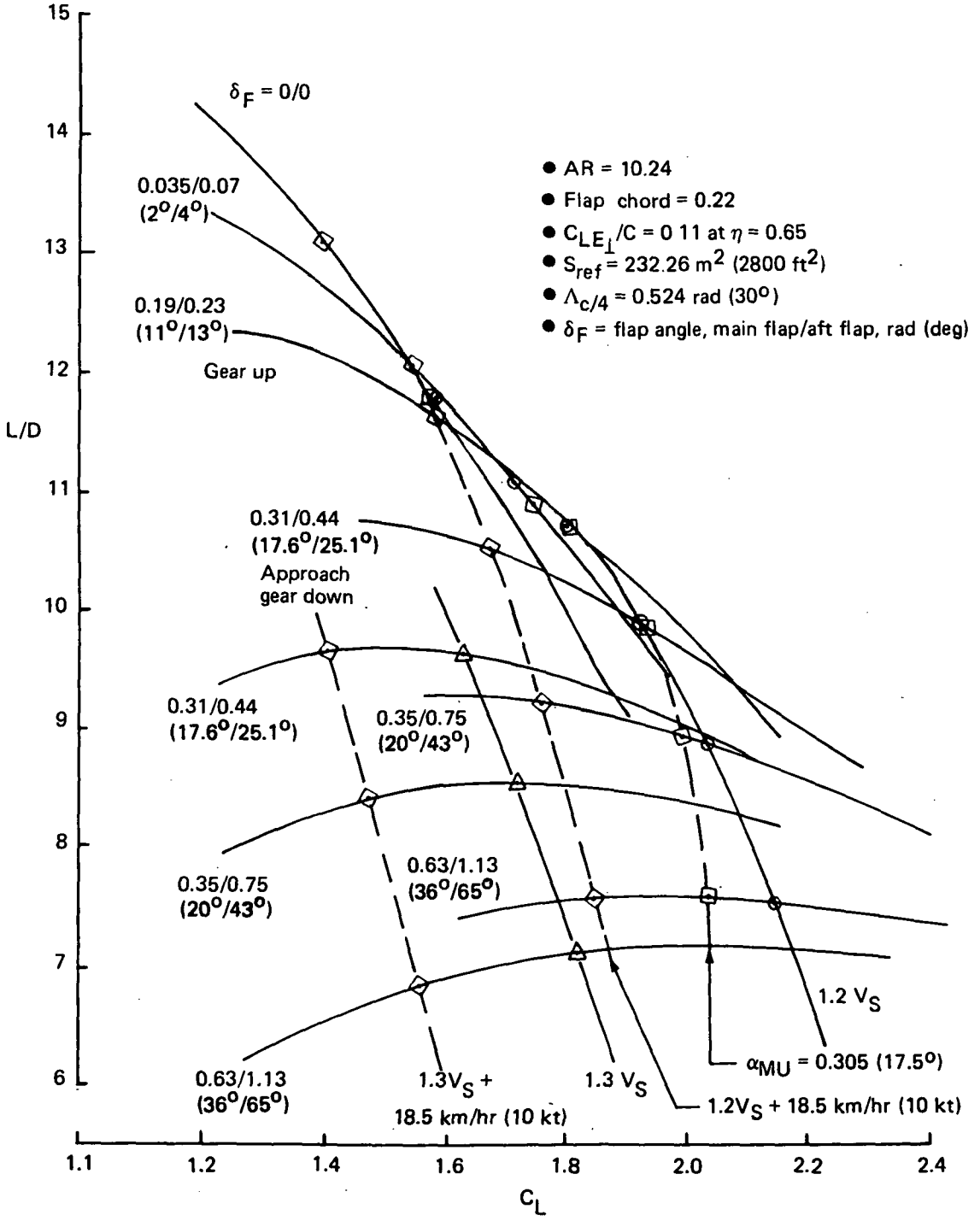

Figure 46. Reference Airplane Low-Speed Characteristics

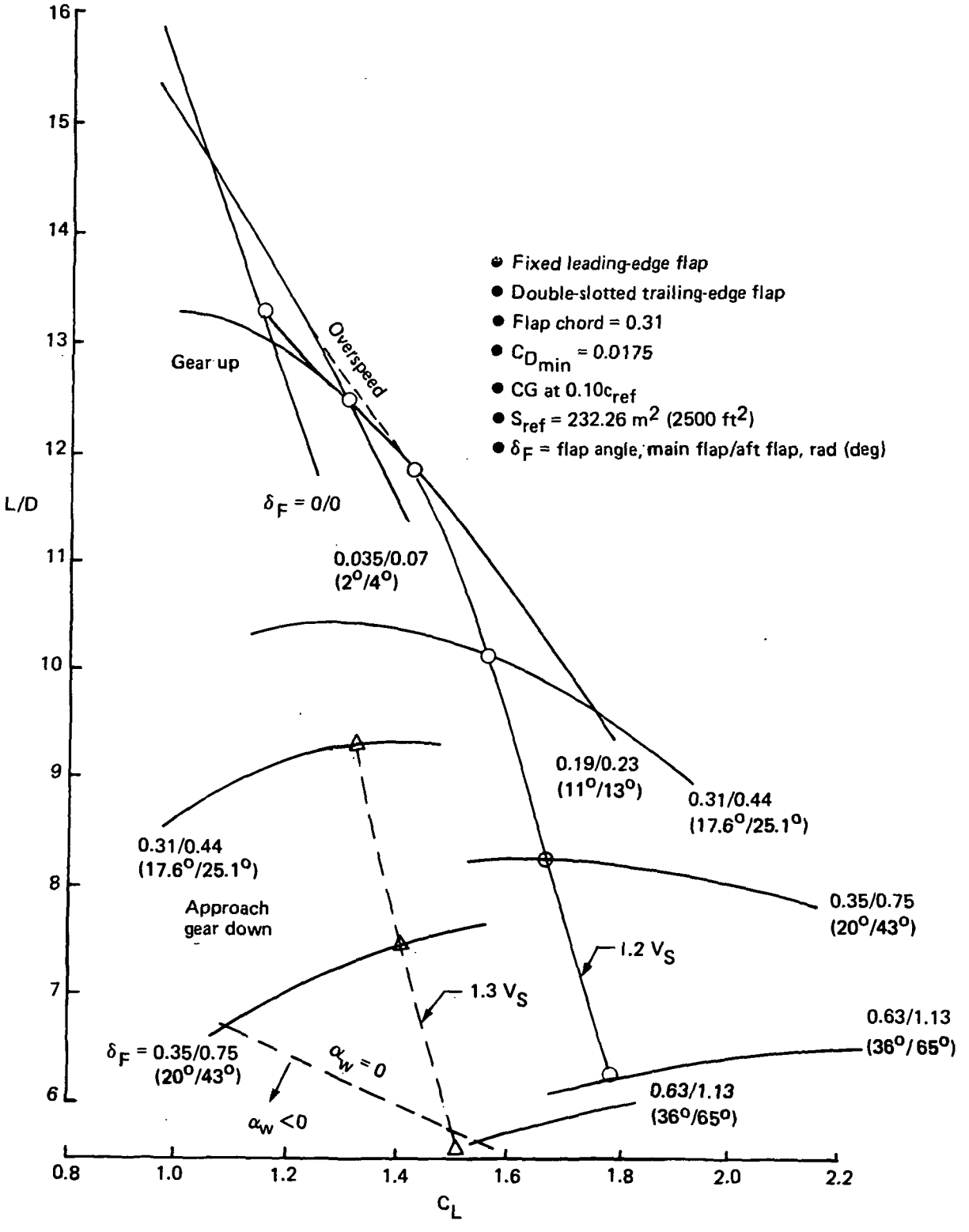

Figure 47. NLF-AR10.24 Airplane Low-Speed Characteristics

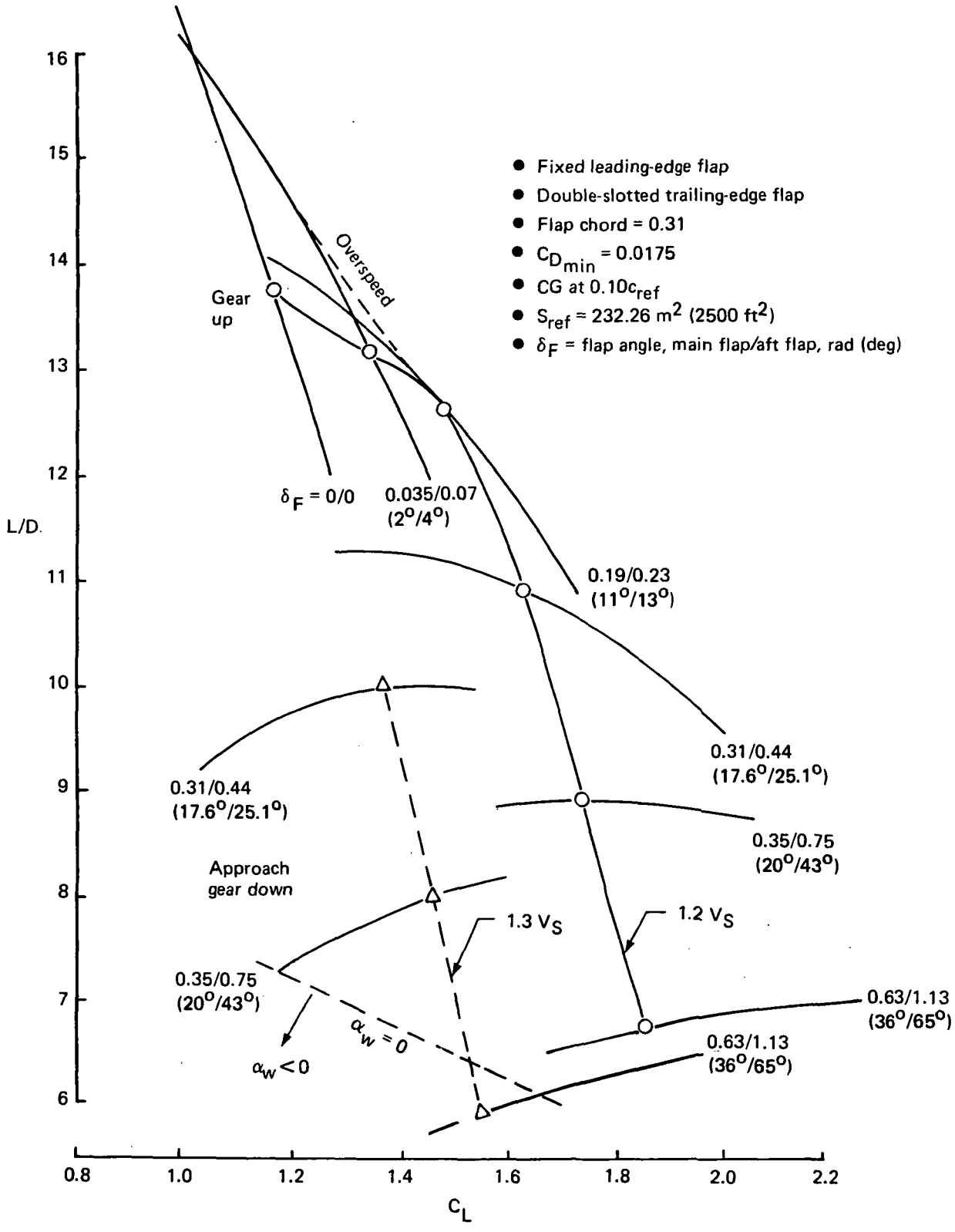

Figure 48. NLF-AR12 Airplane Low-Speed Characteristics

During the development of drag characteristics for the NLF configurations, effects of the following changes were accounted for:

- Moving the engines from the wing to the aft body to eliminate wing boundary-layer interference caused by engine noise and vibration and by the turbulent wedge at the strut
- Reducing the sweep to prevent crossflow instability from causing transition
- Reducing the wing thickness ratio at the side-of-body to 0.11 to maximize the extent of upper-surface laminar flow
- Incorporating a T-tail to clear the exhaust plume of the body-mounted engines
- Lengthening the body 2.45 m (8.04 ft) to accommodate the larger vertical tail

The drag characteristics of model NLF-AR10.24 are shown in Figure 49 for both the turbulent and laminar flow cases. The drag characteristics of the turbulent reference airplane are included for comparison. The transition from turbulent to laminar cruising conditions results in a 15.8% improvement in L/D_{max}. Model NLF-10.24 drag buildup at M = 0.78 is shown in Figure 50.

The drag characteristics of model NLF-AR12 are shown in Figure 51. Transition from turbulent to laminar cruising conditions for this airplane results in an 18.8% improvement in L/D_{max}. Model NLF-AR12 drag buildup at M = 0.78 is shown in Figure 52.

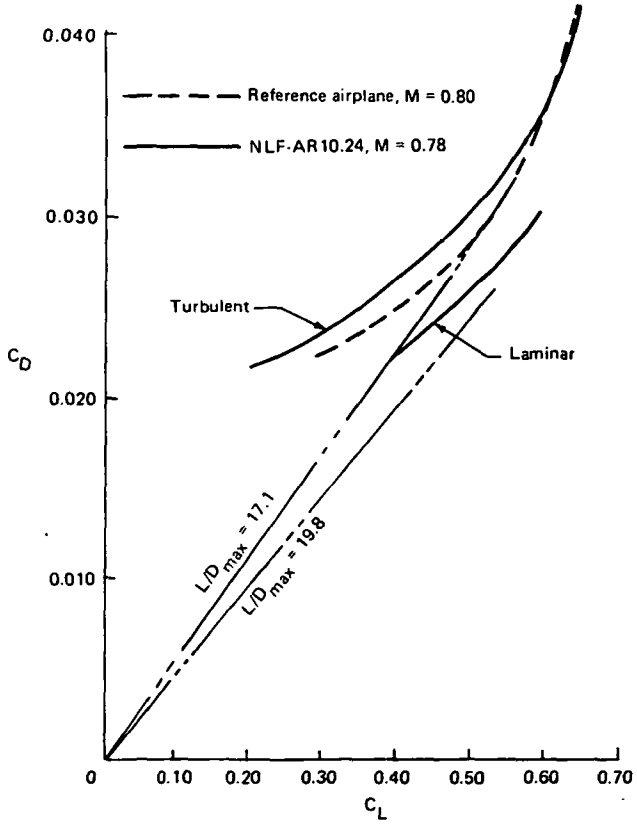

Figure 49. NLF-AR10.24 Airplane Drag Characteristics Summary

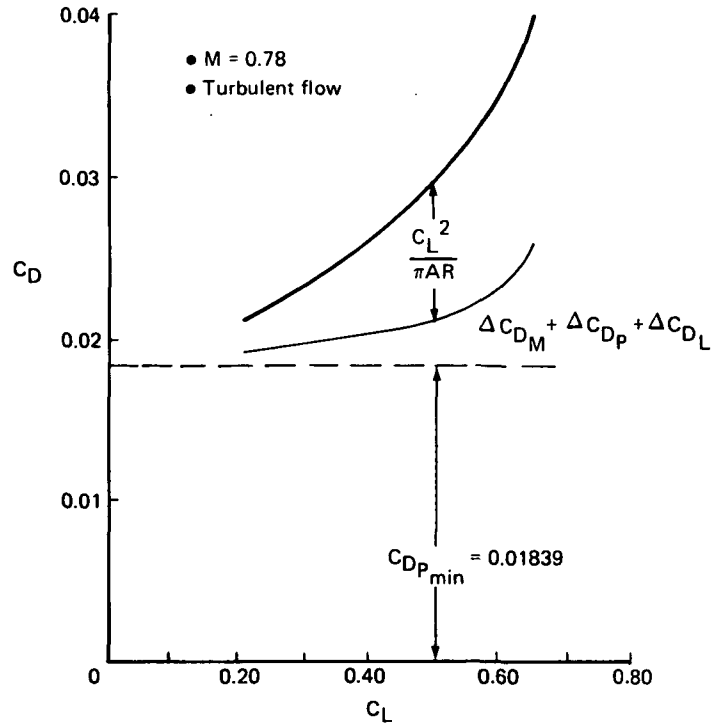

Figure 50. NLF-AR10.24 Airplane Drag Polar

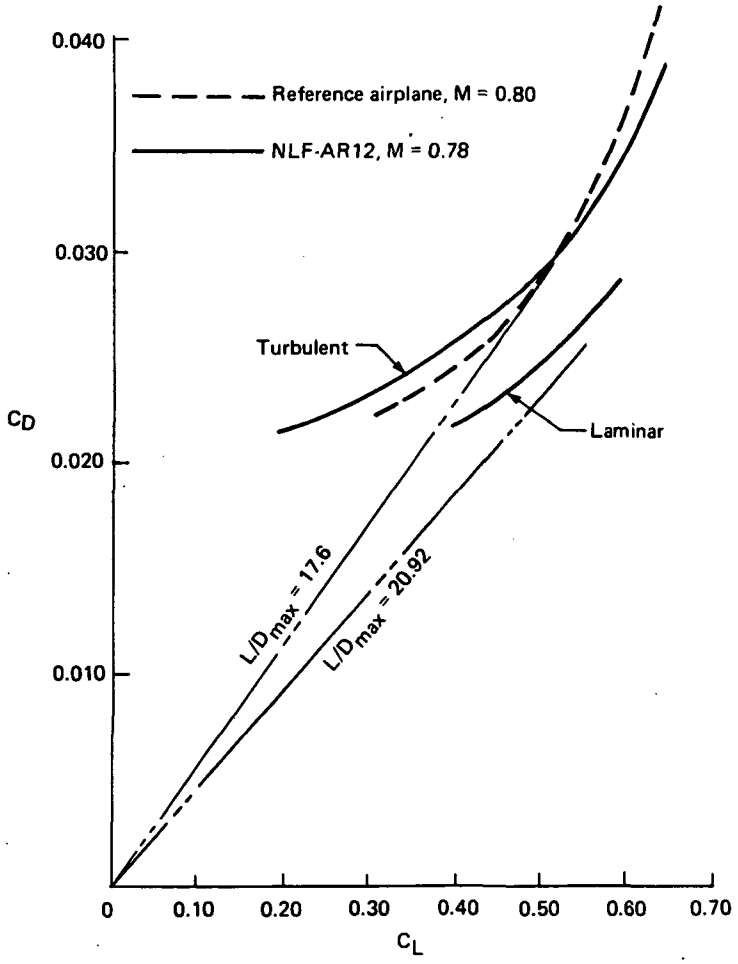

Figure 51. NLF-AR12 Airplane Drag Characteristics Summary

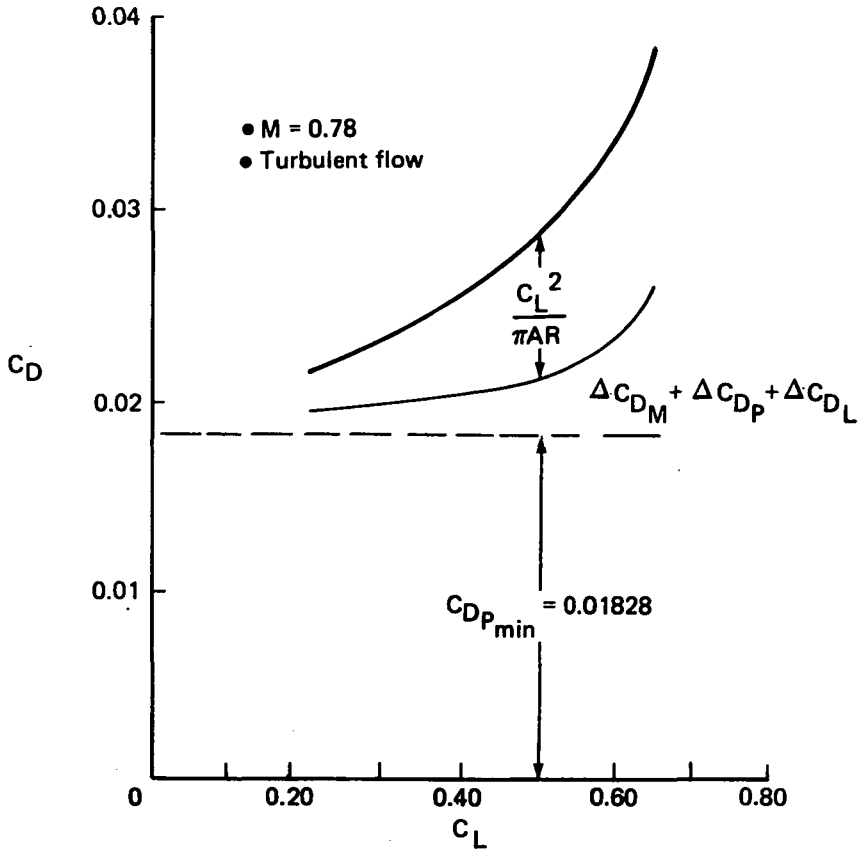

Figure 52. NLF-AR12 Airplane Drag Polar

5.3 AIRPLANE SIZING AND PERFORMANCE

The study airplanes were sized to meet the mission requirements identified in Table II.

The turbulent reference airplane used a Boeing-developed advanced airfoil section. It was necessary to select an NLF airfoil for sizing and performance purposes before the airfoil design task was completed. Therefore, performance results reflected the assumption that for the design conditions, natural laminar flow would exist over the forward 60% of the wing upper surface and over the forward 50% of the wing lower surface, outside of the turbulent wedge at the wing-body intersection. In all other areas of the NLF airplanes, the boundary layer was assumed turbulent. During takeoff, climb, and descent, the wing boundary layer was assumed to be fully turbulent; natural laminar flow existing only during cruise.

Table 11. Sized Airplane Characteristics and Performance Requirements

Mission requirements:

Still-air range, km (nmi)	3 704	(2 000)	Takeoff field length, SL at 29°C, m (ft)	2 286 (7 500)
Payload, 196 passengers, kg (lb)	18 225	(40 180)	Approach speed, km/hr (kt)	231.5 (125)
Initial cruise altitude, m (ft)	10 668	(35 000)	Reserves	ATA domestic
Cruise Mach number				
Reference airplane	0.80			
NLF-AR10.24 and NLF-AR12	0.78			

	Reference airplane	NLF-AR10.24	NLF-AR12
Wing area (ref), m^2 (ft^2)	235.51 (2 535)	309.83 (3 335)	331.57 (3 569)
Wing span, m (ft)	49.11 (161.12)	56.33 (184.80)	58.27 (191.17)
Mean aerodynamic chord, m (ft)	5.23 (17.15)	6.00 (19.67)	6.20 (20.35)
Aspect ratio	10.24	10.24	12.00
Sweep of quarter chord, rad (deg)	0.520 (30.0)	0.037 (2.10)	0.044 (2.53)
Taper ratio	0.3158	0.3158	0.3158
t/c, root/tip gross chord, %	15/10.3	11/10.1	11/10.1
Horizontal tail area, m^2 (ft^2)	51.65 (556)	78.04 (840)	80.36 (865)
Vertical tail area, m^2 (ft^2)	36.14 (389)	55.65 (599)	58.81 (633)
Body length, m (ft)	47.55 (156.00)	50.01 (164.08)	50.01 (164.08)
Body diameter, m (ft)	5.39 (17.67)	5.39 (17.67)	5.39 (17.67)
Engines, quantity, type	Two, scaled CF6-50C	Two, scaled CF6-50C	Two, scaled CF6-50C
Bypass ratio	4.4	4.4	4.4
Seal level static thrust (uninstalled), kN (lb)	16.27 (36 930)	180.55 (40 590)	189.54 (42 610)
Takeoff gross weight, kg (lb)	120 719 (266 140)	135 723 (299 218)	148 982 (328 450)
Operating empty weight, kg (lb)	76 861 (169 450)	91 290 (201 260)	103 669 (228 550)
Block fuel, kg (lb)	19 051 (42 000)	18 928 (41 730)	19 636 (43 290)
Reserves, kg (lb)	6 827 (15 050)	7 548 (16 640)	7 738 (17 060)
Mission landing weight, kg (lb)	101 913 (224 680)	117 063 (258 080)	129 632 (285 790)
Thrust/weight, N/kg (lb/lb)	2.726 (0.278)	2.658 (0.271)	2.550 (0.260)
Wing loading, N/m^2 (lb/ft^2)	5 027.5 (105.0)	4 295.0 (89.7)	4 405.1 (92.0)
Operating empty weight/takeoff gross weight	0.637	0.673	0.696
Payload/takeoff gross weight	0.151	0.134	0.122
Reserves/takeoff gross weight	0.057	0.056	0.052
Initial cruise altitude capability, m (ft)	11 113 (36 460)	12 049 (39 530)	12 259 (40 270)
Average cruise altitude, m (ft)	11 723 (38 460)	12 658 (41 530)	12 869 (42 220)
Range factor, km (nmi)	22 909 (12 370)	27 076 (14 620)	29 225 (15 780)
Lift/drag	18.2	21.9	23.6
Specific fuel constant, kg/hr/N (lb/hr/lb)	0.069 (0.674)	0.068 (0.669)	0.068 (0.669)
$C_{DP_{min}}$	0.01791	0.01309	0.01269
ML/D_{cruise}	14.53	17.05	18.38
C_L at V_2	1.506	1.30	1.40
$C_{L_{app}}$	1.81	1.46	1.51

5.3.1 Sizing and Performance

The turbulent reference airplane was sized, using the design selection chart resulting from the THUMBPRINT analysis (fig. 53), by minimum fuel and gross weight consideration, and by the takeoff field length constraint. Its characteristics and performance are listed in Table 12. As expected, the sizing process resulted in minimal change to the characteristics of the well-developed turbulent reference airplane, as shown in Tables 3 and 12.

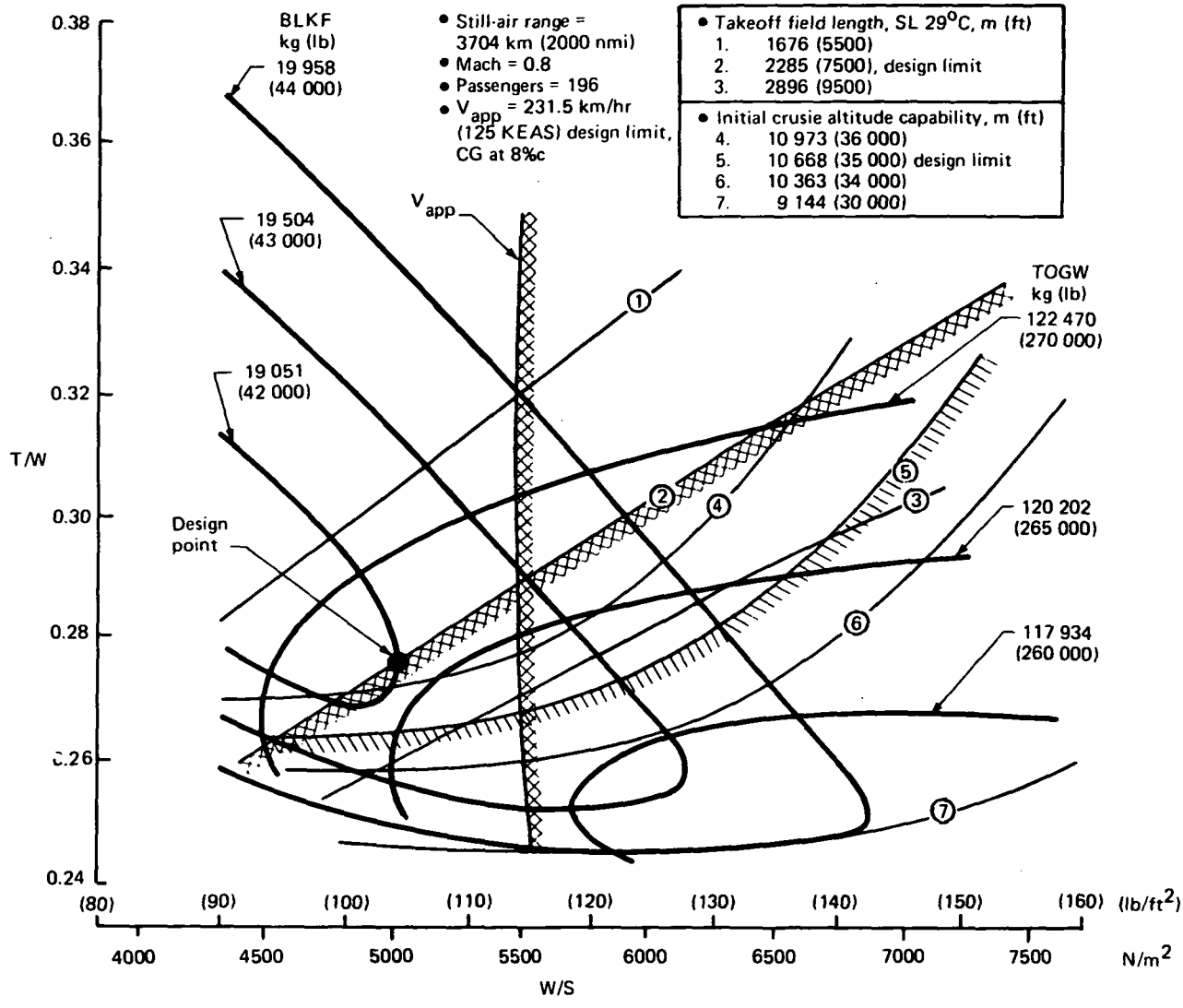

Figure 53. Reference Airplane Design Selection Chart

Table 12. Mission Analysis and Economic Data Comparison

	Reference airplane	NLF final airplane
Payload, kg (lb)	18 225 (40 180)	18 225 (40 180)
Still air range, km (nmi)	3 704 (2 000)	3 704 (2 000)
M_{cruise}	0.80	0.78
Operating empty weight, kg (lb)	76 861 (169 450)	91 290 (201 260)
Manufacturer's empty weight, kg (lb)	71 690 (158 050)	86 119 (189 860)
Brake release gross weight, kg (lb)	121 985 (268 930)	137 490 (303 070)
Block fuel, kg (lb)	20 600 (45 415)	21 310 (46 980)
Block time, hr	4.769	4.885
Reserves (ATA domestic), kg (lb)	6 681 (14 730)	7 058 (15 560)
Relative direct operating cost	Base	*107.8% base

*Based upon 1967 ATA DOC equations adjusted to 1976 costs.

Both NLF airplanes were sized by takeoff and approach speed constraints. Design selection charts for these airplanes are shown in Figures 54 and 55. As predicted by the low-speed aerodynamic analysis, the absence of leading-edge high-lift devices resulted in a requirement for additional wing area as indicated in Tables 4, 5, and 11. A takeoff thrust increase also was required. These increases resulted in larger increases in takeoff gross weight for the NLF airplanes. The greater structural weights of the NLF wings (table 11) also contribute to cause the larger values of wing area, thrust, and gross weight shown in Table 11.

To provide greater visibility of the effects of change in weight and wing area, a wing loading trade study was performed. The results of this study are presented in Figure 56. The magnitude of a 5% change for each parameter evaluated is indicated for reference. The 231.5 km/hr (125 kt) approach speed constraint (at mission landing weight) is shown for each case.

Within the NLF airplane's range of wing loadings, block fuel and initial cruise altitude capability (ICAC) are seen to be relatively insensitive to changes in wing loading. Takeoff gross weight and operating empty weight are strongly affected, with increasing wing loading causing weight reduction. Sea level static thrust also is strongly affected, the thrust requirement increasing with higher wing loading. The relationship between approach speed and wing loading also is shown in Figure 56.

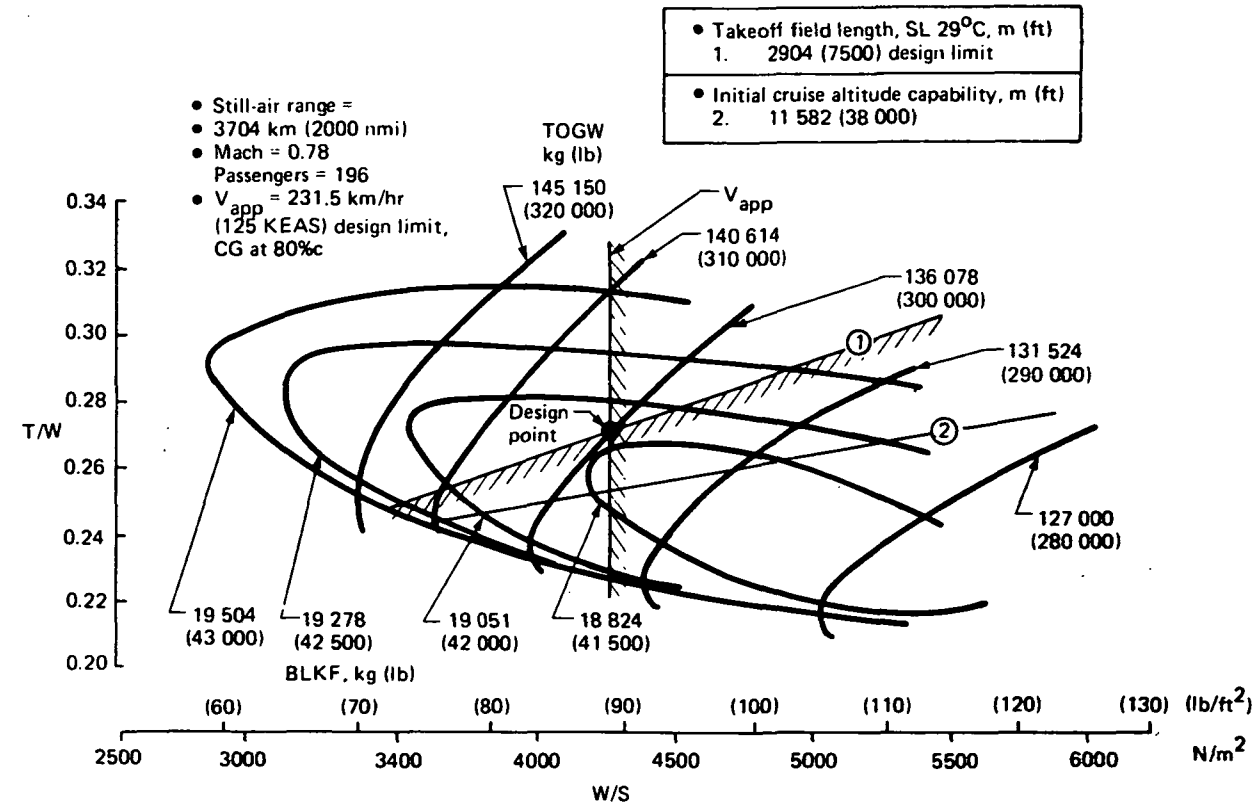

Figure 54. NLF-AR10.24 Airplane Design Selection Chart

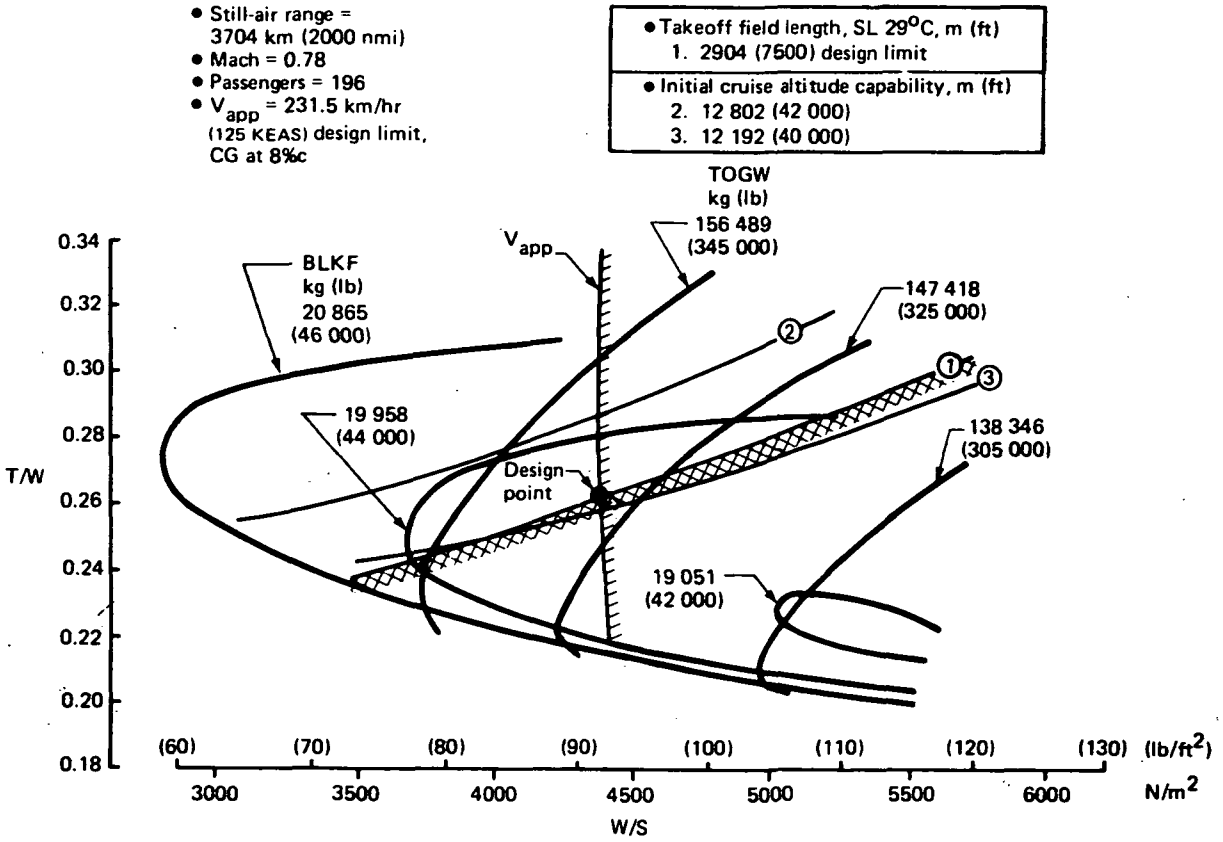

Figure 55. NLF-AR12 Airplane Design Selection Chart

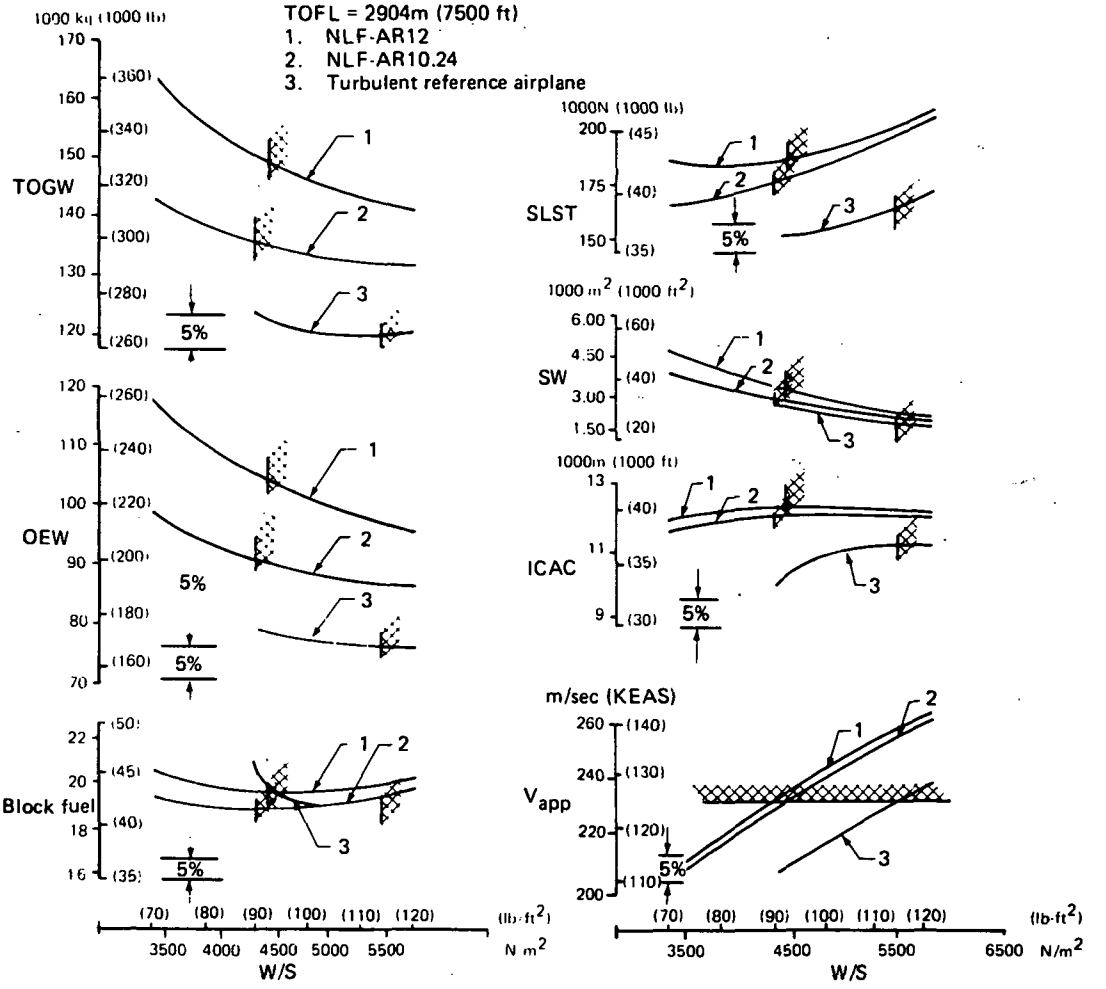

Figure 56. Wing Loading Trade Study

5.3.2 Sensitivity Study

Sized NLF-AR10.24 airplane takeoff gross weight, block fuel requirement, and direct operating cost sensitivity to change of the following unsized airplane parameters was determined with aid of the THUMBPRINT program:

- Operating empty weight
- Cruise drag
- Takeoff thrust
- Wing weight
- Specific fuel consumption

The results are shown in Figure 57. Predictably, change in the input operating empty weight has the most powerful effect on each of the output items considered. Of great importance to the direction of future NLF airplane studies is the finding that wing weight change alone has the same impact on relative direct operating cost, as do cruise drag and specific fuel consumption changes. When the NLF-AR10.24 airplane was sized, a 5% change in wing weight caused a 2-1/2% change in takeoff gross weight and a 1-1/2% change in block fuel and direct operating cost.

- Still air range = 3704 km (2000 nmi)
- Payload = 196 passengers, 18 225 kg (40 180 lb)
- TOFL = 2286m (7500 ft)
- V_{app} = 231.5 km/hr (125 KEAS)
- Cruise Mach = 0.78

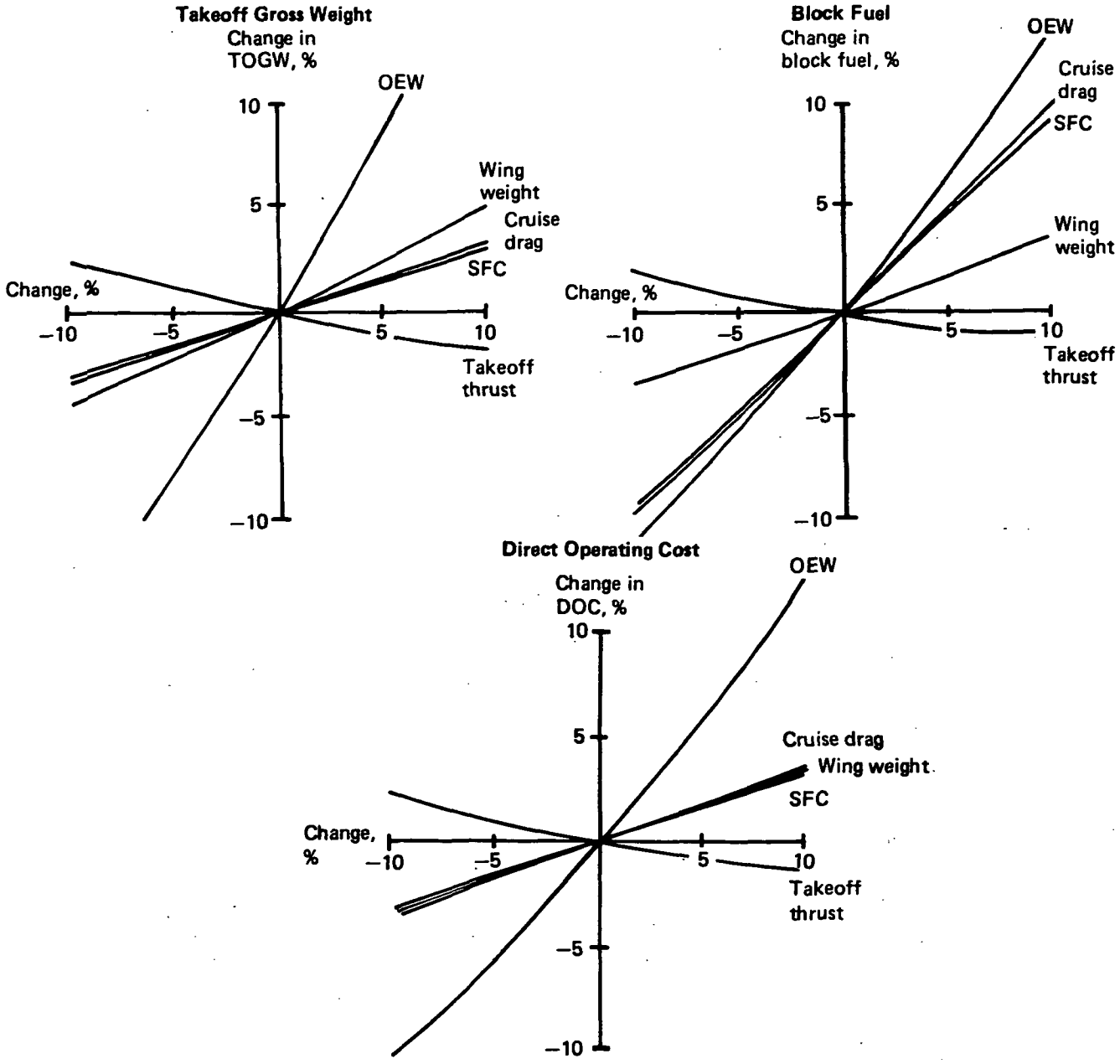

Figure 57. NLF-AR10.24 Airplane Sensitivity to Change in Selected Airplane Characteristics

NLF-AR10.24, the better performer of the two NLF airplanes, was selected as the NLF final airplane. Vertical tail aspect and taper ratio changes, made to accommodate the sized horizontal tail, had no impact upon airplane weight or drag, hence, no effect on THUMBPRINT results.

5.3.3 Mission Analysis

A mission analysis was performed for the final, sized NLF-10.24 airplane shown in Figure 58. The analysis permitted consideration of mission profile effects that only are approximated for airplane sizing purposes by the THUMBPRINT program. For example, THUMBPRINT used cruise drag levels to determine initial cruise altitude, while in the mission analysis, the NLF airplanes were assumed to experience turbulent rather than laminar flow during climb. This resulted in reduction of initial cruise altitude capability.

NLF airplane drag levels were assumed to be those corresponding to turbulent flow below 10 668m (35 000 ft) due to the possible presence of atmospheric ice crystals and to a higher level of atmospheric turbulence. They also were assumed turbulent in descent as well as climb segments, with linear transition to laminar flow taking place during acceleration from climb at M = 0.75 to cruise at M = 0.78. The mission analysis also assumed cruise altitudes conforming to the air traffic control practice of assigning cruise flight levels spaced in 610-m (2000-ft) increments, i.e. 35,000, 37,000, 39,000, etc.

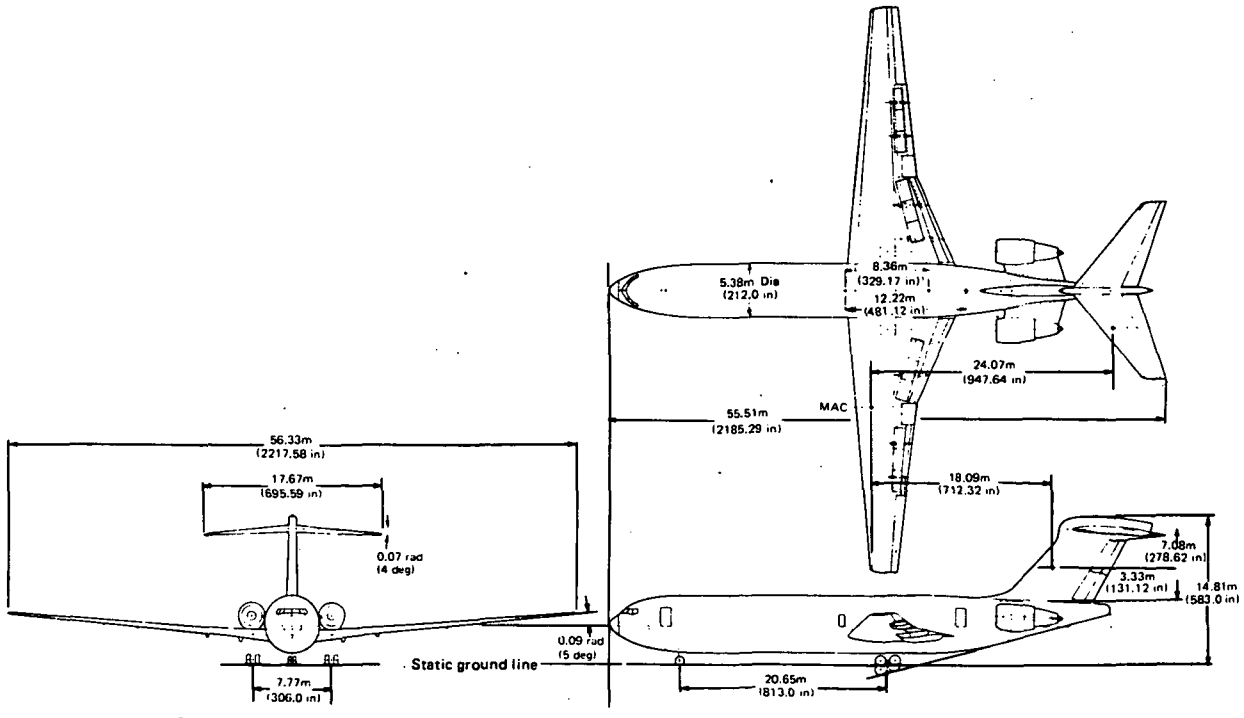

Figure 58. NLF Final Airplane General Arrangement

5.3.4 Turbulent Reference and NLF-AR10.24 Airplane Mission Analysis Comparision

The turbulent reference airplane was assumed to fly at a constant 10 668m (35 000 ft) cruise altitude because it was not capable of the more efficient step-climb cruise incorporated in the NLF mission profile (fig. 59). As a result, the turbulent reference airplane showed a lower average cruise range factor and a greater fuel requirement than the THUMBPRINT sizing process indicated.

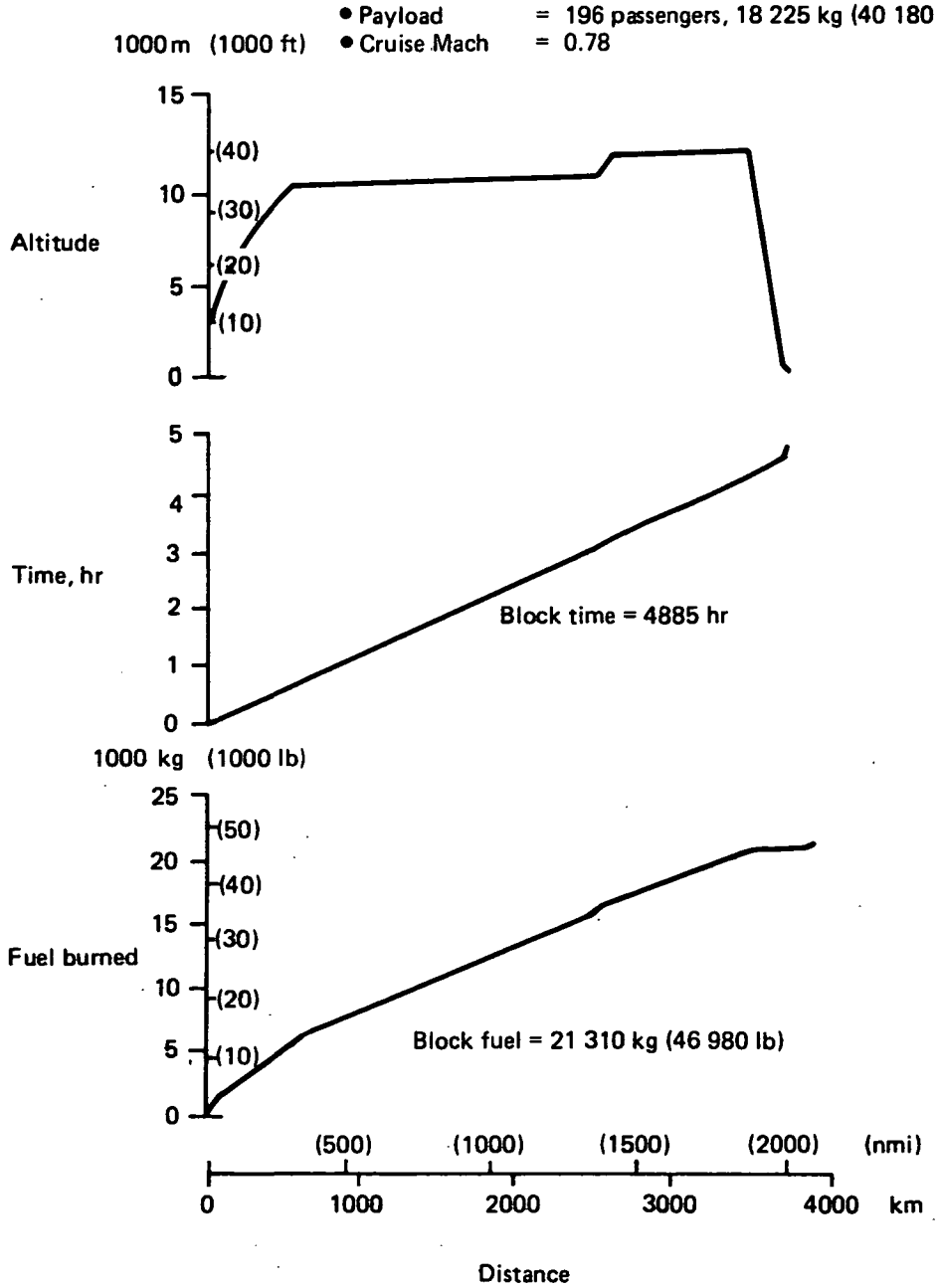

Figure 59. NLF Final Airplane Mission Profile

The NLF-AR10.24 airplane showed a block fuel increase over the THUMBPRINT results due to the requirement that initial cruise altitude be limited to the height that could be reached under turbulent climb conditions.

Both airplanes were penalized by the imposition of realistic 609.6m (2000 ft) cruise altitude increments. A summary of the turbulent reference and NLF-AR10.24 airplane mission analysis comparison is contained in Table 12.

5.4 ECONOMIC STUDY

Results of airplane sizing and mission analyses indicated that the NLF final configuration did not provide an economic advantage when compared to the turbulent reference airplane. Therefore, the economic study was limited to determination of relative direct operting cost (DOC).

The principal manufacturing difference between the turbulent reference and NLF airplanes lies in the wings. The use of bonded-honeycomb primary structure results in substantial reductions in the number of parts and manufacturing complexity. In addition, the NLF wing is simplified by the absence of leading-edge devices and by the existence of a straight (unswept) rear spar. These advantages are offset, however, by the greatly increased area and weight of the NLF wing, and the resultant increase in operating empty weight and engine thrust. For this reason, the cost to produce and, therefore the acquisition cost, was judged to be approximately equal for the turbulent reference and NLF final airplanes. The effects of change in acquisition cost on DOC are such that a 10% error in estimating acquisition cost results in only a 3% change in DOC, if other elements of the DOC formula are unchanged. Table 12 lists the economic comparison input data and the resulting 7.8% increase in DOC for the NLF airplane.

5.5 TRADE STUDY RESULTS

The two NLF airplane configurations proved to have higher DOC and greater block fuel requirements than the turbulent reference airplane. As expected, L/D and ML/D were substantially better for the NLF airplanes, but much greater operating empty weight (OEW) and takeoff gross weight (TOGW) negated this improvement. The turbulent reference airplane was assumed to cruise at M = 0.80, while NLF airplanes had a cruise Mach number of 0.78. If the turbulent reference airplane were to cruise at M = 0.78, an even greater block-fuel difference could be expected.

The effect of wing loading and aspect ratio on sized NLF airplane performance with fixed takeoff field length (TOFL) is shown in Figures 54 and 55. Minimumn block fuel values for the two NLF configurations are limited by the 231.5-km/hr (125-KEAS) approach speed constraint. The turbulent reference airplane (fig. 53) has a 13-km/hr (7-kt) advantage in approach speed at its minimum block fuel point, in addition to having significantly lower TOGW and OEW. Increased takeoff and approach lift coefficients and reduced OEW are necessary if performance of the NLF configurations is to be improved.

A major contributor to the NLF airplane increased OEW was increased wing weight. The NLF-AR10.24 wing was 23% heavier than the turbulent wing of the same aspect ratio area and wing loading. When the NLF aspect ratio was increased to 12.0 and the area held constant, the wing weight was increased by 54% over that of the turbulent wing. Factors that increased weight of the NLF wings include:

- Reduction in wing thickness ratio at the side-of-body (to promote inboard upper-surface laminar flow) reduced the depth of the wing structural box

- Substantially increased gust load factor due to reduction in sweep angle

- Increased bending moment at the side-of-body for the critical zero fuel weight condition due to the OEW increase and an outboard shift of center of pressure

- Increased bending material weight due to the use of bonded aluminum-honeycomb wing skins (for smoothness) in inboard areas where conventional skin-stringer construction would have been more efficient

  Scaling of these designs to achieve mission-sized airplanes resulted in increased wing areas for the NLF concepts to meet approach-speed requirements. This contributed to additional increases in wing weight.

The wing structure required to resist the critical-gust loads was sufficient and no additional material was required to prevent flutter.

Because wing weight proved to have a significant influence on NLF performance and DOC, various weight-reduction possibilities are suggested but have not been analyzed. Two of these suggestions are summarized below:

1. Reconfiguration of the inboard wing box to include additional bending material by sweeping the inboard rear spar rearward. This would reduce the skin-panel end load per unit chord length, allowing a reduction in panel face sheet thickness. If panel loads were greater than optimum for aluminum-honeycomb structure, the design could be refined by adding bonded stiffeners to the basic aluminum- honeycomb panels.

2. Increase of inboard wing thickness ratio. If the increase was made by recontouring the wing upper surface only, the loss of natural laminar flow probably would be restricted to that surface. This would necessitate comparison of the effect of the structural weight decrease associated with increased wing box depth to the effect of a slight increase in cruise drag coefficient.

6.0 CONCLUSIONS AND RECOMMENDATIONS

The magnitude and schedule of the present study precluded thorough investigation of important aspects of natural laminar flow (NLF) that could optimize its application to modern transport aircraft. More specific discussions of study characteristics are contained in preceding parts of the report, and the following conclusions and recommendations are offered with these qualifications in mind.

6.1 NLF AIRFOIL AND WING DESIGN

6.1.1 Conclusions

Assessment of the airfoil and wing design studies provided the following conclusions:

1. The final NLF airfoil (Airfoil 5) has a favorable upper surface pressure gradient to 60% chord and a strong favorable lower surface pressure gradient past 40% chord for the target conditions of $c_\ell = 0.50$, M = 0.78 and Reynolds number of 20×10^6. This airfoil also was free of adverse pressure gradients (to 60% chord on the upper surface, 40% chord on the lower surface) for a reasonable range of M and c_ℓ values.

2. Despite the favorable upper surface pressure gradient to 60% chord, boundary layer stability theory indicated that transition would occur at about 35% chord because of amplification of Tollmien-Schlichting waves beyond an amplification factor equal to 12. A stronger favorable pressure gradient is required to increase the extent of laminar flow on the upper surface.

3. The boundary layer on the lower suface of the airfoil appears to have adequate stability to prevent transition to tubulent flow ahead of 50% chord.

4. Boundary layer stability analysis for a pressure distribution similar to the NLF airfoils studied, indicated that the wing leading-edge sweep should be limited to about 0.087 rad (5 deg) to prevent crossflow-induced transition to turbulent flow. Greater leading-edge sweepback without encountering crossflow-induced transition is very likely achievable but may require sacrificing part of the M - c_ℓ region within which extensive laminar runs are possible. These tradeoffs for a three-dimensional wing have not been investigated in this study.

6.1.2 Recommendations

It is recommended that additional NLF airfoil studies be conducted. These studies should include the following:

1. Determine the sensitivity of boundary layer transition (using a method such as Mack's) to two-dimensional airfoil pressure gradient magnitude and shape.

2. Using airfoils that give the best results (i.e., low peak amplification factors) from the preceding study, determine the Mach-lift coefficient region within which reasonable amplification factors (e.g., n = 12 or lower) can be maintained.

3. The effect of leading-edge sweep on crossflow instability-caused transition should be investigated for several airfoils selected on the basis of results of the two preceding studies. The development of an NLF airfoil that can tolerate at least moderate leading-edge sweepback is highly desirable to prevent spanwise load distributions from shifting outboard, as occurs with the straight wing in flight. Preventing such outboard shifts is vital to attaining wing weight values similar to those for swept turbulent boundary layer aircraft with which NLF applications must compete.

4. Assuming that results of the preceding studies are positive, two-dimensional wind tunnel tests should be conducted to verify the calculated pressure distributions, not only at the design point, but also throughout the predicted M - C_{ℓ} region for NLF application.

6.2 AIRCRAFT DESIGN TRADE STUDY

6.2.1 Conclusions

The following conclusions were derived relative to the final NLF configuration.

1. The final NLF airplane was not competitive with a turbulent airplane of conventional design for the defined 196-passenger, 3704-km (2000-nmi) mission.

2. For such a configuratin, wing weight must be reduced to provide an overall advantage commensurate with reduced NLF drag levels.

3. Takeoff and landing stall speed improvements are necessary to permit higher wing loading and lower thrust loading and, hence, better performance. The low wing loading (large wing area) may be counter-productive in obtaining NLF, due to larger wing chords. The final NLF airplane is likely to be limited in obtaining NLF near the wing root (local RNs are above 40 million). Greater wing root thickness may decrease wing weight significantly, while having a minor effect on actual wing area capable of obtaining NLF.

4. Ride comfort for the two NLF airplanes is inferior to several current production jet transports. A ride quality control system may be necessary.

6.2.2 Recommendations

This study has demonstrated that the combination of boundary layer stability analysis techniques with standard airfoil design techniques can be used to satisfactorily define a two dimensional airfoil having natural laminar flow over a major portion of a wing chord typical of a large contemporary civil transport. However, it has also demonstrated that the integration of such an airfoil into a three-dimensional swept wing is the most challenging problem to be solved before natural laminar flow can be successfully applied to a commercial airplane. The basic problem involved in obtaining natural laminar flow on a swept wing, as opposed to an unswept wing, is that the two basic types of laminar boundary layer instabilities which occur on a swept wing, crossflow instability and Tollmien-Schlichting instability, are affected oppositely by pressure gradient. Crossflow is caused by the combination of sweep and pressure gradient. As a result, a large extent of favorable pressure gradient on a swept wing will result in the development of large crossflow velocities in the boundary layer and large crossflow disturbance amplification rates. On the other hand, a large extent of favorable pressure gradient is required for

the stabilization of Tollmien-Schlichting disturbances. As illustrated in Figure 60, the typical optimum pressure distribution for crossflow stability has very large initial pressure gradients (where the boundary layer is thinner and more stable than further aft). It then rapidly flattens out, resulting in the decay of crossflow disturbances. The typical optimum pressure distribution for Tolmien-Schlichting stability has large favorable pressure gradients occuring over a large percentage of the chord. The integration, in an optimum manner, of a two-dimensional natural laminar flow airfoil (which has been optimized for Tollmien-Schlichting stability) into a three-dimensional swept wing would require that the airfoil be modified to have acceptable crossflow stability characteristics at the desired sweep angle, while not allowing the resulting degradation of Tollmien-Schlichting to become too severe. The resulting pressure distribution would be a compromise between that which is optimum for Tollmien-Schlichting stability and that which is optimum for crossflow stability. There will be some upper bound on the sweep angle beyond which it will not be possible to stabilize both types of disturbances without making other changes to the wing, such as reducing the chord Reynolds number.

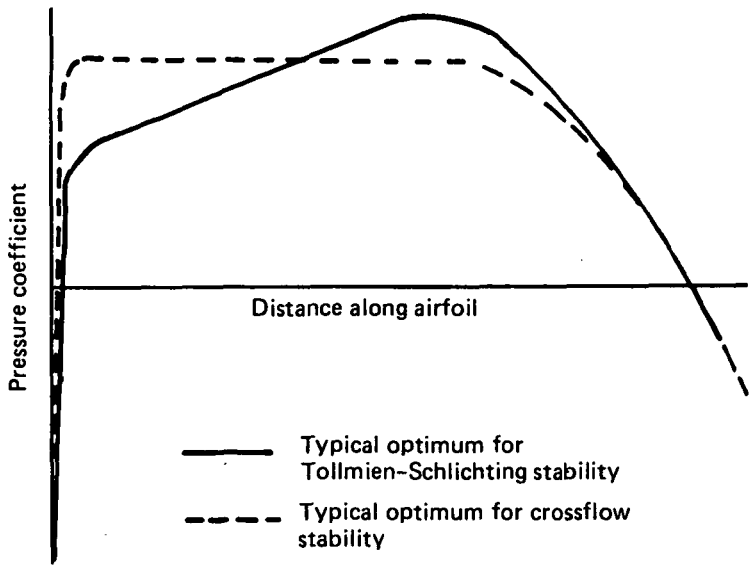

Figure 60. Optimized Pressure Distribution Characteristics

The aircraft trade study identified several areas where futher iterations of the NLF airplane might have improved the design, such as thicker wing section at side-of-body; however, the biggest benefit would result from increasing wing sweep as high as possible. The airfoil-wing integration problem and the resulting determination of a realistic upper bound in the allowable sweep angle is one of the most fruitful areas for additional natural laminar flow studies.

This aircraft design study shows that increased weight due to low wing sweep is the fundamental problem of integrating NLF technology into a short to medium range transport. Successful application of a new technology to conventional-type aircraft cannot always be achieved by the first approach to its integration. However, should

additional NLF airfoil design and validation tests be successful and acceptable solutions to insect contamination be forthcoming, then the following is recommended.

1. Expanded design and configuration studies of several times the magnitude of this program are recommended to permit evaluation of NLF airplanes that represent a good compromise between structural and aerodynamic efficiency.

2. This study has provided insight into the type of trade studies that could be conducted to determine what an optimum airplane configuration might be for maximum NLF potential. Such trades as increasing the wing root thickness to reduce structural weight and use of alternate wing structure such as composites should be investigated. Adding leading-edge devices and reducing wing area also could improve the weight problem. Another option could be investigation of trade study benefits of a wing combining upper-surface laminar flow with a Boeing-747-type leading-edge device. This device, which is faired into the lower surface for cruise, provides protection against erosion and insect impingement upon the fixed leading edge, in addition to substantial improvement in $C_{L_{max}}$.

3. A study should be performed to assess NLF airplanes designed for alternate missions, varying from shorter range and lower speed to very long range.

Each trade study must be conducted in depth sufficient to carefully assess the benefit of reduced weight to potential drag reduction of the remaining natural laminar flow.

7.0 REFERENCES

1. NASA CR-158954, Final Report, "Task 4.1, Study of Surface Coatings for Drag and Erosion Reduction", Contract NAS1-14742, The Boeing Company, January 1979.

2. Bauer, F., Garabedian, P., and Korn, D.: "Supercritical Airfoils", Lecture Notes in Economics and Mathematical Systems, No. 108, Volume II, 1975.

3. Barger, R.L. and Brooks, C. W.: "A Streamline Curvature Method for Design of Supercritical and Subcritical Airfoils", NASA TN D-7770, September 1974.

4. Nash, Y.F. and MacDonald, A.G.Y.: The Calculations of Momentum Thickness in a Turbulent Boundary Layer at Mach numbers up to Unity, Aeronautical Research Council, C.P. No. 963, London, 1967.

5. Reyhner, T.A.: "The Interaction of a Shock Wave with a Laminar Boundary Layer," Dissertation, Stanford University, November 1966, (abbrev. version in the International Journal of Non-Linear Mechanics, Vol. 3, 1968, pp. 173-190).

6. Reyhner, T.A.: "Finite-Difference Solution of the Compressible Turbulent Boundary Layer Equations", in Proceedings Computation of Turbulent Boundary Layers - 1968, AFOSR-IFP-Stanford Conference, Vol. I, pp. 375-383, 1969.

7. Mack, L.M.: "Boundary Layer Stability Theory", Jet Propulsion Laboratory, Document 900-277 (Rev A), Pasadena, California, 1969.

8. Merkle, Charles L.: "The Computation of the Stability Characteristics of Three Dimensional Boundary Layers", December 1977.

9. Schubauer, B. and Skramstad, H. K.: "Laminar Boundary Layer Oscillation and Stability of Laminar Flow", Journal of Aeronautical Science, 14, No. 69, 1947.

10. Smith F. and Highton, D. F.: "Flight Test of a King Cobra FZ440 to Investigate the Practical Requirements for the Achievement of Low Profile Drag Coefficient on a Low Drag Airfoil", ARC Technical Report, R and M 2375, 1950.

1. Report No.	2. Government Accession No.	3. Recipient's Catalog No.
CR-159029		

4. Title and Subtitle	5. Report Date
Final Report - Natural Laminar Flow Airfoil Analysis and Trade Studies	May 1979
	6. Performing Organization Code: B-7220
7. Author(s): Boeing Commercial Airplane Company, Preliminary Design Department	8. Performing Organization Report No.: D6-46694
	10. Work Unit No.
9. Performing Organization Name and Address: Boeing Commercial Airplane Company, P.O. Box 3707, Seattle, Washington 98124	11. Contract or Grant No.: NAS1-14742
	13. Type of Report and Period Covered: Final Report, August 1977 - November 1978
12. Sponsoring Agency Name and Address: National Aeronautics and Space Administration, Langley Research Center, Hampton, Virginia 23665	14. Sponsoring Agency Code

15. Supplementary Notes

Technical Monitor: D. B. Middleton, NASA Langley Research Center

16. Abstract

An analysis of an airfoil for a large commercial transport cruising at Mach 0.8 and the use of advanced computer techniques to perform the analysis are described. Incorporation of the airfoil into a natural laminar flow transport configuration is addressed and a comparison of fuel requirements and operating costs between the natural laminar flow transport and an equivalent turbulent flow transport is addressed.

17. Key Words (Suggested by Author(s))	18. Distribution Statement
Natural Laminar Flow Pressure Gradient	

19. Security Classif. (of this report)	20. Security Classif. (of this page)	21. No. of Pages	22. Price*
Unclassified	Unclassified		

* For sale by the National Technical Information Service, Springfield, Virginia 22161